Pixelated Fourier Transform Plane Filters in Optical Systems

Paul H. Willson

M.Phil.

University of Edinburgh

1991

ABSTRACT

Spatial light modulators (s.l.m.s) are now being used as variable filters which remain in situ in optical systems with the filtering effect controlled by optical or electronic addressing of the devices. These remotely controlled filters are replacing wet-processed or hand-made filters which are manually introduced into an optical system, and which must be changed to suit a particular application.

Pixelation is a feature of some s.l.m.s. That is perturbation of an optical wavefront incident upon the s.l.m. occurs in well-defined, discrete and separately controlled regions of the filter. The effect on the image plane of optical systems which have pixelated filters used in their Fourier transform plane will be studied in this thesis.

An investigation of the optical system with which the s.l.m.s may be used to best advantage will be shown. Experimental results obtained from the use of a working liquid-crystal-over-silicon s.l.m. in a variable-scale-Fourier transform optical system will be given along with a range of results from the use of other pixelated filters.

The optical properties of s.l.m.s have been partly dictated by the nature of the electronic or other addressing system. A part of this thesis deals with filters which simulate some optical properties of s.l.m.s but with designs which have not yet been produced in working devices. Results obtained with these filters are presented.

Finally, the condition under which s.l.m.s may utilise the self-Fourier transforming phenomenon is discussed.

Acknowledgements

My grateful thanks go to my supervisors, Dick Sillitto and David Vass. Thank you too to the other members of the group whose help was invaluable: Norman Fancey, George Bradford, Dick Dougal, Winifred Sillitto, Adil Al-Chalbi and Andy Garrie.

I give my special thanks to Doug McKnight, Ian Underwood, Mike Ranshaw, Alistair Sutherland, Alastair MacGregor, Steve, Ian and Duncan.

Without the assistance of the staff of the Edinburgh Microfabrication Facility, most of the experimental work would have been impossible so I am very grateful to them, especially Tom Stevenson, Alan Gundlach and Bill Gammie.

Thanks to Peter Tuffy for taking and processing some of the photographs.

Finance for the work in this thesis came from S.E.R.C. for two years and form the Dewar fund of the University of Edinburgh for the final year. Thank you for the money.

Finally I would like to thank Bob Imhof of the Photophysics Research Group at the University of Strathclyde without whose patient support this thesis might still be unfinished.

To Derby House: Rona, Mike, Stefano, David, Mike, Craig, Charles, Kevin, Andrew, Scott, Angus, Andrew, Graeme, Gregor, Alan, David, Jamie, Magnus, Brad, Richard, Patrick, Jean, and numerous others who came and went. It was good fun.

Table of Contents

Chapter 1

Introduction

1.1 Historical background

Spatial filtering is the modification of an optical wavefront emanating from an object such that any subsequently formed image of the object is altered. The effects of such optical spatial filtering were first noticed by Abbe, and are described in his paper of 1873 [1.1]. A systematic investigation was carried out by Porter in 1906 [1.2]. Both found that if the diffraction spectrum of an object was filtered at an intermediate stage in an optical imaging system, for example by a lens aperture, the image obtained differed significantly from the object. The spatial filtering effect was recognised, and considered in the design of optical systems during the first half of the 20th century, but it was not until the 1950's that spatial filtering became a subject of study in its own right.

The diffraction spectrum of a plane object illuminated by a monochromatic beam of coherent light is the squared modulus of its Fourier transform (F.T.). The advent of the laser in the early 1960's made it a simple process to produce F.T.s of objects. There have since been many studies of different aspects of F.T. filtering, which can be found detailed in Van der Lugts overview of 1968 [1.3]. The filtering operation has become a more accurate one than was undertaken by Porter since within the F.T. the position of points of

light due to different spatial frequencies present in the object is accurately known.

1.2 Fourier transform filtering

The F.T. of a plane object may be produced by diffractive (e.g. holographic) reflective (e.g. mirror) or refractive (e.g. lens) optical systems. The most common means of producing an optical F.T. of an object in the laboratory utilise the Fourier transforming property of the converging lens. Such optical systems will be discussed in detail in chapter 2. It will be shown that lines of spatial frequency σ present in the object, will produce a spot of light in the F.T. plane of an optical system. This spot will lie on an imaginary line through the centre of the F.T. which is orthogonal to the lines in the object. The distance of the spot from the centre of the F.T. is proportional to the spatial frequency.

Filters placed in the F.T. plane, which modify the F.T. will change the image of the object. The light field in the F.T. plane may be filtered in amplitude and/or phase. The mathematical representation of filters is discussed with some rigour by several authors, whose notation will be used extensively later in the thesis. However, for the moment let us qualitatively consider some of the simple filtering operations.

The method used by Abbe and Porter was binary amplitude filtering. This may be achieved simply by placing apertures and stops in the F.T. plane of an optical system, so that a subsequently formed image is composed of only a known subset of the spatial

frequencies which were present in the object. In 1935, Zernike proposed the phase-contrast technique of spatial filtering [1.4]. Using this method, the phase of spots of light in the F.T. due to different spatial frequencies in the object is changed, causing the image formed at a later stage to be modified. This modification may be in phase only, or in some circumstances, a phase only filter may act as an amplitude filter. In addition to pure phase and binary amplitude filters, grey-scale amplitude filters may be used, which attenuate the contribution of each spatial frequency to the image rather than simply blocking it. Amplitude and phase variations may by combined in complex filters, with applications in optical computing and optical correlation, as well as classical optical processing. However, we shall henceforth consider only relatively simple binary amplitude F.T. filters. These are of four commonly used types: low-pass, high-pass, band-pass and directional filters. A low-pass filter blocks out light due to all spatial frequencies above a cutoff of σ_c and thus an image may be formed which consists wholly of spatial frequencies lower than σ_c. Similarly, a high-pass filter blocks all spatial frequencies below σ_c. A band-pass filter allows only a range of frequencies between two cutoffs to constitute the image. A directional filter allows only spatial frequencies lying in a subset of directions to constitute the image.

1.3 Filtering techniques

The apertures and stops which have traditionally been used as F.T. filters suffer from the disadvantage of being difficult to

align manually, with good accuracy. This is especially true for filters which are more complicated that those illustrated in the last section. Photographic film has been used extensively to produce F.T. filters. The properties of film are discussed in detail by Goodman [1.5]. Although complicated filters may be produced by this method, the technique is not free from difficulties. The major problem associated with photographic film filters in coherent optical processors, is unwanted phase effects which are produced by varying film thickness. This occurs for two reasons. Firstly, the film is generally not produced to be optically flat, and secondly the development process introduces variations in thickness associated with the opacity of the film. Shrinkage of the film during development means that the final filter will differ from the initial specifications. Whilst little can be done about the last point except compensations at the design stage, the optical flatness problem may be overcome by using a liquid gate. This consists of two optical flats, used as two sides of a bath containing oil which approximately matches the refractive index of the film to that of the optical flats, into which the film is placed. In an optical system in which filters are frequently changed this is a messy business! However, photographic filters continue to be widely used.

Since the early 1970's, a range of electronically and optically addressed spatial light modulators (s.l.m.s) have been developed, which may be used as F.T. filters. These devices remain in situ in the F.T. plane, whilst the filtering effect is controlled remotely. S.l.m.s are sometimes pixelated. That is, perturbation of the

optical wavefront which is incident upon them occurs in well-defined discrete and separately controlled areas of the device. Figure 1.1 is a table which gives a summary of some of the optical properties of s.l.m.s commonly encountered in publications [1.6,1.7,1.8].

A great deal has been published on methods of fabrication and electronic specifications of s.l.m.s (e.g. [1.9,1.10,1.11]). However, there have been few reports in the literature relating to the optical effects of pixelation in devices used as F.T. filters in optical systems. A theoretical analysis of the effect of pixelation will be presented and discussed in this thesis. Experimental results from the use of a 16x16 pixel s.l.m designed by Dr. I Underwood of the Applied Optics Group (A.O.G.) at the University of Edinburgh will be compared with expectations from theory.

Three liquid crystal over nMOS silicon s.l.m.s, including the one mentioned above, have been designed by members of the A.O.G. Each of the devices utilises a different optical effect of the liquid crystal, and all have been used for F.T. plane filtering in optical systems. A schematic cross-section of part of a liquid crystal over silicon device is shown in figure 1.2.

Results of experiments in which the 16x16 pixel s.l.m. and other pixelated filters are used in the F.T. plane of an optical system with variable scale F.T. will be presented. The design of the optical system will be given and discussed, and attention will be drawn to the advantages of using pixelated filters in variable rather than fixed scale F.T. optical systems, which will be demonstrated.

In this thesis, for the first time, it will be shown that the

FIGURE 1.1

A summary of the optical properties of some common s.l.m.s.

S.L.M.	MATERIAL	TYPE	CONTRAST RATIO	PIXEL SIZE	PIXEL SPACING	PIXEL NUMBER
UNDERWOOD (A.O.G.)	LIQUID CRYSTAL	BINARY AMPLITUDE	500:1	100x100 μm	200 μm	16x16
MCKNIGHT (A.O.G.)	LIQUID CRYSTAL	BINARY AMPLITUDE	1000:1	45x44 μm	74 μm	50x50
RANSHAW (A.O.G.)	MEMBRANE	PHASE	-	100x100 μm	200 μm	16x16
HUGHES	LIQUID CRYSTAL	AMPLITUDE	100:1	-	-	-
MARCONI	LIQUID CRYSTAL	AMPLITUDE	-	-	14 μm	-
LITTON	GARNET FILM	BINARY AMPLITUDE	-	58x58 μm	76 μm	128x128
PEMSLM	MEMBRANE	PHASE	-	28x33 μm	56 μm	128x128

- INFORMATION NOT AVAILABLE

FIGURE 1.2

A schematic cross-section of part of a liquid crystal over silicon s.l.m.

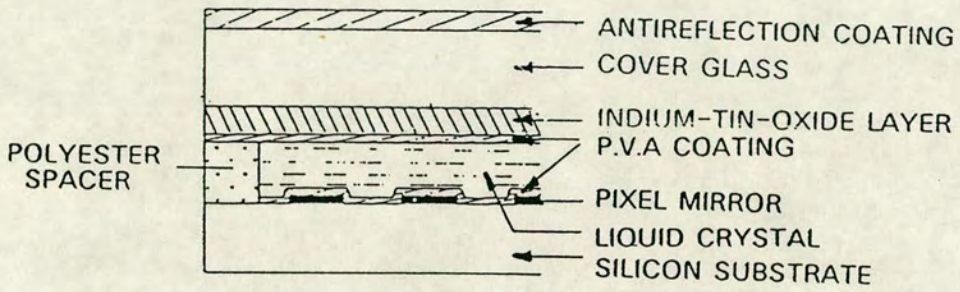

powerful techniques of integrated circuit design and fabrication, which have been used in the production of s.l.m.s, may be used to produce pixelated aluminium mirrors with very precise dimensions on a silicon substrate. The experimental results of mirror arrays produced in this way, used as filters in the F.T. plane of a variable scale F.T. optical imaging system will be given and discussed. The potential for using this technique of producing filters, to simulate the optical properties of s.l.m.s will be assessed in the final chapter of the thesis.

Chapter 2

Fourier transform optical imaging systems

2.1 The production of the Fourier transform

Of the many designs of optical system which have the formation of the F.T. of the object as an intermediate stage, the most commonly used in the laboratory utilise the Fourier transforming property of the converging lens. The simplest systems use a single lens, and figure 2.1 shows schematically three such optical systems which we shall discuss in this chapter. In these cases, the object is illuminated by a) a parallel beam, b) a diverging beam and c) a converging beam. The first is familiar from text-books and gives rise to the f-f, or as it will be referred to later, the fixed-scale F.T. system. Although well understood, this system will be discussed in some detail below to introduce the ideas and algrebraic notation which will be used throughout the subsequent analyses of the more interesting variable-scale F.T. situations which occur in the other two systems. These systems will be seen to be the most flexible for use in conjunction with pixelated F.T. filters.

FIGURE 2.1

Single-lens Fourier-transforming systems

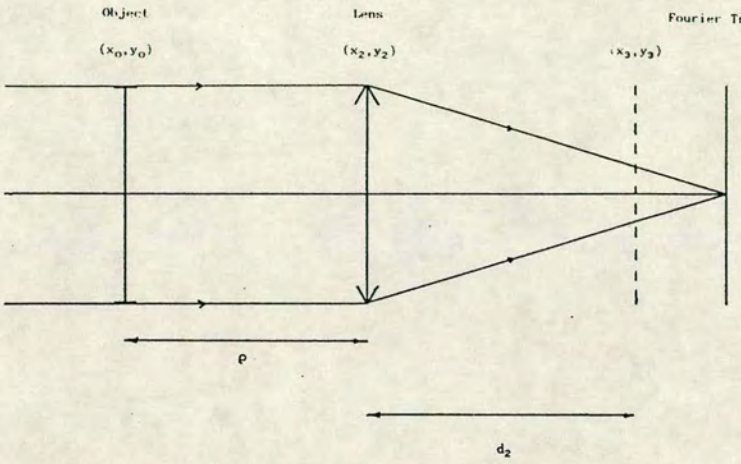

a) Object illuminated by a collimated beam

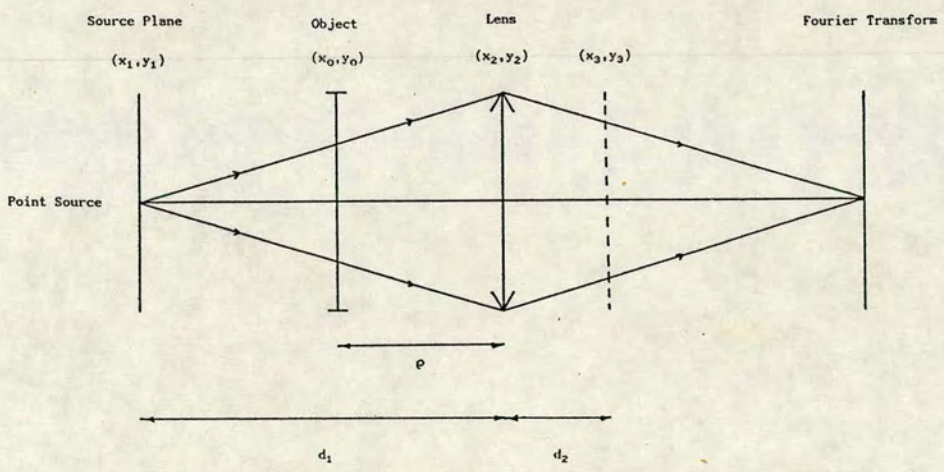

b) Object illuminated by a diverging beam

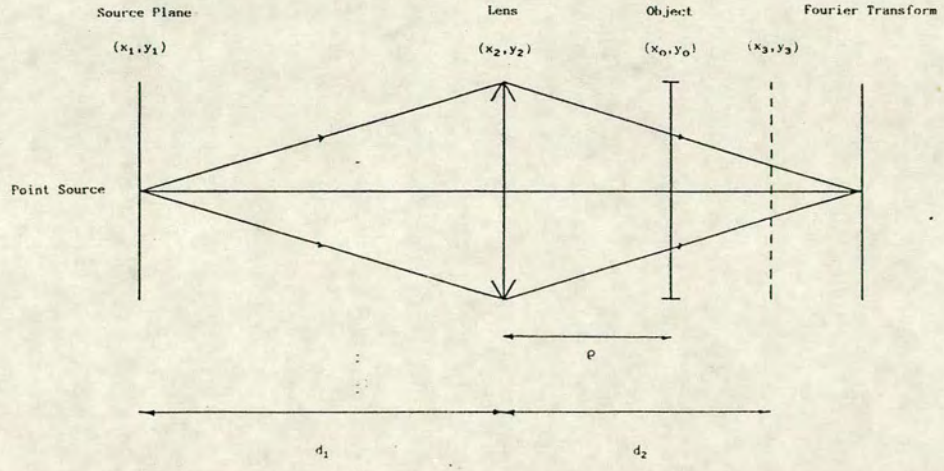

c) Object illuminated by a converging beam

2.1.1 An object illuminated by a plane-wave

Consider figure 2.1.a. If a plane-wave of coherent monochromatic light of constant complex amplitude α is normally incident upon a two-dimensional object of complex amplitude transmittance $t_o(x_o,y_o)$, we may represent the complex amplitude of the light field just after passing through the object as

$$U_o(x_o,y_o) = \alpha t_o(x_o,y_o) \qquad -(2.1)$$

The complex amplitude distribution arriving at the lens may be derived from the Fresnel-Kirchhoff diffraction integral if the distance between the object and lens is greater than the maximum linear dimension of the object [2.1]. Thus we derive the Fresnel diffraction integral which for this case is

$$U_2(x_2,y_2)=\frac{e^{ik\rho}}{i\lambda\rho}\int_{-\infty}^{\infty}\int_{-\infty}^{\infty}U_o(x_o,y_o)e^{\frac{ik}{2\rho}[(x_2-x_o)^2+(y_2-y_o)^2]}dx_o dy_o \qquad -(2.2)$$

which may be written

$$U_2(x_2,y_2)=Ch(x_2,y_2;\rho)\int_{-\infty}^{\infty}\int_{-\infty}^{\infty}U_o(x_o,y_o)h(x_o,y_o;\rho)e^{-\frac{ik}{\rho}(x_o x_2+y_o y_2)}dx_o dy_o \qquad -(2.3)$$

where C represents a complex constant and in general

$$h(x,y;\rho) = e^{\frac{ik}{2\rho}(x^2+y^2)} \qquad -(2.4)$$

If we now consider the lens as an object with complex amplitude transmittance [2.2]

$$t(x_2,y_2) = e^{\frac{-ik}{2f_1}(x_2^2+y_2^2)} = h(x_2,y_2;-f_1) \qquad -(2.5)$$

(in which we have ignored the constant terms), and the pupil function, that is the function which defines the shape and extent of the lens in the (x_2,y_2) plane, associated with the lens is represented by $p(x_2,y_2)$, we may write an expression for the complex amplitude in the arbitrary plane (x_3,y_3):

$$U_3(x_3,y_3) = C\, h(x_3,y_3;d_2) \int_{-\infty}^{\infty}\int_{-\infty}^{\infty}\Big[p(x_2,y_2)U_2(x_2,y_2)h(x_2,y_2;-f_1)$$

$$\times\ h(x_2,y_2;d_2)e^{\frac{-ik}{d_2}(x_2x_3+y_2y_3)}\Big]dx_2dy_2 \qquad -(2.6)$$

Let us remove the complication of the pupil function by considering the lens to be infinite in extent, thus making $p(x_2,y_2)=1$ over the range of integration. We shall however consider the situation where this is not the case later in this chapter.

Subtituting (2.3) into (2.6) yields

$$U_3(x_3,y_3) = Ch(x_3,y_3;d_2) \int_{-\infty}^{\infty}\int_{-\infty}^{\infty}U_0(x_0,y_0)h(x_0,y_0;\rho) \int_{-\infty}^{\infty}\int_{-\infty}^{\infty}\Big[h(x_2,y_2;w)$$

$$\times\ e^{-i2\pi\left[x_2\left[\frac{x_0}{\lambda\rho}+\frac{x_3}{\lambda d_2}\right]+y_2\left[\frac{y_0}{\lambda\rho}+\frac{y_3}{\lambda d_2}\right]\right]}dx_2dy_2\Big]dx_0dy_0 \qquad -(2.7)$$

where

$$\frac{1}{w} = \frac{1}{\rho} + \frac{1}{d_2} - \frac{1}{f_1} \qquad -(2.8)$$

The integral w.r.t. x_2 and y_2 is the F.T. of $h(x_2,y_2;w)$ and may be evaluated as shown in appendix 1.

By evaluating, expanding and rearranging (2.8), we may write for the complex amplitude in the plane (x_3,y_3):

$$U_3(x_3,y_3) = C\, h\left[x_3,y_3;\left[\frac{1}{d_2} - \frac{w}{d_2^2}\right]^{-1}\right] \times \int_{-\infty}^{\infty}\int_{-\infty}^{\infty} U_o(x_o,y_o)h\left[x_o,y_o;\left[\frac{1}{\rho} - \frac{w}{\rho^2}\right]^{-1}\right] e^{-\frac{i2\pi w}{\lambda\rho d_2}(x_o x_3 + y_o y_3)}\, dx_o dy_o \qquad -(2.9)$$

If we now substitute (2.1) into (2.9) we see that if $w=\rho$, or equivalently (from (2.8)) $d_2=f_1$, we may write

$$U_3(x_3,y_3) = C\, h\left[x_3,y_3;\left[\frac{1}{f_1} - \frac{\rho}{f_1^2}\right]^{-1}\right] \times \int_{-\infty}^{\infty}\int_{-\infty}^{\infty} t_o(x_o,y_o)e^{-i2\pi\left[x_o\left[\frac{x_3}{\lambda f_1}\right]+y_o\left[\frac{y_3}{\lambda f_1}\right]\right]}\, dx_o dy_o \qquad -(2.10)$$

which shows that the F.T. of the transmission function of the object multiplied by a complex phase factor appears in the (x_3,y_3) plane. Note that the above is true if $d_2=f_1$, that is the F.T. plane is the back focal plane of the lens. As the object is illuminated with a plane wave, which may be considered to have a point source at an infinitely large distance, the source and F.T. are in conjugate planes relative to the lens. The phase factor is unity if $\rho=f_1$. We have in this case the familiar f-f system. Note that if $\rho\neq f_1$, the centre of the F.T. is still located at the back focal point of the

lens, but the exact F.T. is formed on a spherical surface of radius $f_1^2/(f_1-\rho)$ (which is the distance of the plane of the image of the object from the (x_3,y_3) plane), and the factor is commonly referred to as the phase curvature. Hence a phase factor is introduced for all non-central points of the (x_3,y_3) plane.

2.1.2 Object illuminated by a spherical diverging wave

This case is illustrated in figure 2.1.b. The complex amplitude of the light field leaving the object is

$$U_o(x_o,y_o) = \frac{1}{(d_1-\rho)}\ h(x_o,y_o;(d_1-\rho))t_1(x_1,y_1) \qquad -(2.11)$$

We may follow the analysis of the previous case up to the substitution for $U_o(x_o,y_o)$, giving the complex amplitude in the arbitrary plane (x_3,y_3) represented by (2.9). If we now substitute (2.11) into (2.9) we obtain the expression

$$U_3(x_3,y_3) = Ch\left[x_3,y_3;\frac{d_2}{d_2-w}\right]\int_{-\infty}^{\infty}\int_{-\infty}^{\infty} t(x_o,y_o)h\left[x_o,y_o;\left[\frac{1}{\rho}-\frac{w}{\rho^2}+\frac{1}{d_1-\rho}\right]^{-1}\right]$$

$$\times\ e^{\frac{-i2\pi w}{\lambda\rho d_2}(x_o x_3+y_o y_3)}\ dx_o dy_o \qquad -(2.12)$$

If we choose d_2, which is related to w by (2.8), so that

$$\frac{1}{\rho}-\frac{w}{\rho^2}+\frac{1}{d_1-\rho} = 0 \qquad -(2.13)$$

then

$$\frac{1}{d_2} = \frac{1}{f_1} - \frac{1}{d_1} \qquad -(2.14)$$

and we may write

$$U_3(x_3,y_3) = Ch(x_3,y_3;A)\int_{-\infty}^{\infty}\int_{-\infty}^{\infty} t_o(x_o,y_o)e^{\frac{-i2\pi}{\lambda}\left[\frac{d_1-f_1}{(d_1-\rho)f_1}\right](x_ox_3+y_oy_3)} dx_o dy_o \qquad -(2.15)$$

where

$$\frac{1}{A} = \left[\frac{d_1 - f_1}{d_1 f_1 \rho^2}\right]\left[1 - \frac{d_1(\rho+d_1) - f_1 d_1}{\rho f_1}\right] \qquad -(2.16)$$

which again is the F.T. of the complex transmission function of the object multiplied by a phase curvature factor which is unity if $\rho=f_1$. Notice that (2.14) has the form of the relationship which is commonly known as the lensmakers formula, and shows that the F.T. is produced in the image plane of the point source. This is also the case for the f-f system.

The form of (2.15) appears to differ from that of the previous case in that there is a factor in the kernel of the F.T. which is dependent upon the lens-object distance ρ. For reasons which will be given in the next section, we shall call this the scale factor. Note however that this case is a special case of the previous one, and in the limit as ρ tends to infinity, (2.15) becomes (2.10). A scale factor also occurs in the final case which we shall consider.

2.1.3 Object illuminated by a spherical converging wavefront

Refer now to figure 2.1.c. The complex amplitude of the light field leaving a plane object (represented by the transmission function $t_o(x_o,y_o)$) illuminated by a spherical converging beam is

given by

$$U_o(x_o,y_o) = \frac{1}{d_1-\rho}\, h(x_o,y_o;-\rho)t_o(x_o,y_o) \qquad -(2.17)$$

The pupil function of the lens producing the beam is considered to be unity as before.

Using the Fresnel diffraction equation, we obtain the following expression for the complex amplitude in the plane (x_3,y_3):

$$U_3(x_3,y_3) = \frac{1}{i\lambda(d_2-\rho)}\; h\left[x_3,y_3;\frac{2}{d_2-\rho}\right] \times \int_{-\infty}^{\infty}\int_{-\infty}^{\infty} t_o(x_o,y_o)e^{\frac{-ik}{\rho}(x_ox_3+y_oy_3)}\, dx_o dy_o \qquad -(2.18)$$

which we recognise as the F.T. of the complex amplitude transmittance of the object multiplied by a phase curvature factor.

In this case, we have predetermined the position of the centre of the F.T. by choosing d_1 and f_1 and because

$$\frac{1}{d_1} + \frac{1}{d_2} = \frac{1}{f_1} \qquad -(2.19)$$

as was the situation in the previous case (2.14) in which the source plane, lens and image plane configuration is the same. So again the F.T. is formed in the conjugate plane to the source plane relative to the lens, that is the image plane of the point source. As in the previous case, a factor is present in the kernel which affects the scale of the F.T. We shall now look more closely at the scale factor.

2.2 The variable scale factor

In general, a 2-dimensional F.T. has the form

$$V(\sigma,\tau) = \int_{-\infty}^{\infty}\int_{-\infty}^{\infty} U(x,y)e^{-\frac{i\lambda\pi}{\gamma}(x\sigma+y\tau)}\,dxdy \qquad -(2.20)$$

Where σ and τ are spatial frequencies which are present in the x and y directions in the object respectively, and γ is a dimensionless constant.

In a F.T. optical system, light diffracted by spatial frequency (σ,τ) in the object arrives at the point $(\gamma\sigma\ \lambda f, \gamma\tau\ \lambda f)$ in the F.T. plane. Variation of γ changes the off-axis distance of this spot of light in the F.T. plane. Thus F.T.s of the same object in systems of different γ will appear to be of different 'size'. The effect is analogous to magnification in an imaging system.

We have seen that whereas in the fixed scale F.T. system, the factor γ is fixed as unity for a lens with a given focal length, in the other two systems discussed, it is a function of the separation of the object and lens and thus if we can vary this separation, we have some control over the F.T. scale.

In the case of the object illuminated by a spherical diverging beam, we saw that the scale factor was

$$\frac{1}{\gamma} = \frac{d_1-f_1}{d_1-\rho} = \frac{1}{M(1-(\rho/f_1))+1} \qquad -(2.21)$$

and in the case of illumination by a spherical converging beam

$$\frac{1}{\gamma} = \frac{f_1}{d_2-\rho} = \frac{1}{(M+1)-(\rho/f_1)} \qquad -(2.22)$$

Where $M = d_2/d_1$ $-(2.23)$

is the magnification of the system.

Figure 2.2 is a graph showing how γ varies with the parameter ρ/f_1 for the values M = 0.5, 1, 2. It is drawn as if the lens is infinitely thin, in effect as if the object is moved through the lens from one side (diverging illuminating wave) to the other (converging wave). In each case the scale factor increases as the object is moved away from the lens. Only in the case where the source and F.T. are equidistant from it is the variation symmetrical about the lens. The diagram below the graph shows the relative positions of the point source, lens and F.T. corresponding to each of the graphs.

Notice that in each case, when the object is in the front focal plane of the lens, the scale factor is unity i.e identical to that of a fixed scale system with a lens of the same focal length. Notice also that in each case the Fourier plane is conjugate to the source plane.

2.3 The effect of the lens aperture upon the Fourier transform

In the preceding discussions of the production of F.T.s, the effect of the size of the lens aperture was neglected in order to focus attention on the variable scale phenomenon. The pupil (or

FIGURE 2.2

A graph illustrating the variation of Fourier transform scale with separation of object and lens, with a schematic diagram of the optical system

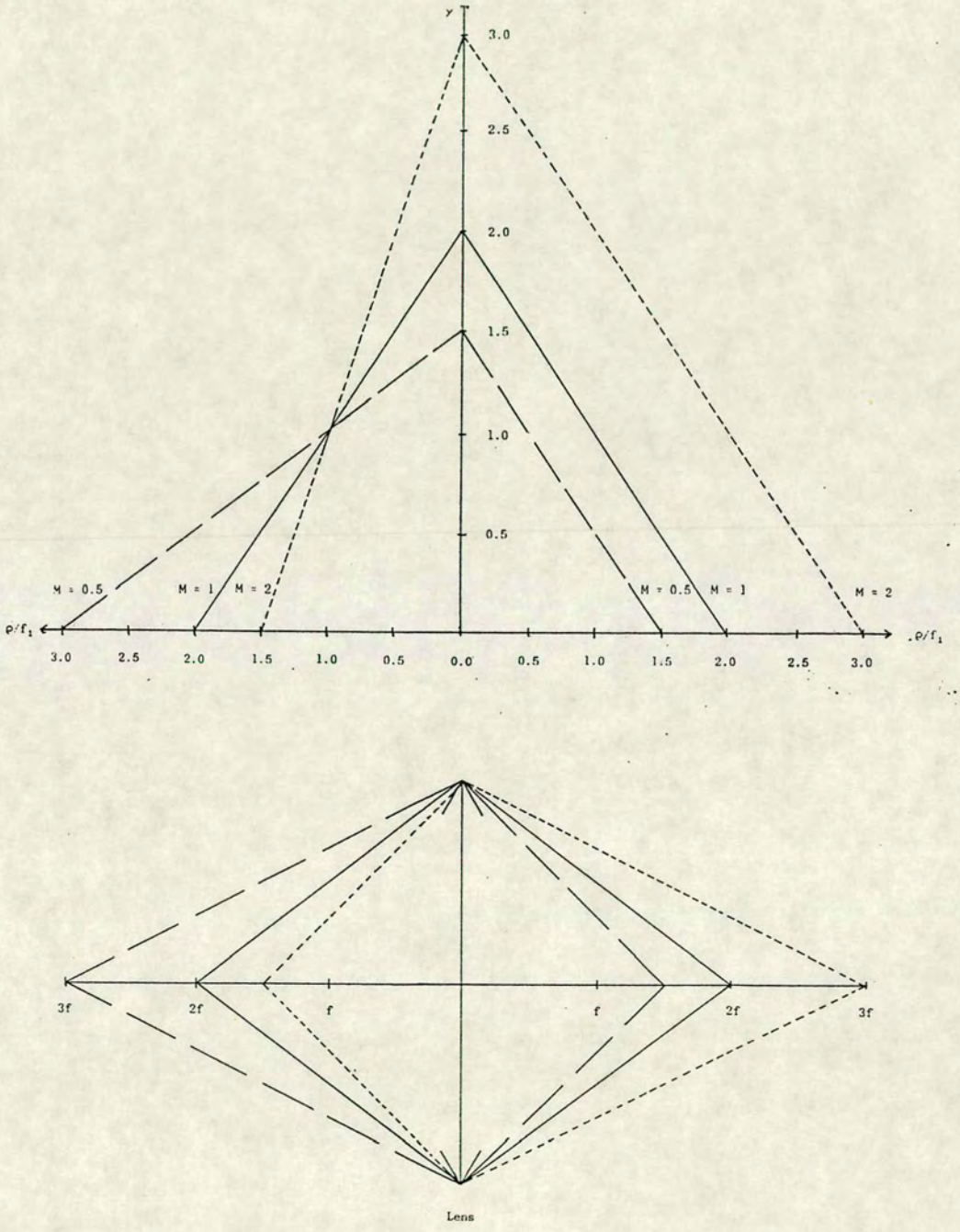

aperture) function of the lens in those cases was considered to be unity over the range of integration; that is the lens was regarded as being of infinite extent. Let us now consider a more realistic, if less simple case.

We saw in the earlier analyses that the complex amplitude in the F.T. plane of a system in which an object is illuminated either by a plane or spherical diverging wavefront may be expressed as in (2.7), a planewave being considered as a wavefront diverging from an infinitely distant point and therefore being a special case in the diverging wave analysis. Reinserting the previously removed pupil function, this becomes

$$U_3(x_3,y_3) = Ch(x_3,y_3;d_2)\int_{-\infty}^{\infty}\int_{-\infty}^{\infty}U_o(x_o,y_o)h(x_o,y_o;\rho)\left[\int_{-\infty}^{\infty}\int_{-\infty}^{\infty}p(x_2,y_2)\right.$$

$$\left.\times\, h(x_2,y_2;w)e^{\frac{-i2\pi}{\lambda}\left[\frac{(x_ox_3+y_oy_3)}{\rho}+\frac{(x_2x_3+y_2y_3)}{d_2}\right]}dx_2dy_2\right]dx_ody_o \qquad -(2.24)$$

This expression contains the F.T. of the product $p(x_2,y_2)h(x_2,y_2;w)$ which may be evaluated, yielding

$$U_3(x_3,y_3) = Ch(x_3,y_3;\frac{d_2^2}{d_2-w})\int_{-\infty}^{\infty}\int_{-\infty}^{\infty}U_o(x_o,y_o)h(x_o,y_o;\rho)h\left[x_o,y_o;\frac{-\rho^2}{w}\right]$$

$$\times\left[p\left[\frac{x_ow}{\rho}+\frac{x_3w}{d_2},\frac{y_ow}{\rho}+\frac{y_3w}{d_2}\right] * h\left[\frac{x_ow}{\rho}+\frac{x_3w}{d_2},\frac{y_ow}{\rho}+\frac{y_3w}{d_2};w\right]\right.$$

$$\left.\times\, e^{-i2\pi\left[x_1\left[\frac{x_3}{\lambda f_1}\right]+y_1\left[\frac{y_3}{\lambda f_1}\right]\right]}\right]dx_ody_o \qquad -(2.25)$$

Where * denotes a convolution.

For the case of plane-wave illumination this reduces to

$$U_3(x_3,y_3) = Ch\left[x_3,y_3;\frac{f_1^2}{f_1-\rho}\right]\int_{-\infty}^{\infty}\int_{-\infty}^{\infty} t_o(x_o,y_o)\left[p\left[x_o+\frac{x_o\rho}{f_1},y_1+\frac{y_o\rho}{f_1}\right]\right.$$

$$\left.* h\left[x_o+\frac{x_o\rho}{f_1},y_1+\frac{y_o\rho}{f_1};\rho\right]\right] e^{-i2\pi\left[x_o\left[\frac{x_3}{\lambda f_1}\right]+y_o\left[\frac{y_3}{\lambda f_1}\right]\right]} dx_o dy_o \qquad -(2.26)$$

where we have substituted for $U_o(x_o,y_o)$ from (2.1) and let $w=d_1$.

In the case of spherical diverging wave illumination, (2.15) becomes

$$U_3(x_3,y_3) = Ch(x_3,y_3;A)\int_{-\infty}^{\infty}\int_{-\infty}^{\infty} t_o(x_o,y_o)\left[p\left[\frac{x_o w}{\rho}+\frac{x_3 w}{d_2},\frac{y_o w}{\rho}+\frac{y_3 w}{d_2}\right]\right.$$

$$\left.* h\left[\frac{x_o w}{\rho}+\frac{x_3 w}{d_2},\frac{y_o w}{\rho}+\frac{y_3 w}{d_2};w\right]\right] e^{\frac{-i2\pi\gamma}{\lambda f_1}(x_o x_3+y_o y_3)} dx_o dy_o \qquad -(2.27)$$

The above equation is exact, but difficult to evaluate. Following the example of several other authors, and using the ray-tracing procedure used by Goodman [2.3], we may deal with the problem diagrammatically as in figure 2.3. Figure 2.3.a shows the fixed-scale system and 2.3.b the variable scale case (the diverging illumination as shown and the converging illumination by interchange of the F.T. and source planes in the diagram.) By projecting rays back from points in the F.T. plane to the object via the aperture, it can be seen that the contribution to the intensity of the F.T. as we

FIGURE 2.3

Diagrams illustrating vignetting using ray-tracing

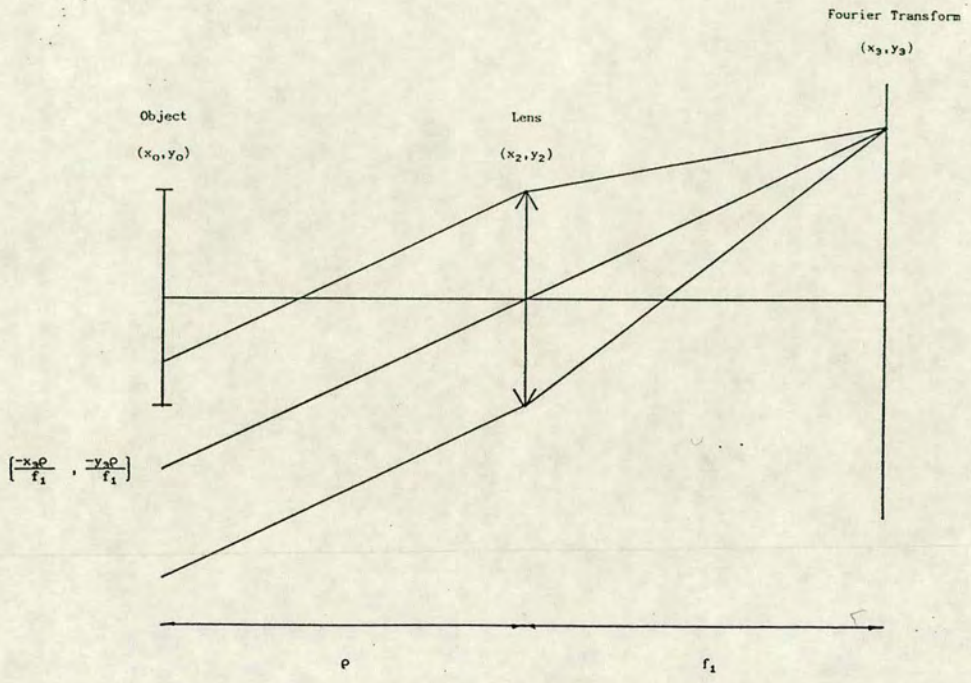

a) Vignetting in an f-f system

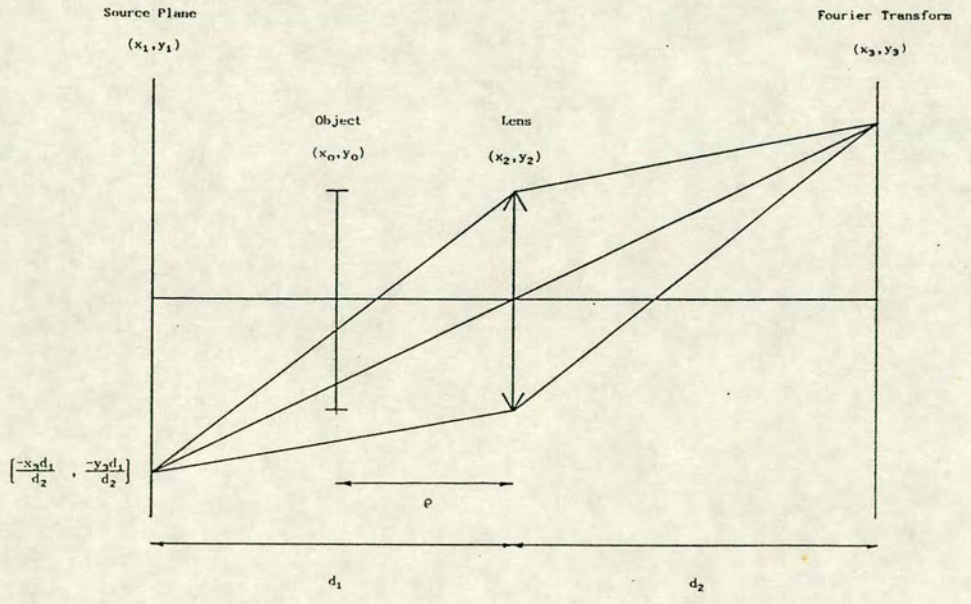

b) Vignetting in a variable-scale F.T. system

move from its centre outward is due to an increasingly smaller portion of the object. This is called vignetting. In an experimental system the F.T. would be seen to be finite in extent and decrease in intensity away from its centre. The edge of the F.T. occurs at a point where the object is no longer included in the aperture projection.

Vignetting can be minimised in an optical system by keeping the object as close to the lens as possible, or making the lens as large as possible. Obviously if the object is larger than the beam illuminating it, vignetting occurs throughout the F.T. This introduces an upper limit to the scale which can be achieved in practical systems [2.6].

The effect of vignetting will be returned to in the next chapter in relation to imaging systems.

2.4 Imaging systems

2.4.1 A two-lens system

The F.T. of the F.T. of a 2-dimensional function is simply the inverse of that function, as shown in appendix 2. Thus we may produce the image of an object by using a single converging lens acting on the F.T. of an object. This results in a 2-lens imaging system such as that shown schematically in figure 2.4. The F.T. of the object is produced in the plane (x_3,y_3) and the lens of focal

FIGURE 2.4

A two-lens imaging system

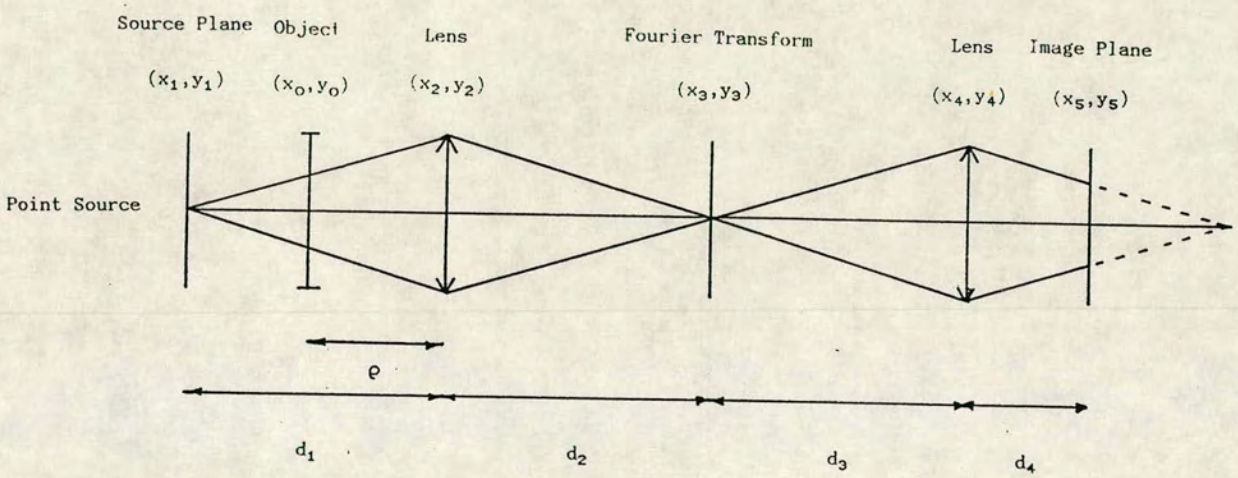

length f_2 is in the plane (x_4,y_4). Following the same procedure as in the previous examples, the complex amplitude in the plane (x_5,y_5) may be written

$$U_5(x_5,y_5) = Ch\left[x_5,y_5;\frac{d_4^2}{d_4-z}\right]\int_{-\infty}^{\infty}\int_{-\infty}^{\infty}U_3(x_3,y_3)h\left[x_3,y_3;\frac{d_4^2}{d_4-z}\right]$$

$$\times\, e^{\frac{i2\pi z}{\lambda d_3 d_4}(x_3x_5+y_3y_5)}\,dx_3dy_3 \qquad -(2.28)$$

where $$\frac{1}{z} = \frac{1}{d_3} + \frac{1}{d_4} - \frac{1}{f_2} \qquad -(2.29)$$

This expression is valid whether the object is illuminated by a plane-wave or a spherical diverging wave. Note that (2.28) and (2.29) are of the same form as (2.9) and (2.8) respectively.

Consider the plane-wave illumination situation. In this case $U_3(x_3,y_3)$ is given by (2.10). Substituting into (2.28) gives

$$U_5(x_5,y_5) = Ch\left[x_5,y_5;\frac{d_4^2}{d_4-z}\right]\int_{-\infty}^{\infty}\int_{-\infty}^{\infty}\int_{-\infty}^{\infty}\int_{-\infty}^{\infty}t_o(x_o,y_o)$$

$$\times\, e^{-i2\pi\left[x_o\left[\frac{x_3}{\lambda f_1}\right]+y_o\left[\frac{y_3}{\lambda f_1}\right]\right]}dx_o dy_o\Big]h(x_3,y_3;B)$$

$$\times\, e^{\frac{-i2\pi z}{\lambda d_3 d_4}(x_3x_5+y_3y_5)}\,dx_3dy_3 \qquad -(2.30)$$

where $$\frac{1}{B} = \frac{1}{d_3}\left[1 - \frac{z}{d_3}\right] + \frac{1}{f_1}\left[1 - \frac{\rho}{f_1}\right] \qquad -(2.31)$$

If we now write in the outer integral

$$x_3 \text{ as } (\lambda f_1)\frac{x_3}{\lambda f_1} \qquad \text{and} \qquad y_3 \text{ as } (\lambda f_1)\frac{y_3}{\lambda f_1} \qquad -(2.32)$$

(2.30) becomes

$$U_5(x_5,y_5) = Ch\left[x_5,y_5;\frac{d_4^2}{d_4-Z}\right]\int_{-\infty}^{\infty}\int_{-\infty}^{\infty}t_o(x_o,y_o) \times e^{-i2\pi\left[x_o\left[\frac{x_3}{\lambda f_1}\right]+y_o\left[\frac{y_3}{\lambda f_1}\right]\right]}dx_o dy_o\Big]h\left[\frac{x_o}{\lambda f_1},\frac{y_o}{\lambda f_1};\frac{B}{(\lambda f_1)^2}\right] \times e^{-i2\pi\left[\left[\frac{-f_1 z}{d_3 d_4}\right]x_5\left[\frac{x_3}{\lambda f_1}\right]+\left[\frac{-f_1 z}{d_3 d_4}\right]y_5\left[\frac{y_3}{\lambda f_1}\right]\right]}d\left[\frac{x_3}{\lambda f_1}\right]d\left[\frac{y_3}{\lambda f_1}\right] \quad -(2.33)$$

If $1/B=0$, the above is a F.T. relationship. For this to be the case, $z=d_3$ and $d_4=f_2$. The phase term outwith the integrals is unity if $z=f_2$. Making these substitutions and evaluating yields

$$U_5(x_5,y_5) = Ct_1\left[-\frac{f_1}{f_2}x_5,-\frac{f_1}{f_2}y_5\right] \quad -(2.34)$$

This is the inverted image of the object magnified by f_2/f_1. Note that for ease of analysis, we have assumed no vignetting in the F.T. plane.

A similar analysis may be carried out for the other two cases of object illumination by making the relevant substitution for $U_3(x_3,y_3)$. Thus for the case of the spherical diverging wave illumination, we obtain

$$U_5(x_5,y_5) = Ch\left[x_5,y_5;\frac{d_4^2}{d_4-z}\right]t_1\left[-\frac{\rho d_2 z}{d_3 d_4 w}x_5,-\frac{\rho d_2 z}{d_3 d_4 w}y_5\right] \quad -(2.35)$$

where $\frac{d_3 d_4 w}{\rho d_2 z}$ is the magnification of the inverted image.

For the final case of an object illuminated by a spherical converging wavefront we obtain

$$U_5(x_5,y_5) = Ch\left[x_5,y_5;\frac{d_4^2}{d_4-z}\right]t_1\left[\frac{-z(d_2-\rho)}{d_3 d_4}x_5,\frac{-z(d_2-\rho)}{d_3 d_4}y_5\right] \quad -(2.36)$$

where $\frac{d_3 d_4}{z(d_2-\rho)}$ is the magnification of the inverted image.

It bears repetition that in each case the centre of the F.T. is at a point which is conjugate to the point source illumination relative to the transforming lens. The centre of the image is conjugate to the object centre. In the two latter cases, moving the object changes the scale of the F.T. and changes the magnification of the image as well as changing its phase curvature and position.

2.4.2 A three-lens system

We shall now consider some characteristics of a particular optical system which has been used to study optical filters. Discussion of the results of its use in experiments will appear later in this thesis. In the system it was found necessary to include a means of keeping the position of the image constant whilst the scale of the F.T. is varied. This may be achieved by replacing the second transforming lens by a 2-lens varifocal system. This also enables the image to be magnified.

The focal length of the varifocal system is given by the equation

$$\frac{1}{f_T} = \frac{1}{f_3} + \frac{1}{f_4} - \frac{L}{f_3 f_4} \qquad -(2.37)$$

where f_3 and f_4 are the focal lengths of its components and L is their separation.

The system which was used experimentally had an object

illuminated by a spherical diverging wavefront. Thus the complex amplitude in the image plane of its reconstruction system may be obtained from (2.35) by simple substitution

$$U_5(x_5,y_5) = Ch\left[x_5,y_5;\frac{d_4^2}{d_4-z'}\right]t_1\left[-\frac{\rho d_2 z'}{d_3 d_4 w}\,x_5,-\frac{\rho d_2 z'}{d_3 d_4 w}\,y_5\right] \qquad -(2.38)$$

The position of the image plane is given by

$$\frac{1}{d_2}\left[1-\frac{w}{d_2}\right]+\frac{1}{d_3}\left[1-\frac{z'}{d_3}\right]=0 \qquad -(2.39)$$

where $$\frac{1}{z'}=\frac{1}{d_3}+\frac{1}{d_4}-\frac{1}{f_T} \qquad -(2.40)$$

The complex amplitudes in the image planes of the other optical systems described are similarly modified by the substitution of a zoom system. In each case the magnification or position of the image may be varied independently of the F.T. scale. Note however, that the phase curvature factor also varies, as it is dependent upon the focal length of the reconstruction system.

2.4.3 The effect upon the image of the aperture stop of the system

The aperture stop of variable scale F.T. processors is coplanar with the F.T. plane [2.5]. Thus, the intensity distribution which occurs in the image is determined by the convolution of that of the object with the F.T. of the aperture stop. In a perfect system, the aperture would be infinite in extent. However, we have seen that vignetting in the F.T. plane causes an effective stop for any system

with finite sized lenses, and we would expect this to affect the image. We may also modify the aperture stop in order to perform filtering operations as described in the next section.

2.5 Fourier transform filtering

We may use the fact that changing the field distribution in the F.T. plane of an imaging system modifies the image in a controlable way. Such filtering operations were described briefly in chapter 1. Gaskill [2.6] has approached the subject with some rigour, but has also shown that the general characteristics of different filters may be illustrated diagramatically with 1-dimensional examples. We shall discuss here the effect of four common filtering operations upon the image of an object whose unfiltered image intensity is represented in figure 2.5.a. Following Gaskills example, the one-dimensional object will be used to give a general indication of how a variation of F.T. scale affects the image for each of the filtering operations. The diagrams for figure 2.5 were computed using a fast F.T. program. They are normalised in width (i.e. image size) but not in height (image intensity); however qualitative characteristics of filtered images and relative intensities may be seen.

FIGURE 2.5

One-dimensional graphical representation of filtered images

a)

b)

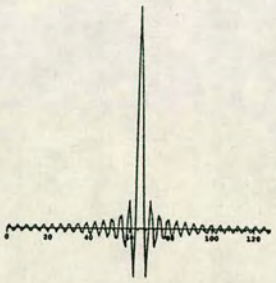

c)

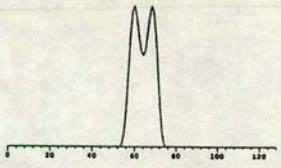

d)

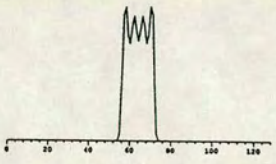

e)

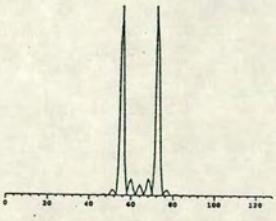

f)

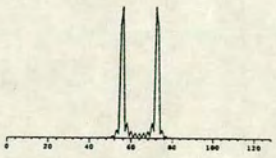

g)

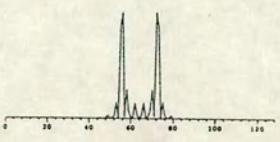

h)

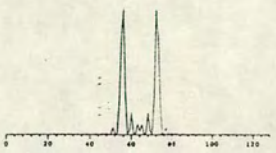

2.5.1 Low-pass filtering

The low-pass filtered object is illustrated in figures 2.5.c and d. In d, the scale of the F.T of the object has been halved, that is the cutoff frequency of the filter doubled. Figure 2.5.b shows a sinc function, the F.T. of a low-pass filter. It can be seen in both cases that the edges of the image are less well defined than the object, and intensity variations appear in the image in positions corresponding to those where the object was of uniform intensity. Such an intensity variation is commonly known as ringing. Notice that the 'ringing frequency' increases with the cutoff frequency. Low-pass filtering is experimentally realised by placing an aperture in the F.T. plane of an optical imaging system, allowing to pass all spatial frequencies below the cutoff and none above. Filtering of this type due to lens apertures was observed by Abbe and Porter ([1.1],[1.2]).

2.5.2 High-pass filtering

The high-pass filtered object is shown in figures 2.5.g and h. A high-pass filter allows only spatial frequencies above a well-defined cutoff frequency to form the image, and occurs when a stop is placed in the centre of the F.T. plane of an optical system. By Babinets principle, the F.T. of a high-pass filter is an inverted sinc function. We see from the illustrations that the edges of the image are still well-defined after filtering, but that ringing is also observed.

2.5.3 Band-pass filtering

Band-pass filters may be thought of as a combination of the previous two, allowing to pass only a band of spatial frequencies to form the image. Two cases are illustrated in figures 2.5.e and f. In this case, the low-pass filter is the same for each (with a cutoff frequency twice that of 2.5.d) and the high-pass filter as in e and f respectively. Under certain conditions, band-pass filters are used to perform edge enhancement.

2.5.4. Directional filters

Directional filters are by necessity 2-dimensional and cannot be illustrated by 1-dimensional diagrams. The effect of such filters is to allow only spatial frequencies arising from certain directions in the object to form the image. Thus all frequencies are allowed in some directions and none in another.

Figure 2.6 shows typical designs of 2-dimensional filters. We shall take a more quantitative approach to spatial filtering in following chapters when numerical information from this section will be used to predict the effect of 2-dimensional filters upon images.

FIGURE 2.6

Two-dimensional representation of F.T. filters

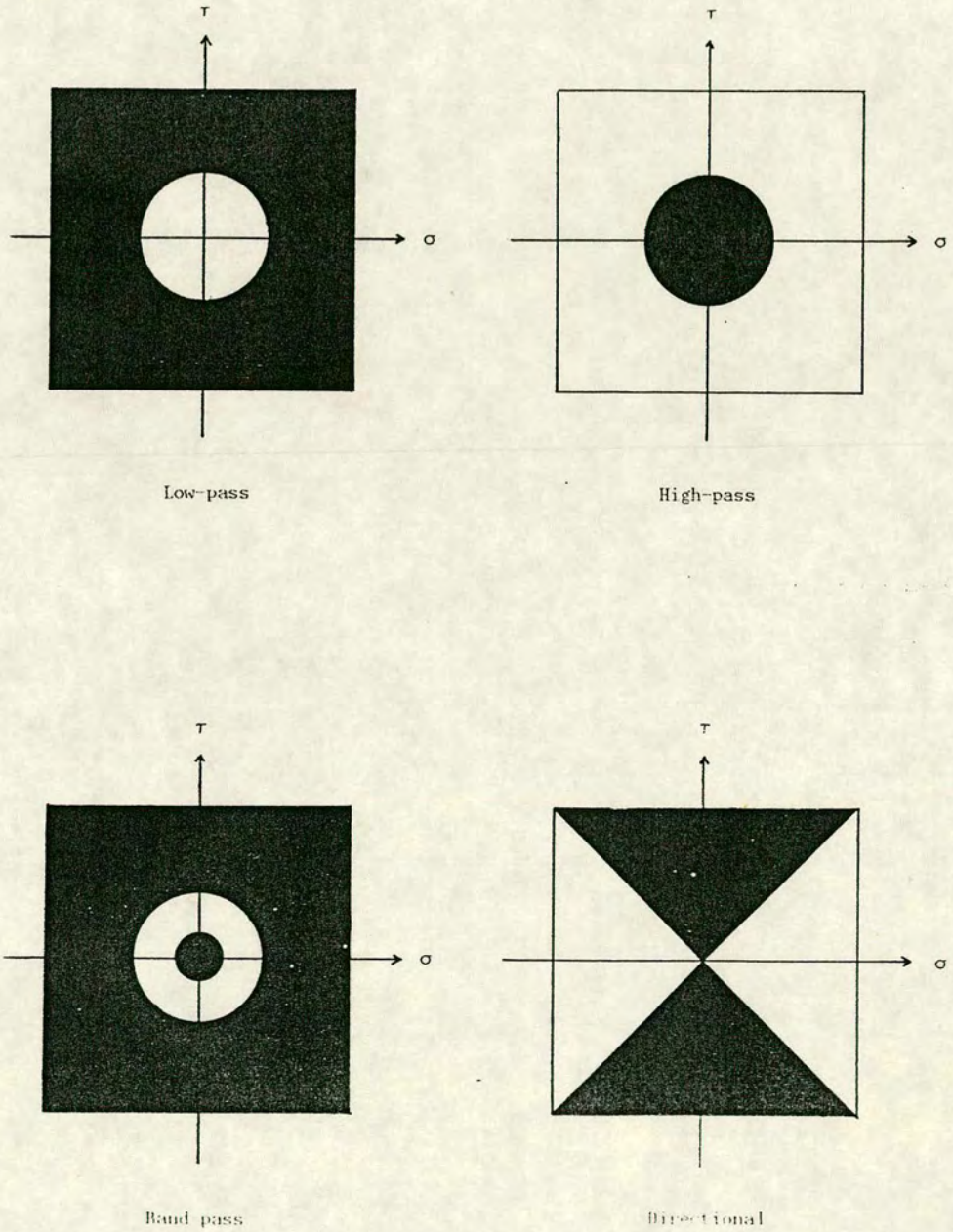

Low-pass

High-pass

Band pass

Directional

2.6. Fourier transform plane pixelation

We have now seen that modification of the light field in the F.T. plane of an optical imaging system results in modification of the image, and we have considered the use of apertures and stops as filters. The analysis and uses of images modified by these methods have been discussed in great detail in the published literature (for example [1.3]). On the other hand, pixelated filters which are now in wide use for some of the practical reasons outlined in chapter 1, have been discussed in depth in relatively few publications. Pixelation of the F.T. plane of an optical system, however, introduces some constraints on its design which will need to be considered in relation to the experimental optical system discussed in the next chapter. We shall extend the analysis of section 2.5 to include pixelated F.T. plane filters to derive previously unpublished results.

2.6.1. Filters of infinite extent

For a 3-lens imaging system of the type considered in 2.4.2 above, the complex amplitude in the image plane is given by

$$U_5(x_5,y_5) = Ch\left[x_5,y_5;\frac{d_4^2}{d_4-z'}\right]\int_{-\infty}^{\infty}\int_{-\infty}^{\infty}U_3'(x_3,y_3)h\left[x_3,y_3;\frac{d_3}{z-d_3}\right]$$

$$\times\, e^{\frac{-i2\pi z'}{d_3 d_4}(x_3x_5+y_3y_5)}\,dx_3dy_3 \qquad -(2.41)$$

where $U'(x_3,y_3)$ is the complex amplitude of the light field in the F.T. plane.

If the F.T. plane contains a pixelated filter of infinite extent, the complex amplitude of the light field in that plane may be expressed as

$$U_3'(x_3,y_3)=\sum_{m=-\infty}^{\infty}\sum_{n=-\infty}^{\infty}\delta(x_3-ml,y_3-nl)U_3(x_3,y_3) \qquad -(2.42)$$

where the pixels are represented by dirac δ-functions equally spaced with separation l in the x and y directions. $U_3(x_3,y_3)$ is the complex amplitude of the light field incident upon the filter.

In the optical system under discussion, the object is illuminated by a spherical diverging beam of light. Hence, $U_3(x_3,y_3)$ is given by (2.15). Substituting (2.15) and (2.42) into (2.41) yields the (at first sight) formidable expression

$$U_5(x_5,y_5)=Ch\left[x_5,y_5;\frac{d_4^2}{d_4-z'}\right]\int_{-\infty}^{\infty}\int_{-\infty}^{\infty}\int_{-\infty}^{\infty}\int_{-\infty}^{\infty}t_o(x_o,y_o)h\left[x_o,y_o;(d_1-\rho)+\frac{\rho}{\rho-w}\right]$$

$$\times\, e^{\frac{-i2\pi w}{\lambda d_1 d_2}(x_o x_3+y_o y_3)}\,dx_o dy_o\Big]\sum_{m,n=-\infty}^{\infty}\sum^{\infty}\delta(x_3-ml,y_3-nl)$$

$$\times\, h(x_3,y_3;B)e^{\frac{-i2\pi z}{\lambda\rho d_2}(x_3x_5+y_3y_5)}\,dx_3dy_3 \qquad -(2.43)$$

However, continuing in a similar manner to that seen in (2.30) to (2.34) we find that

$$U_5(x_5,y_5)=C\sum_{m,n=-\infty}^{\infty}\sum^{\infty}\delta\left[x5 - \frac{md_3d_4w^2\lambda z'}{\rho^2 d_2^2 l},\ y_5 - \frac{md_3d_4w^2\lambda z'}{\rho^2 d_2^2 l}\right]$$

$$* t_o\left[\frac{-\rho d_2 z'}{d_3 d_4 w} x_5\ ,\ \frac{-\rho d_2 z'}{d_3 d_4 w} y_5\right] \qquad -(2.44)$$

which shows that myriad images of the magnified, inverted object now appear in the image plane. The centre to centre separation of these replicas is $(d_3d_4w\lambda z')/(\rho^2 d_2^2 l)$. Thus if a single replica is larger than this, the replicas will overlap, obscuring the detail. Fortunately, in this optical system the F.T. size may be varied, so varying the replica size. The use of this to the optical designer's advantage will be shown in the next chapter.

2.6 2. Other pixelated filters

The pixelated filter just discussed was infinite in extent and had infinitesimally small pixels. This is not a situation which is physically realisable. A general pixelated filter may be described by the transmission function

$$\Phi(x,y)=G(x,y)\left[H(x,y)*\sum_{m,n=-\infty}^{\infty}\sum \delta(x - ml, y - nl)\right] \qquad -(2.45)$$

where the function H(x,y) represents the shape and size of the pixel and G(x,y) represents the extent of the filter. A one-dimensional form of the function is illustrated graphically in figure 2.7. By following the Fourier transformation rules given in appendix 2, the

FIGURE 2.7

Graphical illustration of a one-dimensional pixel function

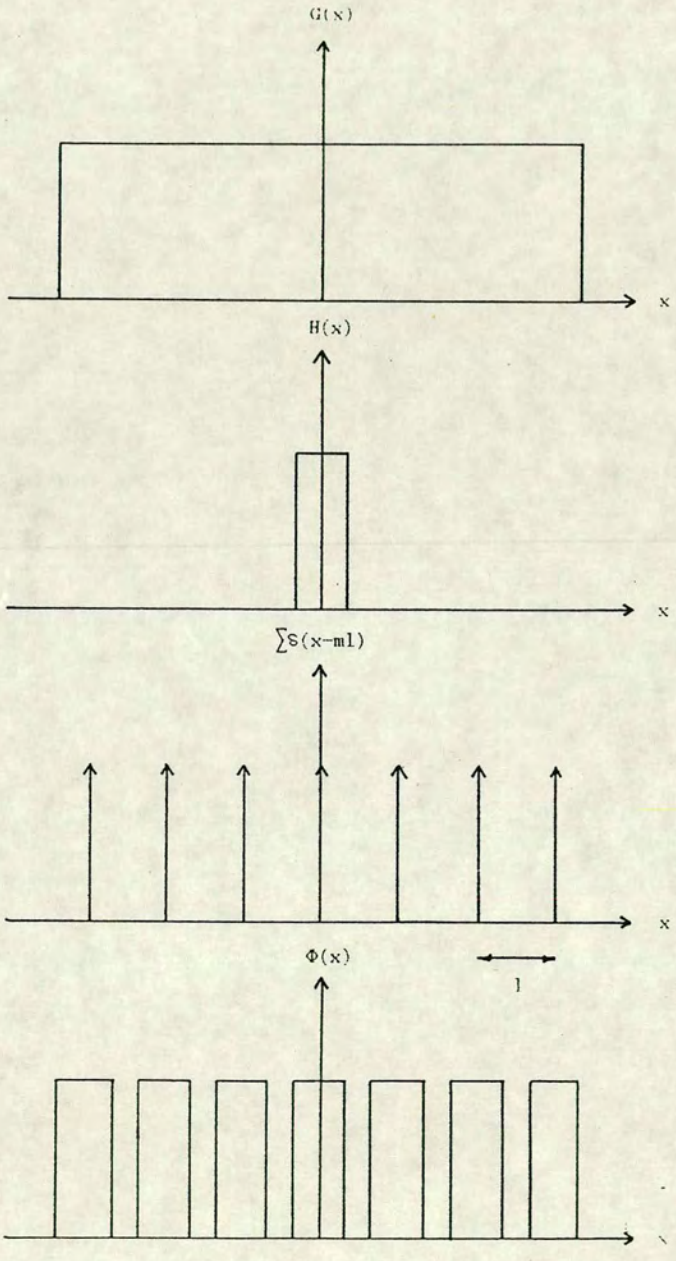

complex amplitude in the image plane is found to be given by

$$U_S(x_S,y_S)=F.T.[H(x_S,y_S)]\times\Big[F.T.[G(x_S,y_S)]$$

$$*\sum_{m,n=-\infty}^{\infty}\sum^{\infty}\delta\Big\{x_S-\frac{md_3d_4w^2\lambda z'}{\rho^2d_2^2l}y_S-\frac{\lambda z'md_3d_4w^2}{\rho^2d_2^2l}\Big\}$$

$$*t_1\Big\{\frac{-\rho d_2Z'}{d_3d_4w}x_S,\frac{-\rho d_2Z'}{d_3d4w}y_S\Big\}\Big] \qquad -(2.46)$$

Thus, each replica is convolved with the F.T. of the extent of the filter in the F.T. plane, and each is thus identical and filtered as we would expect in the non-pixelated case. However, the image plane amplitude distribution is multiplied by the F.T. of the pixel shape function. Thus a variation of the replica intensity has been introduced. This subject will be returned to in experimental detail in chapter 4.

2.7 Discussion

In this chapter we have drawn attention to the variable-scale phenomenon which may be produced in a single-lens F.T. system. This effect enables us to have control over the position of light diffracted due to specific spatial frequencies in the object in a way which the more familiar fixed-scale system does not. This may be used to advantage in filtering systems.

The major characteristics of images filtered in different ways have been indicated. We see that, using the variable-scale system, the cutoff frequencies of high-pass, low-pass and band-pass filters may be selected simply by moving the object relative to the

transforming lens. To vary the cutoff frequency in a fixed-scale system, we would have to change the filter.

The price which has to be paid for this flexibility is phase curvature in the F.T. and image planes, and an image plane which changes position with varying F.T. scale, as object and image planes are conjugate. Vignetting may also be a problem with a widely separated object and lens. We have shown that the image plane may be kept in a constant position by using a zoom reconstruction system. This has the added benefit of the ability to magnify the image. Again, however, attention should be paid to exit pupil limitation by lens apertures.

We have given a familiar analysis of F.T. systems and extended it to describe, in a notation consistent with that work, characteristics of a particular variable-scale F.T. imaging system. It has been shown that this system is well suited for use with pixelated F.T. plane filters, allowing a range of object sizes to be used without overlapping image replicas.

Use will be made in the next chapter of the results derived in this one for the design of an optical imaging system specifically for use with pixelated filters. Experimental illustrations of some of the results derived here will be presented.

Chapter 3

Experimental use of Fourier transform imaging systems

Due to its planar F.T., and the corresponding ease of analysis, the fixed-scale imaging system has become the most commonly used in the laboratory. In this chapter, we shall illustrate with experimental examples some of the results derived in the previous chapter in relation to this type of system. We shall then go on to discuss a design for a variable-scale-F.T. system for use with a specific set of F.T. filters, and again illustrate some of the results of the previous chapter relating to this system. Finally we shall discuss the advantages and limitations of this type of system when used with pixelated F.T. filters.

3.1 Filtering using a fixed scale system

Figure 3.1 is a photograph of a fixed-scale F.T. system such as that described in section 2.1. It is a 4-f system with an additional lens which collimates light from the laser/spatial filter assembly, and an auxiliary lens which may be used to magnify the image. The scale of the F.T. produced by this system is calculated from (2.20) to be 0.63 lp/mm/mm. This is large enough that the desired accuracy of filtering for this general-purpose system may be attained using relatively crude apertures and photographically

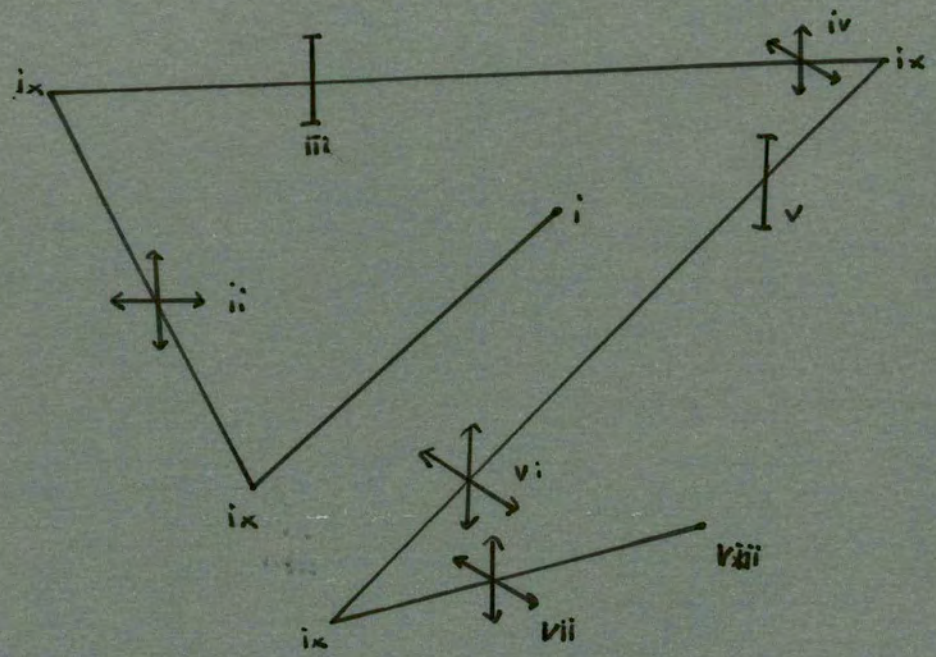
ix
iii
iv
ix
v
i
ii
ix
vi
viii
ix
vii

FIGURE 3.1

A photograph and schematic diagram of a fixed-scale Fourier transform system, with table showing system specifications

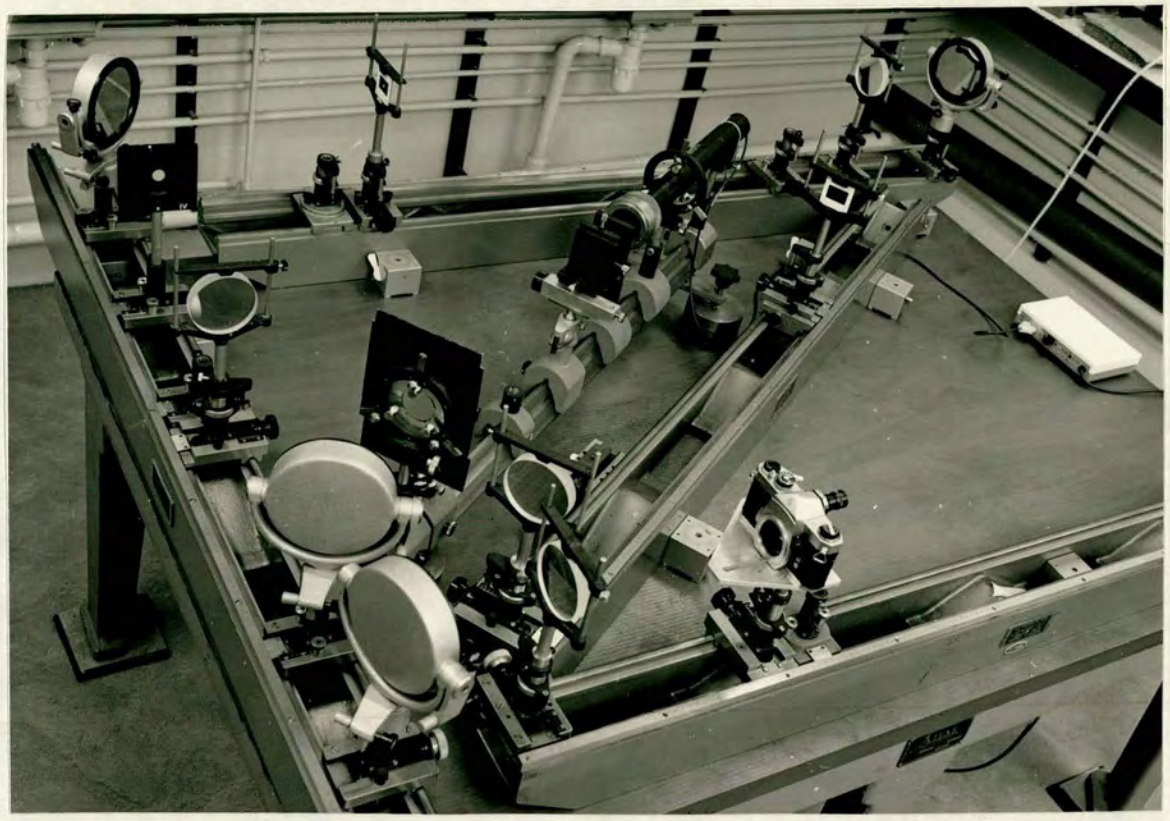

i) 10mW He-Ne laser and spatial filter assembly
ii) Collimating lens, f = 1000mm, diameter 100mm
iii) Object
iv) Transforming lens, f = 1000mm, diameter 100mm
v) Fourier transform plane
vi) Transform lens, f = 1000mm, diameter 100mm
vii) Auxiliary lens, f = 1000mm, diameter 100mm
viii) Image plane camera
ix) Mirrors

produced filters, which have limited precision of dimension. However, the long focal length lenses make it necessary to fold the optical path of the system, and a schematic diagram is also given in the figure to aid interpretation of the photograph. A table identifies and gives the specifications of the pieces of the apparatus which are numbered in the photograph and diagram.

Figure 3.2.a is a photograph of the image plane of the optical system with an equilateral triangular aperture with 1mm long sides as object. Figure 3.2.b is a photograph of the F.T. plane. There is no obvious degradation of the image due to vignetting, indeed defects in the sides of the aperture are clearly visible. This is as we may intuitively expect as the objects largest dimension is some 1/100th the diameter of the lens. Indeed, using results seen in the last chapter (figure 2.36), the frequency cutoff of the F.T. due to vignetting is 32.1 lp/mm which occurs at a distance of 50.7 mm from its centre.

The triangle will be used as object throughout the following experimental work. There are two main reasons for its use, i) it has been used previously in studies of edge-enhancement and ii) when considering image replication produced by pixelated F.T. filters it is easy to see the intersection of replica triangles, as when the apex of one crosses the side of another.

The image plane resulting from a pixelated filter placed in the F.T. plane of the optical system is shown in figure 3.3.a. A photograph of the F.T. plane is shown in figure 3.3.b and a table of filter specifications and expected effects is given in figure 3.3.c. The filter is a photographically produced 16x16 square array of

FIGURE 3.2

Photographs of an image and Fourier transform produced by the fixed-scale system

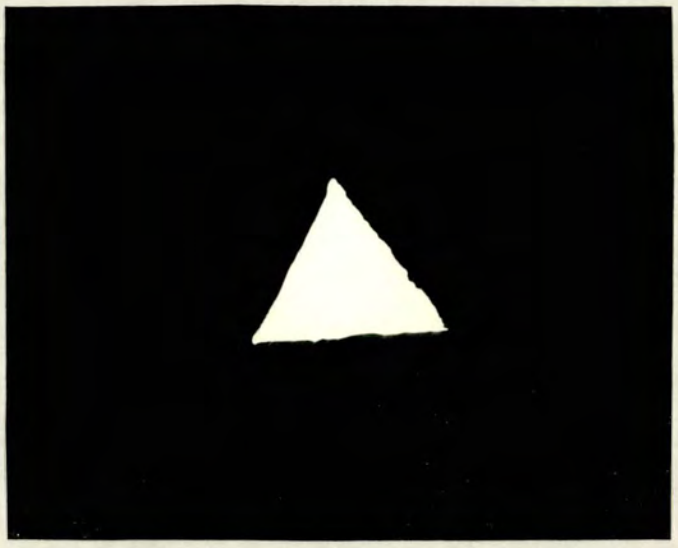

a) The image of an equilateral triangular aperture with 1mm sides

b) The Fourier transform of the triangle

FIGURE 3.3

The effect of Fourier transform-plane pixelation

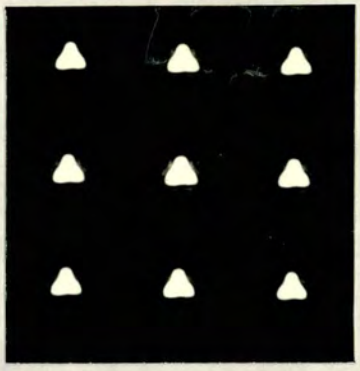

a) A photograph of the image plane showing replicated images

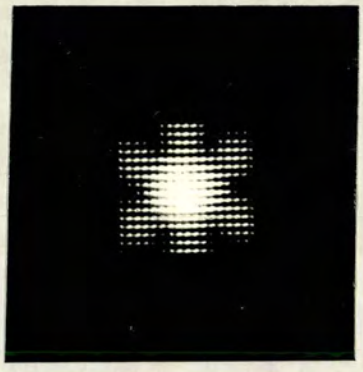

b) A pixelated filter in the Fourier transform plane

Filter size: 3.2mm x 3.2mm, 2.7 lp/mm horizontal, 2.9 lp/mm diagonal
Pixel size: 100 m x 100 m
Pixel number: 16 x 16
Pixel spacing: 200 m
Expected image spacing: 7.9mm
Horizontal position of envelope 1st minimum: 14mm

c) A table of specifications of the filter and expected effect upon the image plane

square pixels designed to have sides of 100 μm and a mark to space ratio of 1:1. Thus the actual size of the filter is 3.2 mm x 3.2 mm giving a high-frequency cutoff across its narrowest part of 2.7 lp/mm, and across its widest of 2.9 lp/mm. We would expect from calculations using (2.44) that the separation of the image replicas in the image plane would be 7.9 mm or almost 8 object lengths. This is obviously not the case. The reason for this is two-fold. Firstly, upon microscopic examination emulsion shrinkage was observed to have caused the pixel centres to be separated by 220μm, so causing the replicas to be closer than anticipated. Secondly, the image is quite severely low-pass filtered and spread out so that the images appear larger than in the unfiltered case, as we saw in the one-dimensional representation of low-pass filtered images in section 2.6. From the orientation of the filter, with its side parallel to one leg of the F.T., we would expect that one side of the triangle should be more severely low-pass filtered than the other two. The effect of this 0.2 lp/mm difference however is not visible in the photograph. The intensity envelope in the image plane due to the shape of the filter gives rise to the differing intensities of the image replicas. The actual size of the pixels was measured as 110 μm, and the sides were observed to be rounded. If, for ease of calculation we nevertheless assume them to be square, and hence the intensity envelope in the image plane to be a squared sinc function we would expect the first minimum to occur at approximately 14 mm from the centre (using (2.44)), and hence the central and two diffracted orders to lie within this. This is consistent with what we see in the photograph, with the second and

third orders horizontally and vertically of approximately the same intensity, and the second order in the diagonal sense of a much lower one. As pictures of filtered F.T.s convey little information, image photographs will henceforth be accompanied only by a table of information, specifying the filter and its expected and actual properties.

Observe that the replicas in figure 3.3.a are widely spaced. This is an example of inefficient filtering. In effect, the filter is sampling the F.T., and the Whittaker-Shannon sampling theorem states that for a bandlimited object, the critical sampling interval (that is the largest separation of samples which can be used without losing information about the object) is the inverse of the extent of the its F.T. In our case the critical interval is the inverse of the size of the object, as the F.T. is being sampled, and thus the critical spacing is 1.5 mm. We are oversampling in the example we have seen by a factor of 6. The critical sampling interval occurs when the object is fully recoverable i.e. the replicas do not overlap and the samples are as widely separated as possible. We shall term this spacing the Nyquist spacing for the object. It follows from the above argument that the filter already seen has pixels which are at the Nyquist spacing for a larger object than the one used. Figure 3.4 is a photograph of the image plane when a larger object triangle is used. The edges of the replicas are sharper in this case, but the low-pass filtering is still manifested in the structure which can be seen in the centre of some of the replicas. Note that as the filter is the same in both the cases of figure 3.3 and figure 3.4, the intensity envelope of the image plane

FIGURE 3.4

A photograph of the image plane when the 1mm tringle is replaced by a 3mm triangle

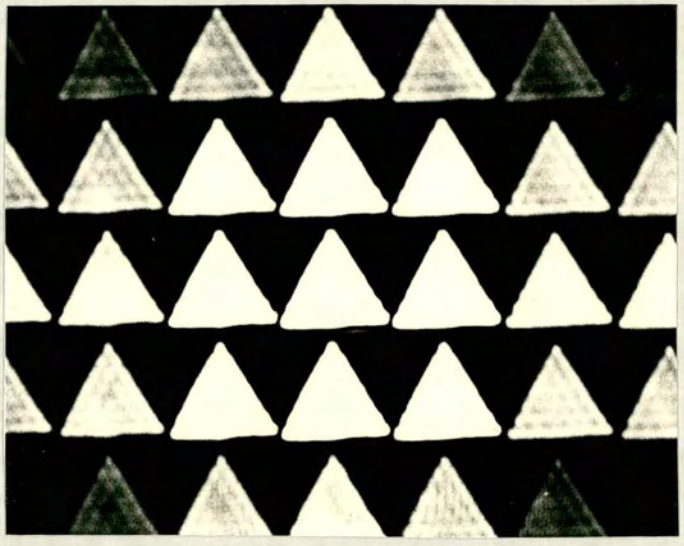

is unchanged. As we expect from (2.45), the intensity of each replica is determined by the position of its centre in the image plane, and thus we see no intensity modulation of a single replica due to the intensity envelope.

When using pixelated F.T. filters we would ideally wish to have pixels at the Nyquist spacing for the object. This may be possible in situations where the object is always the same or where a large supply of filters is available. However, in a multi-purpose system or automated systems using s.l.m.s such as those mentioned in chapter 1, the pixel spacing is fixed. Using a variable magnification F.T. system, we may vary the scale of the F.T., an equivalent situation to varying the pixel spacing. Thus we may sample at the Nyquist spacing for a range of objects.

3.2 Design and use of a variable-scale Fourier transform imaging system.

3.2.1 The system design.

Figure 3.5 is a photograph of the variable scale F.T. imaging system (which will henceforth be referred to as the variable scale system) designed for use with reflective liquid crystal over nMOS silicon s.l.m.s. The photograph is accompanied by a schematic diagram giving dimensional information and a table giving component specifications. A 10 mW He-Ne laser and spatial filter [i] were

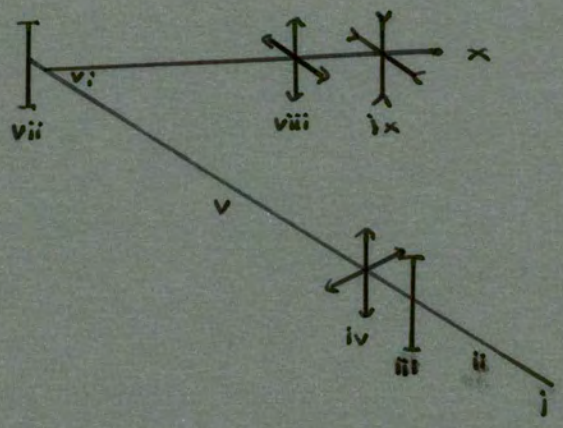
vii
vi
viii
ix
x
v
iv
iii
ii
i

FIGURE 3.5

A photograph of a variable-scale-Fourier transform optical system with schematic diagram and table of specifications

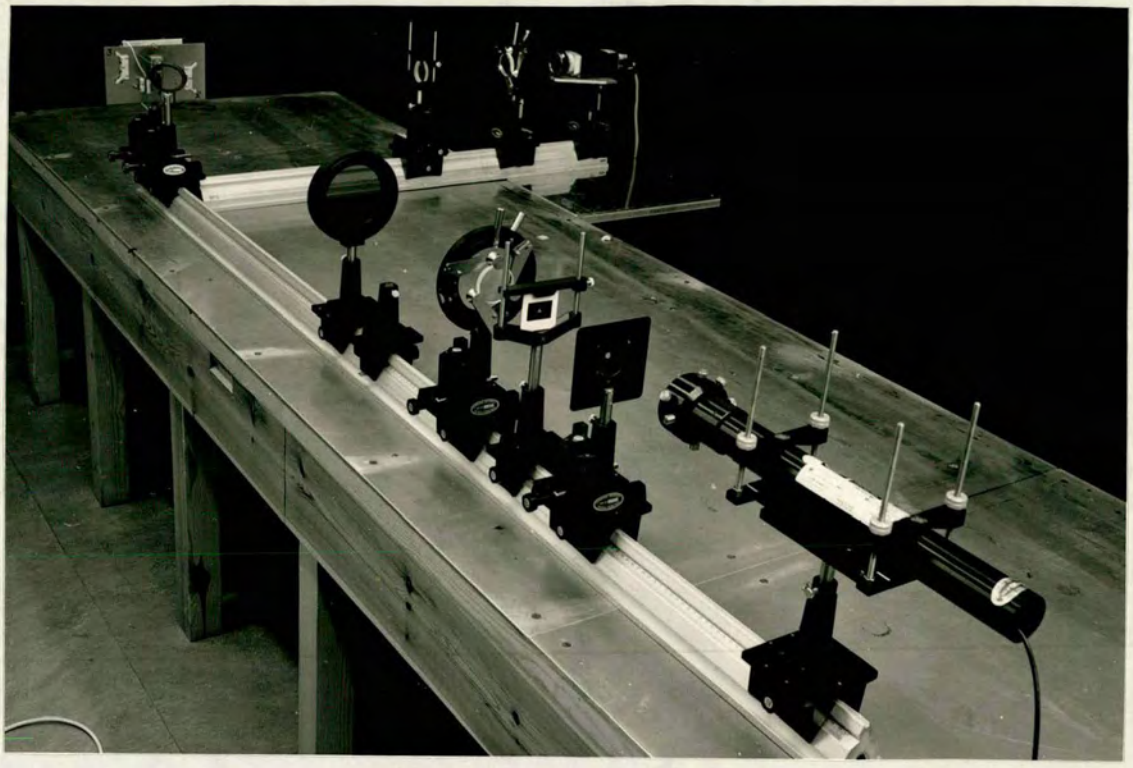

i) 10 mW He-Ne laser and spatial filter assembly
ii) Iris
iii) Object
iv) Biconvex achromatic doublet, f = 300mm, diameter 50mm
v) Polariser
vi) Pellicle beamsplitter
vii) Fourier transform plane
viii) Biconvex achromatic doublet, f = 300mm, diameter 50mm
ix) Concave meniscus achromatic doublet, f = -150mm, diameter 50mm
x) Image plane camera

d_1 = 600mm

d_2 = 600mm

$d_3 + d_4$ = 500mm

used for produce a diverging beam of coherent radiation (of wavelength 633 nm). An iris [ii] was used to prevent stray laser light entering the system. The object [iii] in the photograph is placed in the diverging beam. We have seen however, that a variable scale effect can be achieved in the F.T. when the object is placed either in the diverging or converging beam. It was seen to be necessary to utilise both configurations. The converging beam illumination has advantages in terms of lower aberrations, which will be discussed in the next section. However, on occasion optical components such as the polariser (the s.l.m. is operated in polarised light) [v] and drive electronics for the s.l.m.s had to be accommodated between the lens and the F.T. plane. The F.T. system was therefore designed to be symmetrical (i.e. magnification M=1) so that the object position for equivalent F.T. scales on each side of the lens could be easily located without recourse to calculation. A pellicle beamsplitter [vi] was used to redirect light reflected by the filter, which was held in a mount [vii] in the F.T. plane. A varifocal reconstruction system was used to form the image of the object in the plane of the camera [x].

It was noted in chapter 2 that the object and image planes of the system are conjugate. Thus as the object position is varied to change the F.T. scale, the position of the image plane also varies. To avoid having to move the camera (photographic, video, or in the case of the photograph, CCD array) the varifocal system was used. This enabled the image plane to be kept in a constant position whilst the object was moved, and also enabled the image to be magnified.

3.2.2 Some considerations of aberrations and vignetting in the F.T. plane.

We have seen that unlike the fixed scale F.T. system, a variable scale system may introduce phase variations across the F.T. and image planes. Let us consider the F.T. plane. Figure 3.6 is a graph of the variation of phase curvature with object to lens distance. The filter to be used with the system was 3.2 mm x 3.2 mm in size. Thus we would wish to use a range of object to lens distances for which vignetting would not add to the low-pass filtering effect of the filter. We see from figure 3.6 that we may move the object between the lens and 0.5 m from it without incurring this problem. We also see that the maximum phase curvature which we may encounter is 1.5 m^{-1} in the latter case.

Up to now we have considered the lens to be infinitely thin. Indeed we have said the the F.T. is infinite in extent when ρ is zero. This is obviously not the case. However, we can say that the F.T. extends more than 60mm from the centre and we are only concerned with filters which are 4.5 mm in largest dimension so this need not concern us.

Traversal of the finite lens may deform the wavefront i.e introduce aberrations. We are of course only concerned here with monochromatic aberrations. Of the five primary aberrations,

FIGURE 3.6

A graph showing the variation of phase curvature with separation of object and lens

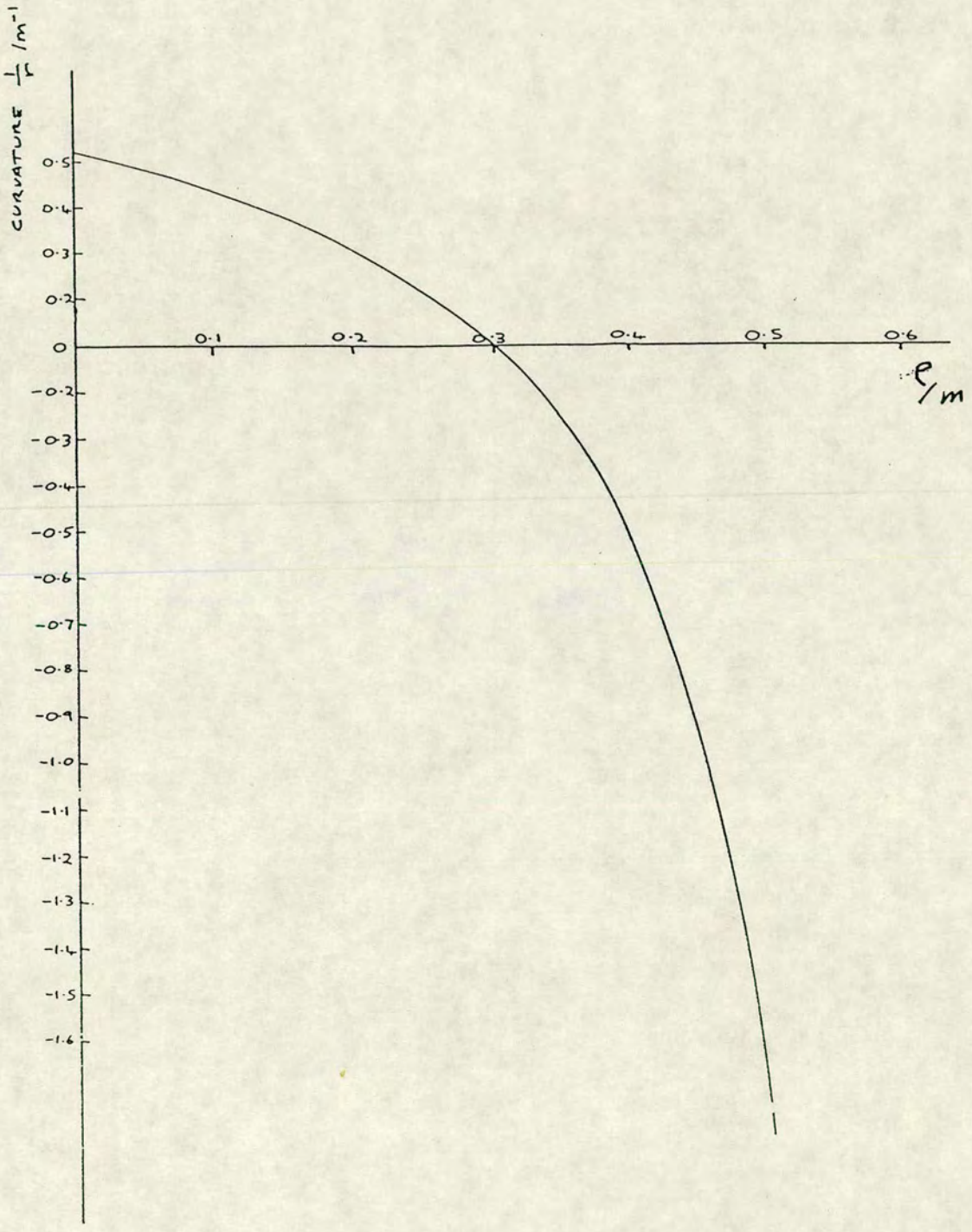

spherical aberration, coma and astigmatism tend to degrade the image by blurring, whilst field curvature and distortion may distort the image even though it remains unblurred. Achromatic doublets were chosen for all the lenses considered so far as these have negligible spherical aberration and coma.

Joyeux and Lowenthal [3.1] suggest that the configuration which gives the lowest aberrations in the F.T. plane is the converging beam system, which is a possible configuration for the system designed.

3.2.3 Use of the system

A photograph of the image plane of the system with an equilateral trianglular aperture with 3mm sides as object is shown in figure 3.7. The object was touching the lens and hence we would expect no observable low-pass filtering due to vignetting. Notice however that the corners are not sharp. This is due to the photo-etching production process, and a better guide to the large bandwidth of the image is the absence of 'ringing' structure around the sharp sides.

3.2.3.1 Photographic filters

Figure 3.8 is a photograph of the image plane when the 16x16 pixel filter which has already been described is placed in the F.T. plane. Notice in this case the intensity envelope and the intensity structure within the replicas due to the pixel size and filter size

FIGURE 3.7

A photograph of the image of a 3mm sided equilateral trianglular aperture in the image plane of the variable-scale system

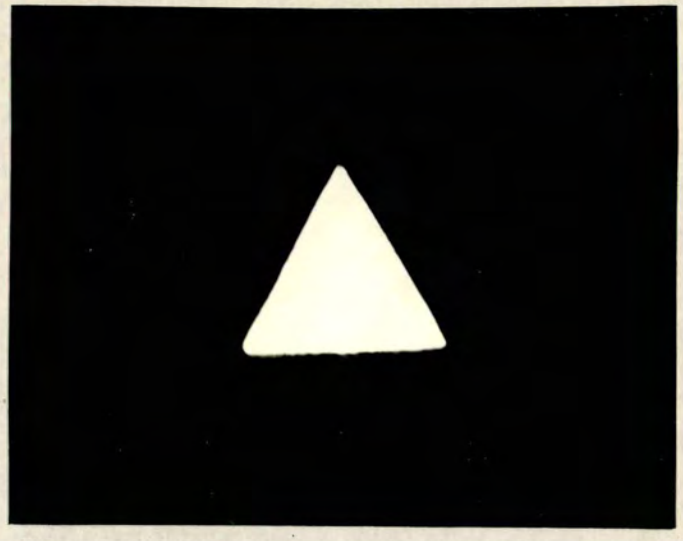

FIGURE 3.8

A photograph showing replicated images of the object in the image plane when a pixelated filter is placed in the Fourier transform plane

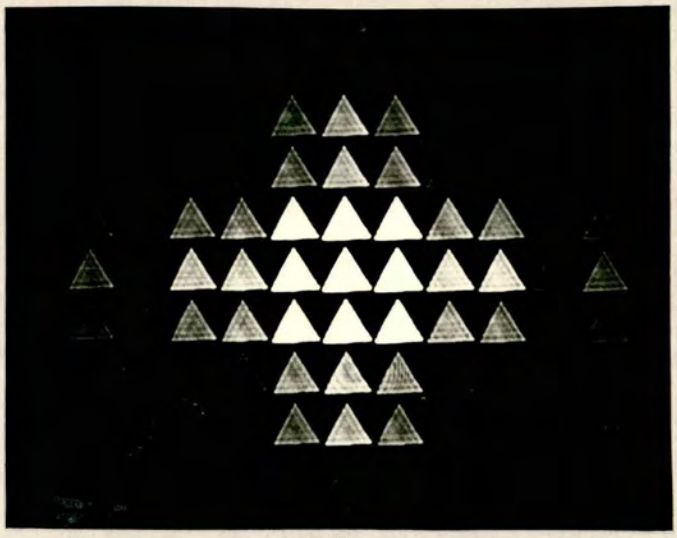

respectively. Figure 3.9 illustrates the case of undersampling, where image replicas overlap. This photograph shows well the phase problem associated with photographically produced filters. In some instances there is constructive interference between overlapping replicas, causing the small bright triangles, and in some cases destructive interfrence causes dark triangles. Some examples of these are indicated in the photograph. In subsequent experiments in which it was necessary to use binary transparencies, a lithographic rather than photographic process was used.

3.2.3.2 S.L.M.s

Details of the design, architecture and electronic addressing system of the reflective, adaptive F.T. filters for which the optical system was primarily designed may be found in the paper by Underwood, Willson, Sillitto and Vass which is bound into this thesis as appendix 3(ii). Let us here, however, pick out some of the points which are relevant to the optical properties of the device. The pixels are arranged in a square array of 16x16 with centre to centre separation of 200μm. Each pixel is 110μm x 110μm in size.

Consider first the back-plane of the device. Each mirror is formed by evaporation of an aluminium-copper-silicon (95%,4%,1%) alloy on top of a thin silicon dioxide layer, which insulates the mirror from the substrate. The mirrors were tested to be flat by white light interferometry to within $\pm$25nm. VLSI circuitry is

FIGURE 3.9

A photograph illustrating the effect on the image plane of undersampling the Fourier transform

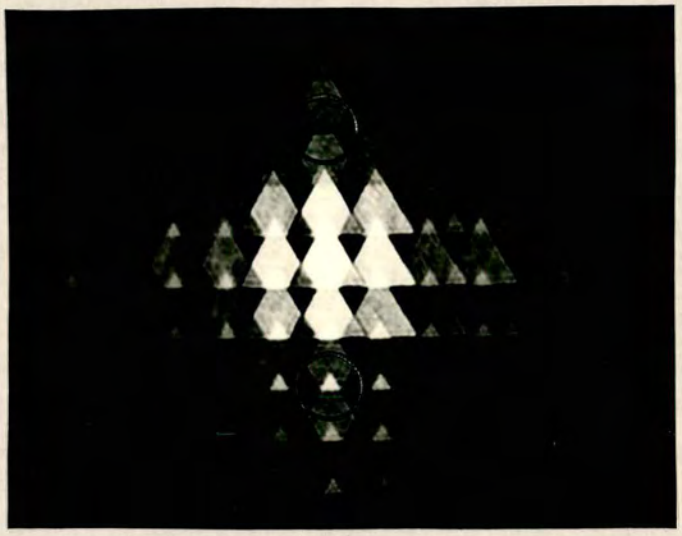

contained within the spaces between the pixel mirrors. A photograph of a back-plane is shown in figure 3.10. A large mirrored area can be seen outside the array of pixels and a set of pads for electronic connections on each of the sides.

As a first test of the optical system, the mirrored area was masked and the back-plane used as a F.T. filter. The resulting image plane was recorded in the photograph figure 3.11, in which low-pass filtering is observed as expected, and indicated by the structure within and around the replicated triangles. Notice however, that the replicas do not fall within a symmetrical intensity envelope. A possible explanation for this is that some light is reflected by circuitry between the pixels, in effect making the repeated pattern in the filter more complicated that the simple square.

In the completed device, which was shown in schematic cross-section in figure 1.2, the pixel mirrors become electrodes, over which is placed an approximately 12μm thick layer of liquid crystal and a cover glass with an indium-tin oxide coating on its inner surface, acting as a second electrode. The liquid crystal may be changed from transparent to opaque by applying a voltage across the electrodes, each pixel being controlled separately. A 1000:1 contrast ratio is possible. The device was designed such that the liquid crystal over the circuitry remains opaque during the operation of the device.

Figure 3.12 is a photograph of the image plane when a prototype s.l.m. was used as a F.T. filter. The effectiveness of the liquid crystal as a screen may be judged by comparison with figure 3.11.

FIGURE 3.10

A photograph of an s.l.m. back-plane

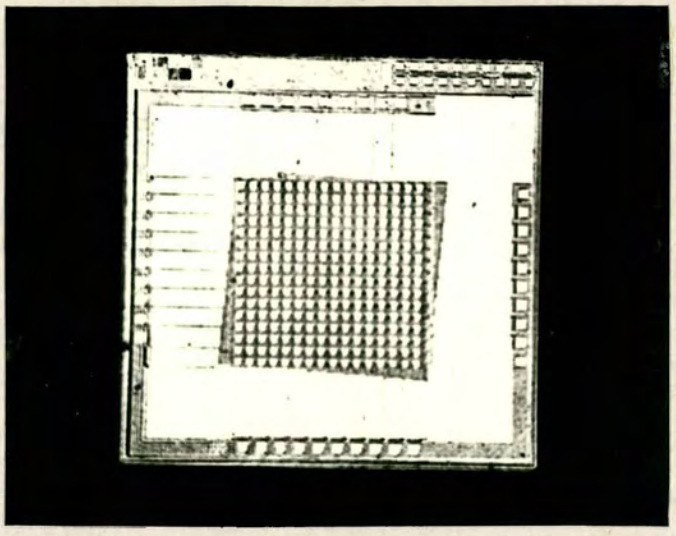

FIGURE 3.11

A photograph showing the image plane resulting from use of an s.l.m. back-plane as a Fourier transform filter

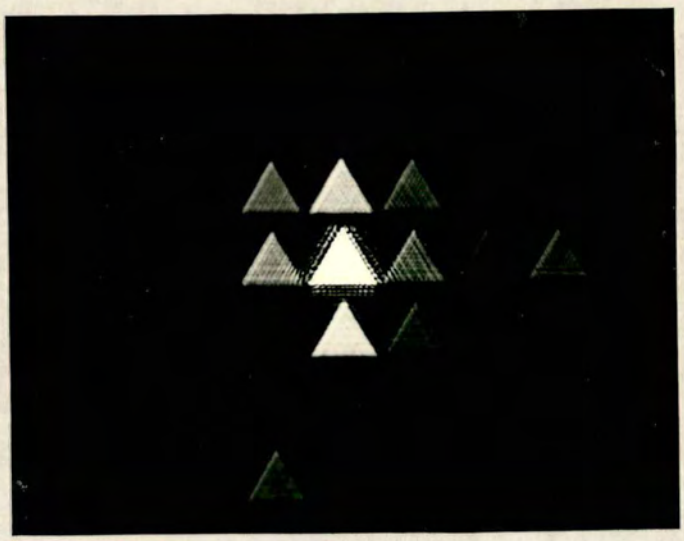

FIGURE 3.12

A photograph of the image plane produced with a prototype s.l.m. used as a Fourier transform filter

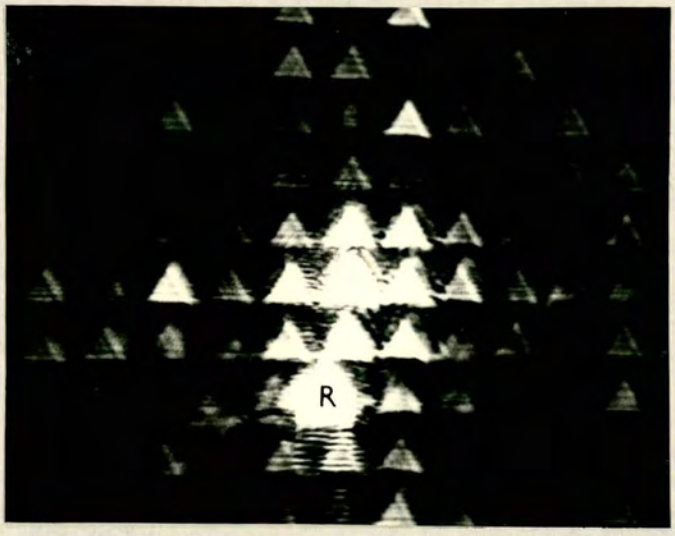

The image plane is noisier in this case as we may expect as we have considerably complicated the filtering process, adding phase effects due to liquid crystal and glass. However, it is obvious that the intensity envelope in the image plane is not symmetrical, but nor is it identical to that seen in figure 3.11. We may perhaps assume partial shielding of the circuitry by the liquid crystal. Indeed the envelope was seen to vary from device to device pointing again to the liquid crystal as the cause, the optical properties of the other components of the device being constant. The large triangle denoted by the letter R is a reflection from the indium-tin oxide used as a conducting coating for the back surface of the the glass.

3.3 Discussion

An experimental optical system with variable F.T. scale has been shown in this chapter. It was designed for use with physically small filters for which neither the problem of phase curvature of the F.T. nor of vignetting was critical. This enabled small diameter, general purpose lenses, albeit with consideration of aberrations to be used, rather than more costly specifically designed lenses. Using photographic filters, the effect of sampling both at the Nyquist interval and at a larger spacing has been illustrated. Attention has been drawn to the phase effects associated with photographic filters, and the even more drastic shortcomings of the available s.l.m.s.

Chapter 4

Production of Fourier transform filters using V.L.S.I. techniques

The design and fabrication of s.l.m.s is a capital and time intensive operation, as is the solution of optical and electronic problems associated with devices after fabrication. It is therefore impractical to experiment with the pixelated structure of devices. Pixel arrays are therefore usually simple. Because of this some opportunities for the development of s.l.m.s as F.T. filters may have been neglected.

There are several ways to simulate s.l.m.s in order to determine optical characteristics. In some cases, simple calculation may yield required information such as expected intensities of images in the image plane as was shown in the last chapter. For more complicated designs, computer simulation is a very useful and powerful tool, but relates only to perfect systems, and will not show unexpected results which may arise, for example from fabrication errors. Finally, photographic and other filters may be used to simulate F.T. filters but these introduce effects of their own which may mask those due to the filter which is required to be simulated as we have already seen.

It is the purpose of this chapter to show that the techniques of V.L.S.I. design may be used to produce mirror arrays with very precise specifications which simulate s.l.m.s and to assess their

viability for use as an aid to s.l.m. design.

4.1 Array production

It has been stated previously that s.l.m. design and fabrication is a time consuming process. Although the mirror arrays which will be described below are simple in comparison to the design of working s.l.m. backplane, much of the effort in this project has gone into their production in close cooperation with the Edinburgh Microfabrication Facility (E.M.F.). The technique described later in this chapter for simulating s.l.m.s with pixels turned off (i.e equivalent to having opaque liquid crystal over pixel mirrors) has never before been attempted.

4.1.1 Production techniques

There are several different technologies on which integrated circuits may be based. That used for the design of the mirror arrays followed closely the nMOS (negative Metal Oxide Silicon) process used for the production of the 16x16 pixel s.l.m. This allowed wafer fabrication to be carried out at the E.M.F. following the same production route as the working devices.

Integrated circuit structures are formed on a silicon substrate by a series of patterning deposition and etching processes. The silicon substrate consists of a wafer which is 3" in diameter and 0.38 mm thick, which is cut from a single crystal.

The required pattern is produced on the wafer by imaging a mask

onto its surface. The mask contains the shapes designed to be produced on the finished silicon chip. The pattern is repeated over the surface forming typically 26 dies (a chip which is stil part of a wafer) on the 3" disk. Each die is lcm xlcm.

In our case, the complexity of the task was considerably reduced by the need for only one mask, used to define the mirror arrays in aluminium. It may be found necessary to have as many as ten masks (i.e. 10 layers) in a working device.

In a device such as the 16x16 s.l.m. the mirrored pads are electrically isolated from the silicon substrate by a 55 nm thick silicon dioxide layer. The mirror arrays were designed in the same way even though no electrical contacts were to be made, to mimic the s.l.m. production as closely as possible. Upon this was deposited a layer of Al-Si alloy (99%-1%)of thickness 500nm$\pm$10% which was being used at the time for s.l.m. production. The metal is then covered with a layer of photoresist. The mask is used to define the unwanted areas of metal in photoresist, and after exposure, the unwanted areas are etched away leaving the metal on silicon dioxide.

4.1.2 Mask design

The masks were designed using the GAELIC suite of programs on the PRlME F computer at the Rutherford Appleton Laboratory (R.A.L.). This language was developed for easy production of repeated patterns. Upon completion of the mask design, the completed GAELIC program file was passed to the electron beam lithography facility, also at R.A.L., for mask making.

The design is produced as gaps in a chromium film on glass by an electron beam pattern generator. The reticle is ten times the desired pattern size to aid resolution in the process.

4.2 Array specifications

There are four variables which need to be considered when designing pixel arrays: i) pixel number, ii) pixel array configuration, iii) pixel size and iv) pixel shape. Let us deal with each of these in turn.

i) Given that a 16x16 S.L.M. had already been designed and was working, but not perfectly, it was decided to design one mirror array as a simulation of this device. In order to make direct comparisons between all the arrays, all would therefore be arrays of 256 pixels. The die size was 1cm x 1cm and the 16x16 array size was 3.2mm x 3.2mm, allowing 9 designs to be fitted onto the die.

ii) Petersen and Middleton [4.1] have applied the mathematical methods of sampling theory to N-dimensional objects of infinite extent with band-limited F.T.s. Considering the 2-D case and using the Fourier integral theorem to apply their results to the case in which we are interested, we find the following: The efficiency of a particular pixel configuration can be defined as the area of each image replica in the image plane divided by the area which each replica could fill without overlapping any other. The most efficient filter is therefore the one for which the replica is the same shape and size as that maximum unit cell. This is illustrated

in figure 4.1 It is clear that the most efficient filter for a particular application depends upon the shape of the object, and that if replicated images do not tessilate then 100% efficiency is not possible. In experimental image processing systems, the object is usually a photographic transparency or incoherent to coherent converter, which are usually rectangular and circular respectively. We shall therefore confine ourselves to pixel configurations which produce a rectangular or, as circles obviously do not tessellate but may be close-packed, hexgonal structure.

We have limited ourselves in this thesis to consideration of pixelated filters to be used as 'classical' F.T. filters. That is we are interested in looking at a single image replica. It can be seen from the diagram in figure 4.2, showing the intensity envelope and position of the centre of replicas in one dimension, that as the mark to space ratio increases, the intensity of the central replica relative to the first order becomes greater. The limiting case is of course that where the pixels are touching and the filter can be considered unpixelated. An attempt should therefore be made to make mirror arrays with the mirrors as close together as the process will allow. In the case where the mirrors are not touching, as may be necessary in practice where circuitry must be placed between mirrors, a better choice of pixel may be the circle. As shown in figure 4.3 it is not possible for the intensity maxima of the first and subsequent orders to be as great as for the square pixel of equivalent linear dimension.

Figure 4.4.a is a plot of the mask design for the die to produce the 9 mirror array designs; a large plot of this mask and

FIGURE 4.1

A schematic diagram showing an image plane resulting from the use of a 100% efficient pixelated filter in the F.T. plane

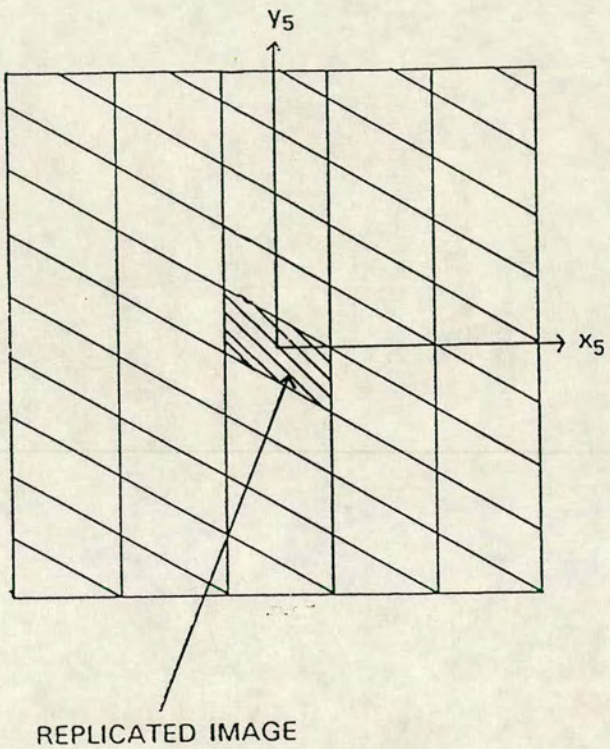

FIGURE 4.2

A one dimensional representation of a sinc^2 intensity envelope

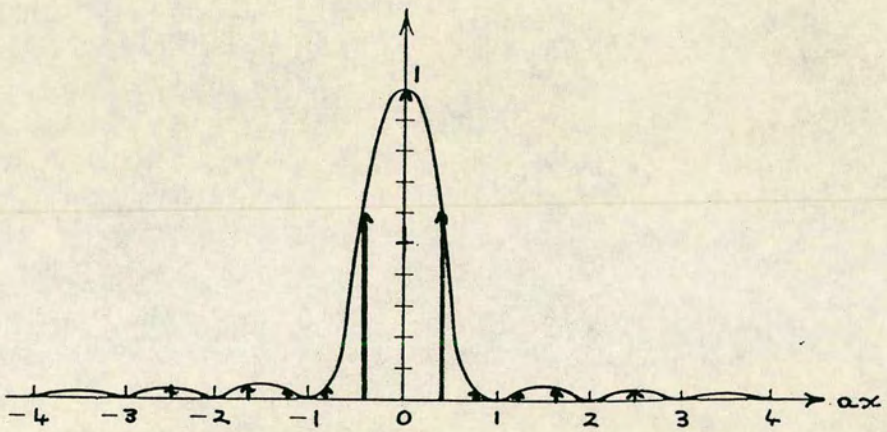

FIGURE 4.3

A one dimensional representation of a squared Bessel function intensity envelope

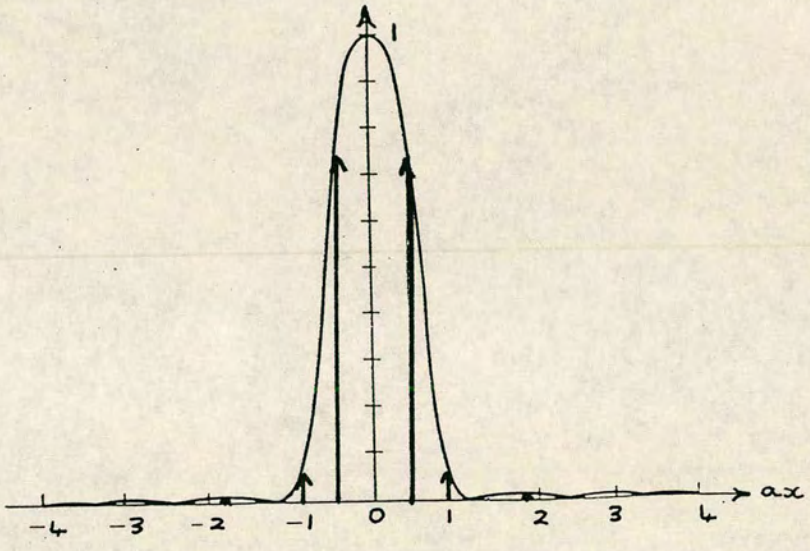

all others mentioned in this chapter may be found in appendix 4. Figure 4.4.b shows enlarged portions of the of each design in the same relative positions as for figure a, with each assigned an identifying letter. A photograph of the fabricated die is shown in figure 4.4.c, and dimensional specifications of each of the arrays is given in the table, figure 4.4.d.

The arrays fall into three groups, those with mirrors on a rectangular grid, an hexagonal grid, and a quasi-hexagonal grid. Arrays A,D,G,B, and E fall into the first group and are all candidates for working devices based on the 16x16 pixel s.l.m. design. A and D have square mirrors, the former with dimensions the same as those in the working device, and the latter with mirrors as close together as advised possible by staff at the E.M.F. whilst still being separated. D and E have circular pixels with the same diameter as the side of the square mirror. Array G has smaller circular pixels, their diameter chosen arbitrarily so as to give a central image replica which could be seen easily whilst being small enough to give a broad centre to the envelope. Arrays C, F, and I are closely packed rectangles, circles and hexagons on an hexagonal grid. Array H is a quasi-hexagonal grid. That is, square mirrors in a 'brick wall' structure with alternate rows shifted by one half-pixel length.

4.3 Experimental use

Upon fabrication, the dies were separated (chipped) and the separate chips were mounted in 40 pin DIN packages so that they

FIGURE 4.4

A)16x16 square array of square mirrors 200 µm centre to centre horizontally and 200 µm centre to centre vertically (200-200 µm). 100x100 µm mirrors.
This mimics the 16x16 device already described with perfect shielding, to determine by comparison the actual degree of shielding achieved by the liquid crystal.

B)16x16 square array of square mirrors 200-200 µm centre to centre 196x196 µm mirrors.

A similar array to the previous one but with mirrors as large as possible. If the mirrors were made any larger there would be the possibility of their joining during fabrication.

C)15x16 hexagonal array of Rectangular mirrors 200-173 µm centre to centre 196x169 µm mirrors.

These are rectangular mirrors on a regular hexagonal lattice, again as closely packed as possible.

D)16x16 array of circular mirrors 200-200 µm centre to centre 100 µm diameter.

Circular mirrors replacing square ones in a cell of the same dimensions as previously.

E)16x16 square array of Circular mirrors 200-200 µms centre to centre, 196 µm diameter mirrors.

Circular mirrors of same diameter as the sides of the large square mirrors.

F)15x17 hexagonal array of circular mirrors 200-173 µms centre to centre 196 µm diameter mirrors.
Closest possible packing of circular mirrors with almost the same number of mirrors as the square array for comparison.

G)16x16 square array of circular mirrors 200-200 µm centre to centre 20 µm diameter mirrors.

Mirrors are as small as possible whilst still giving a reasonable reflection intensity.

H)15x17 hexagonal array of square mirrors 200-200 µms centre to centre 196x196 µm mirrors.

Array of large square mirrors with alternate rows shifted to investigate any increase in efficiency.

I)15x17 hexagonal array of hexagonal mirrors 200-173 µms centre to centre 196 µm mirrors A/F.

Hexagonal array of hexagonal mirrors which makes better use of space than the circular mirrors, but with higher symmetry than the square.

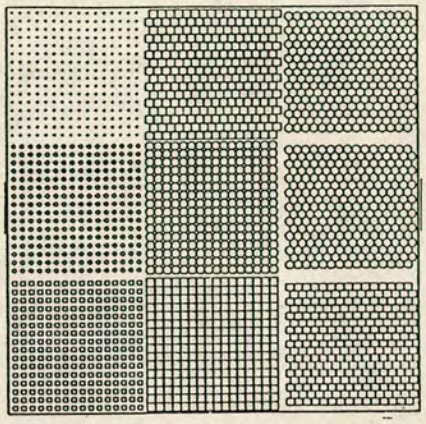

A plot of a mask to be used for the production of 9 pixelated mirror designs

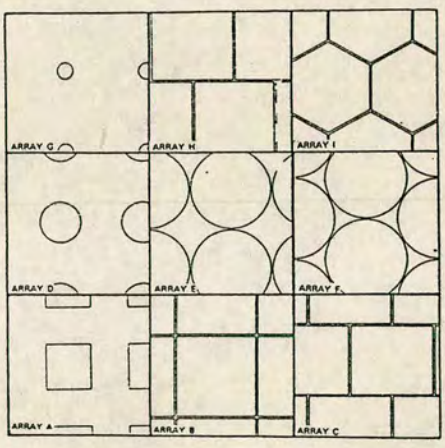

Magnified plots of the 9 designs.

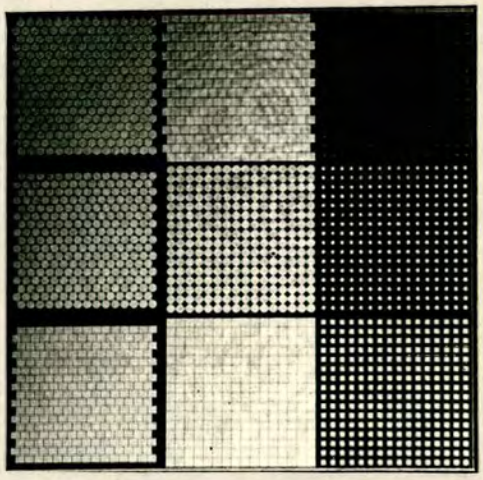

(Note that the photograph is reversed relative to the plot)

could be placed in the holder used for the s.l.m. Initial microscopic inspection showed that each of the close packed designs was separated. This is confirmed by the results from a talystep surface profile measurement reproduced in figure 4.5.

Figure 4.6 is a set of photographs of the image plane resulting from use of each of the mirror arrays as a filter in the F.T. plane. The object and experimental setup was the same as that used previously for the experiments shown in the last chapter. The photographs are all overexposed to show clearly the intensity envelope produced by the pixel shape function. There is excellent agreement and the image plane is as expected, with a single exception. Consider the image plane produced by array G. The central image replica is much brighter than we would expect. This is due to the oxide between the metal mirrors reflecting laser light. This is an unfortunate consequence of following the s.l.m. design conditions too closely. However, this affects *only* the central replica. The other replica orders should be as we expect.

4.4 Filtering

It would be possible to produce mirror arrays to act as pixelated high-pass, band-pass and directonal filters in the same way as described previously, by forming repeated patterns of mirrors but leaving some mirror sites vacant to simulate 'off' pixels. This method was considered but would be time consuming in both design and

FIGURE 4.5

A reproduction of a typical talystep surface profile measurement of an array of close-packed pixels

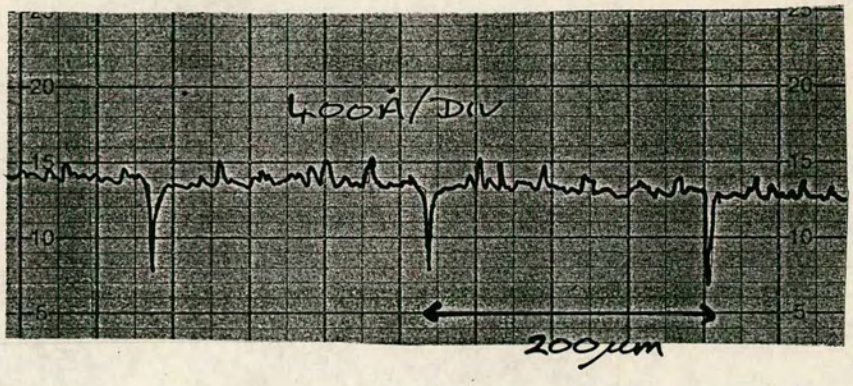

FIGURE 4.6

Replicated images in the image plane resulting from the use of the various pixel arrays as F.T. filters

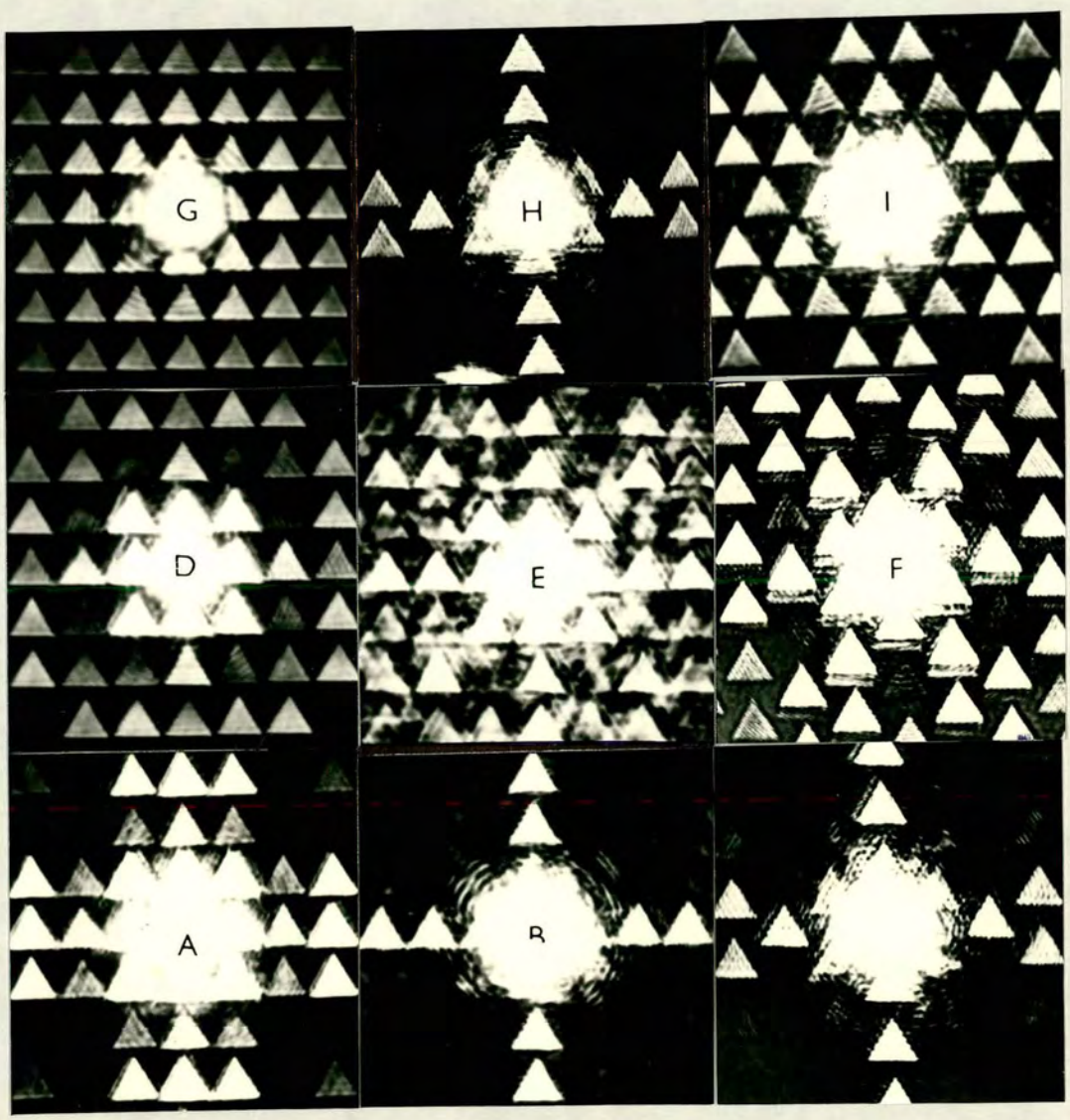

fabricaton. Instead nine masks were produced which define areas where no mirrors are required. These were used by the E.M.F. as templates to chemically remove the metal layer from filters which had already been fabricated. This technique had not previously been used by the E.M.F. The nine masks are shown in figure 4.7.a identified by a number. A table giving the specification and desired effect of each mask is given in figure 4.7.b

The masks were produced in house using the pattern generator at the E.M.F. from a GAELIC mask design program. As the pattern generator (unlike the electron beam method used by the R.A.L.) is able to produce only manhattan geometries, sloping or curved lines had to be replaced by a stepped pattern, as shown in the magnified portion of the mask, figure 4.8.

4.5 Processing problems

Figure 4.9 shows one of the completed filters, in this case a directional filter. Notice that instead of a uniform unpixelated region, the positions once occupied by removed pixels are darker than the surrounding surface. This is because the etching process attacked the oxide layer, roughening the surface.

The difficulty of producing the filters is manifested in the processing errors. Some filters were found to be mis-aligned relative to the mirror array, as two mask design processes were being used, making the filter non-symmetrical or giving half-pixels. Attempts were made in the latter stages of production to align the

FIGURE 4.7

Filter mask designs and their specifications

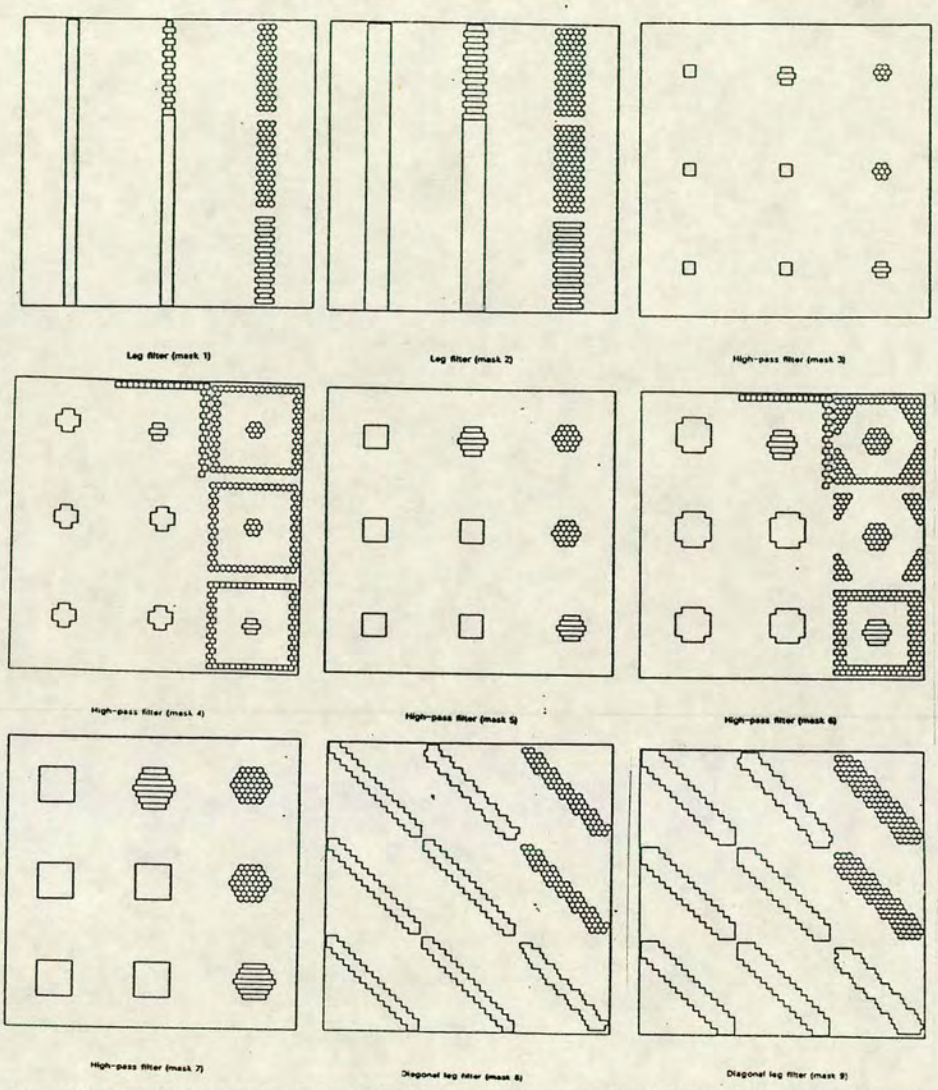

1) A mask to remove two columns of pixels, or the equivalent in the hexagonal grid structures.

When used to form a filter, this would be used to remove a leg of the Fourier transform, which would cause high-pass filtering and the removal of an edge in the image.

2) A wider version of the last mask, this time to remove four columns of pixels or the equivalent.

A filter formed using this mask would have a similar effect to the last but with a higher low-frequency cutoff

3) A group of four pixels in the rectangular structures or five in the hexagonal, would be removed.

This is a mask to form a high-pass filter.

4) A similar mask to the last, with more pixels removed. Some pixels are also removed from the outer edges of some arrays, to increase the low-pass filtering effect.

5) A high-pass filter with more pixels removed.

6) Again, a mask to remove more pixels to form a high-pass filter. Also, with pixels removed from the edges of the arrays to investigate the increased low-pass filtering effect

7) The high-pass filter mask with the highest low-frequency cutoff.

8) A mask to remove pixels on a diagonal across the filter. This would have the same use as the first two filter masks, but used to investigate the effect of the jagged edges which must be used with diagonal filters.

9) A similar mask to the previous one but with more pixels removed.

FIGURE 4.8

A magnified portion of a mask showing the stepped structure

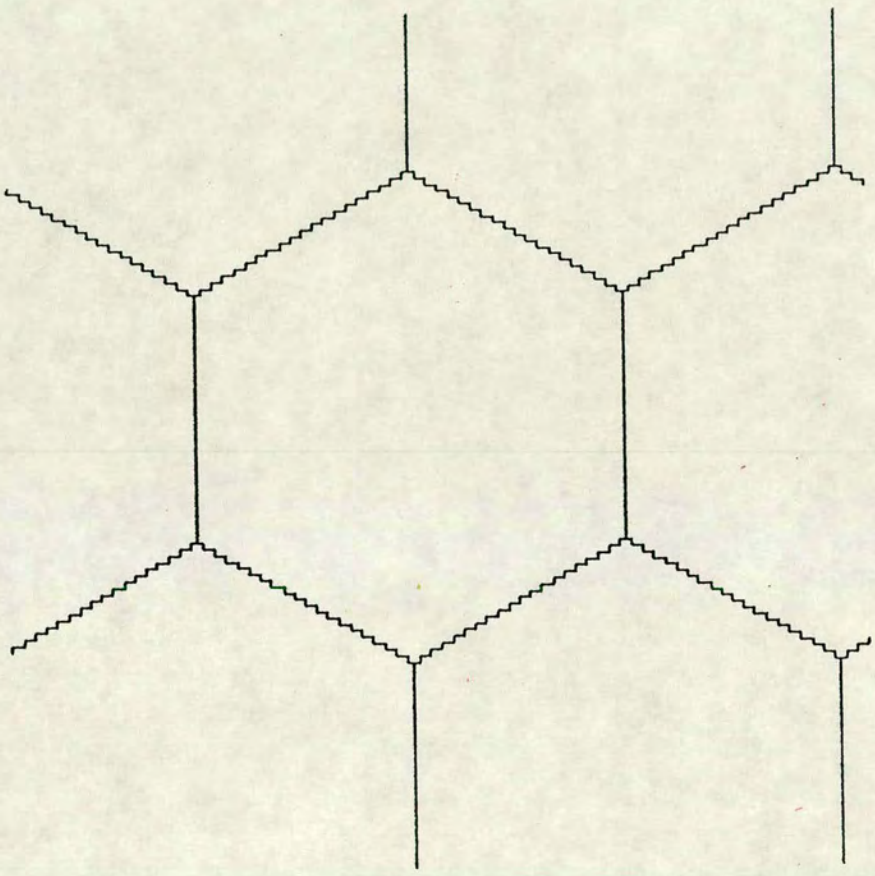

FIGURE 4.9

A filtering array produced by the mask-etch process

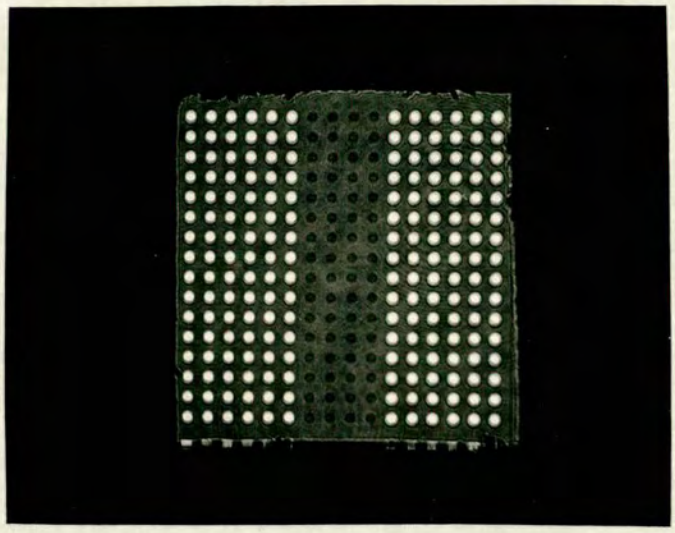

masks by eye, making this a time and resource intensive operation. Another error is observed when a pixel which should have been removed for an unknown reason remains as, as shown in the photograph figure 4.10. This is interesting because this type of problem is often observed in working s.l.m.s, when a pixel ceases to function.

4.6 Experimental use

It would take a great deal of space to illustrate the effect of each of the filters produced. However, we shall illustrate a few cases to show that the filtering effect is in evidence and that the method of filter production is successful. This is of course with the exception of the problem of the bright central replica which remains unfiltered. We shall draw attention to the differing filters which would have to be considered equivalent due to the quantised nature of the filtering in pixelated filters. For example a set of six missing pixels in an hexagonal array and four in a rectangular array forming a high-pass filter; Figure 4.11 illustrates this situation with two examples. Figure 4.12 shows two leg filters formed by removing vertical rows of pixels and figure 4.13 shows the equivalent filter produced by removing pixels across a diagonal of the filter.

4.7 Discussion

Let us first consider the photographic results from the use of the mirror arrays. As can be seen from the data accompanying the

FIGURE 4.10

A filtering array exhibiting an error

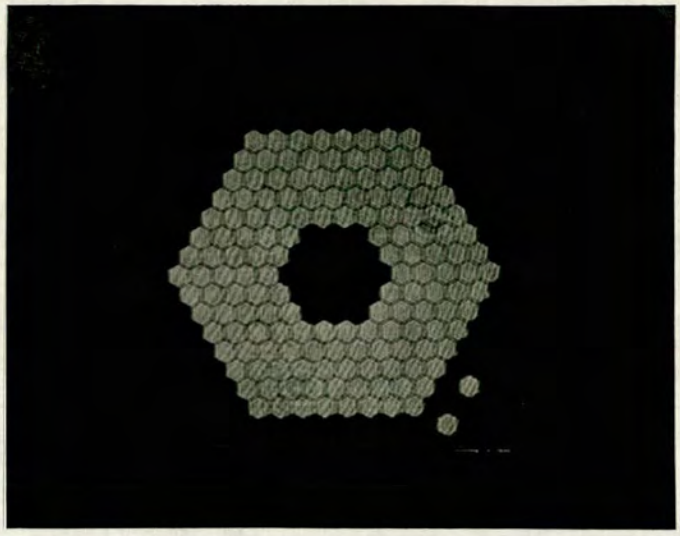

FIGURE 4.11

Two examples of 'equivalent' filters

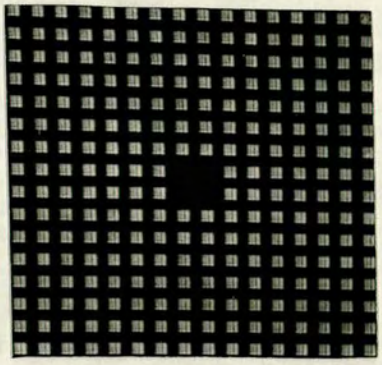

Filter A3

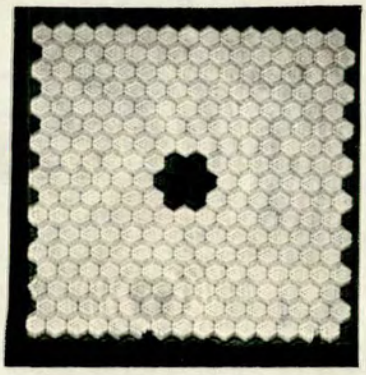

Filter I3

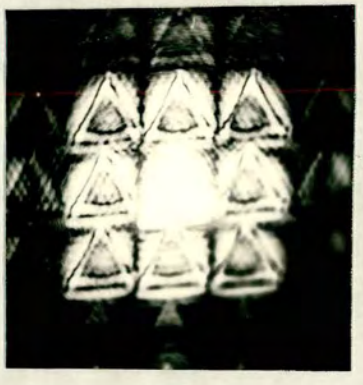

FIGURE 4.12

Leg (high-pass and side) filtering arrays and the filtered images resulting from their use

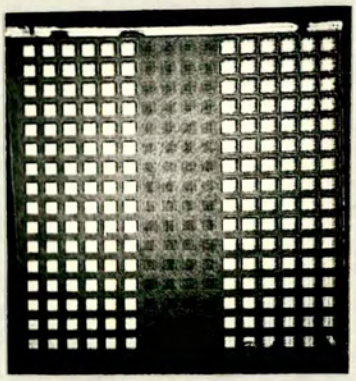

Filter A2

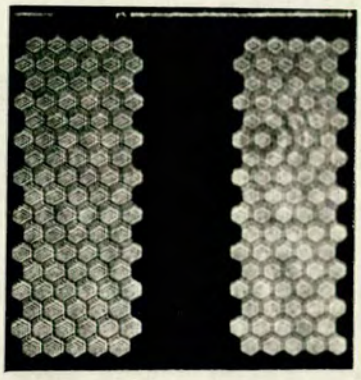

Filter I2

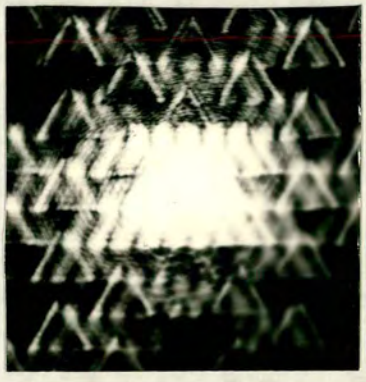

FIGURE 4.13

Diagonal leg filtering arrays and the filtered images resulting from their use

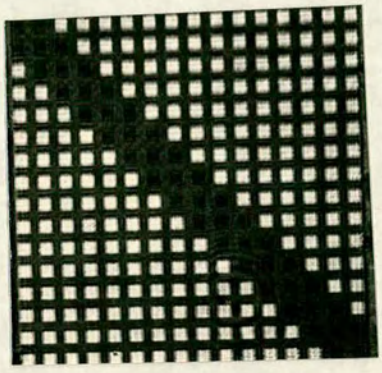

Filter A9

Filter I9

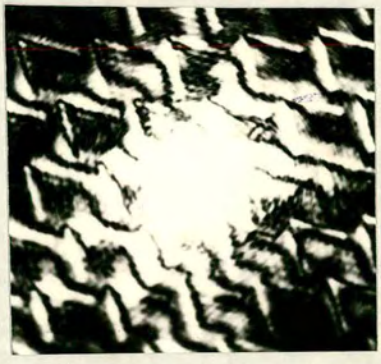

photographs, the expected results are obtained in terms of the size and shape of the intensity envelope and the number of image replicas contained therein. It is interesting to note that in each case, the overexposed central reflection exhibits 'ringing' characteristic of low-pass filtering. Low-pass filtering is also apparent in some replicas where intensity structure of the type seen in chapter 3 is present. It is interesting to note that this structure appears to change little between the various pixel configurations, indicating that any increase in sampling efficiency due to closer spaced pixels in hexagonal arrays than rectangular ones is negligible in this case. Notice also that due to the large spaces between pixels in arrays A and D, the bright reflected triangle is more intense in these cases than in others.

The presence of the bright central triangle prevented comparison of the intensities of the central replicas produced using the various arrays and also the intensities of the various orders within one image plane. However, the effect of the intensity of a whole replica being determined by the position of its centre within the intensity envelope is shown very clearly in the case of filter F where replicas at or near a zero in the intensity envelope appear to be 'missing'.

Unfortunately, but unsurprisingly, the filter arrays suffer from reflection from the silicon dioxide layer in the same way as the arrays. It is probable that the roughness of the areas where the pixels have been removed mean that they reflect diffusely and do not add to the intensity of the central image, but the decreased intensity of the filtered triangle means that the overexposed

reflection affects the photographs of the filtered replicas more than those of the unfiltered case. The intensity and distribution of the replicas due to the intensity envelope are obviously the same as in the non-filtering arrays using the same pixel sizes and spacings. The purpose of the experiments was therefore seen to be to observe the effect of the shape of the removed pixel area of a filter on the replicated triangles.

In each of the photographs of the filtered images, a dark line appears around the sides of the triangle. This is a feature of high-pass and band-pass filtering. In the case of the leg filters, one of the sides of the triangle is also missing.

A visual inspection of the pairs of high-pass filtered images shows the image produced by the hexagonal array to be'cleaner', that is the bright line bordering the dark lines are narrower. The same is true of the leg and diagonal filters.

In the above examples, the small size of the mirror arrays and the associated low-pass filtering effect made assessmment of the quality of the images produced using the various filters difficult. However, some differences are noticeable as mentioned above for the hexagonal filter, but not enough to favour the one filter over another.

The problem encountered with the reflection of light from between the mirrors affects only the central image replica, allowing the effect of the filtering operation to be seen in the other replicas. The reflection problem could be decreased in future by making the background diffusely reflecting as is the case where the pixels have been removed.

Chapter 5

Self-imagery and self-Fourier transformation in optical processing systems

Although it has been stated previously that we shall not discuss diffractive methods of F.T. production in general, one method is of particular interest when considering pixelated filters, and is worthy of discussion here, that is self-Fourier transformation. The phenomemon of self-imaging of objects which consist of periodically repeated patterns has been known for over one hundred and fifty years [5.1]. Using coherent light, the phenomenon of self-Fourier transformation may occur. In this chapter we shall look at the conditions under which it occurs and at the theory as published in recent papers. We shall then reappraise the theory by a novel method. Experimental results obtained using a pixelated filter will be shown.

5.1 Theory of self-Fourier transformation

Most noteworthy of papers published on self-imagery and self-Fourier transformation in recent years have been those by Kolodziejczyk, Kalestynski and Smolinska [5.2],[5.3].

Kolodziejczyk has described the case in which a self-Fourier transform of an object is obtained by illuminating with coherent

monochromatic light, the object sampled by a pinhole array. We shall show in the following analysis that such a sampling array of pinholes may be considered as a pixelated Fresnel-zone plate.

Let us first consider the theory as presented by Kolodziejczyk. Figure 5.1 is a schematic diagram showing object, pinhole array and Fourier transform plane. A rectangular array of infinitesimally small pixels may be represented by the transmission function

$$t_o(x_o,y_o) = \sum_{m=-\infty}^{\infty}\sum_{n=-\infty}^{\infty} \delta(x_o-ml,y_o-nl) = \frac{1}{l^2}\mathrm{Comb}\left\{\frac{x_o}{l},\frac{y_o}{l}\right\} \qquad -(5.1)$$

where l is the separation of the pixels, m and n are integers. We may represent an object in the same plane as the pinhole array by $U_o(x_o,y_o)$. The complex amplitude in the plane z=d may be represented by the Fresnel diffraction integral and written,

$$U_1(x_1,y_1) = \frac{e^{ikd}}{i\lambda d}\, e^{\frac{ik}{2d}(x^2+y^2)} \int_{-\infty}^{\infty}\int_{-\infty}^{\infty} U_o(x_o,y_o)$$

$$\times \sum_{m=-\infty}^{\infty}\sum_{n=-\infty}^{\infty} \delta(x_o-ml,y_o-nl)\, e^{\frac{ik}{2d}(x_o^2+y_o^2)}\, e^{-\frac{ik}{d}(xx_o+yy_o)}\, dx_o dy_o \qquad -(5.2)$$

This is the Fourier transform of the product

$$U_o(x_o,y_o)\sum_{m=-\infty}^{\infty}\sum_{n=-\infty}^{\infty} \delta(x_o-ml,y_o-nl) \qquad -(5.3)$$

FIGURE 5.1

A schematic diagram showing a two-dimensional object and pixel array in the same plane, and the F.T. plane separated form them by a distance d

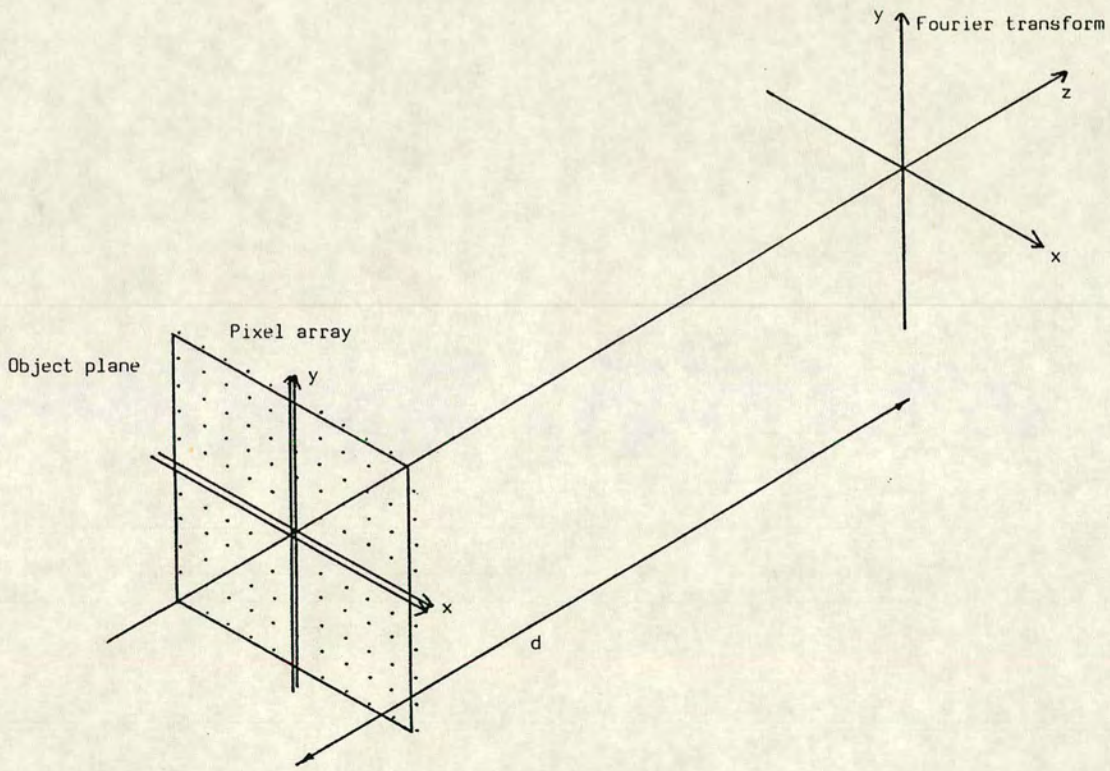

if the condition

$$e^{\frac{ik}{2d}(x_o^2+y_o^2)} = 1 \qquad -(5.4)$$

is fulfilled.

We see that for this particular array or sampling filter,

$$x_o = ml \ , \ y_o = nl \qquad -(5.5)$$

and thus the condition for self-Fourier transformation from (5.4) becomes

$$d = \frac{l^2}{2\lambda N} \qquad -(5.6)$$

where N is an integer.

Note that the above expression for the plane in which the F.T. is produced has the same form as that for the focal length of a Fresnel zone-plate. Consider now the array of pinholes as a pixelated zone-plate of the Soret type, that is with zones either completely opaque or perfectly transparent. Figure 5.2 shows an array of pixels with Fresnel-zone boundaries indicated. The radius of the central zone is the distance from the centre of a group of four pixels to any one of those pixels. Let us call these four pixels the first shell. The distance is $(\sqrt{2}l)/2$. A zone-plate with a central zone of this radius would have a primary focal length

FIGURE 5.2

A rectangular array of pixels (considered to be small and lying at the centre of the crosses) with superimposed Fresnel zones

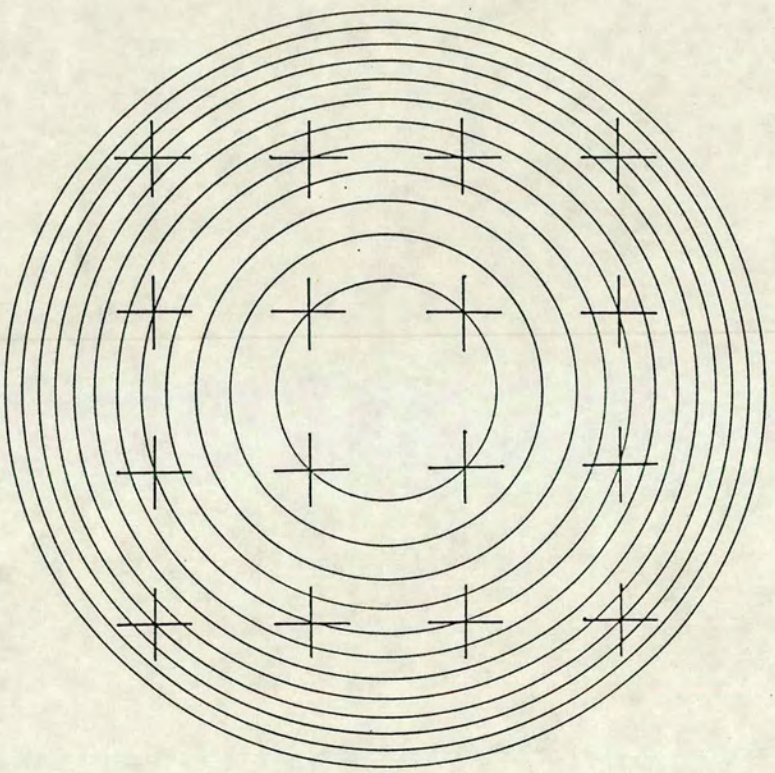

$$F = \frac{r^2}{\lambda} = \frac{l^2}{2\lambda} \qquad -(5.7)$$

which is the focal length arrived at in (5.6) by a different method.

If we continue in this manner, and consider other zone radii, we see that pixel shells do not fall on each zone boundary, but on every fourth. Changing the zone radii by an infinitely small amount, so that the first shell of pixels is either included in the centre zone or in the second zone, and adjusting the other zone radii accordingly, we see that the pixels only fall into zones which we would expect to be transparent in a zone-plate of the same primary focal length. If we had chosen a pixel as the centre of our zone-plate structure as shown in figure 5.3, we see that the same zone-plate radii would include pixels in each alternate zone.

This type of analysis, although alluded to in the published literature has not been given explicitily.

When considering sampling arrays with pixels of finite size, the condition for the formation of the Fourier tranform, according to Kolodziejczyk becomes

$$e^{2\pi i\left\{\frac{(ml+\Delta)^2+(nl+\Delta)^2}{2\lambda d}\right\}} = 1 \qquad -(5.8)$$

where Δ is the radius of a pixel (assuming them to be circular).

For practical filters, this reduces to the inequality

$$\frac{2(m+n)N\Delta}{l} \ll 1 \qquad -(5.9)$$

which is satisfied if d is large or Δ/l is small.

Consider now a sampling array with square pixels of side length

FIGURE 5.3

Fresnel zones centred on a pixel. The pixel and zone spacing is the same as that in figure 5.2

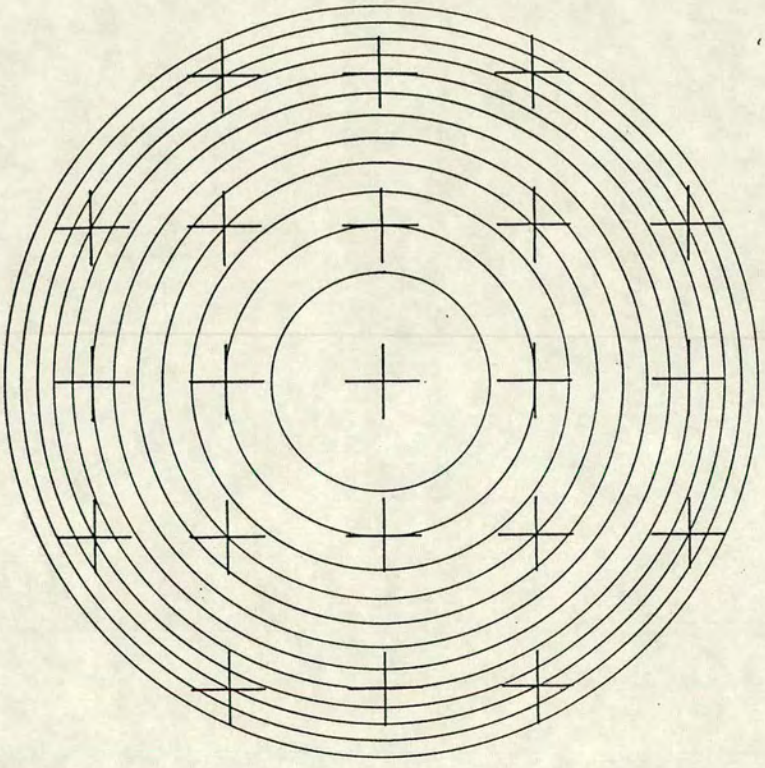

Δ as a pixelated zone-plate. As shown in figure 5.4, if $\Delta/l = 0.5$ only one pixel falls completely into a zone. Pixels which fall across two or more adjacent zones have a diminished focussing effect as light from these zones destructively interferes. A set of sampling arrays for which Δ/l is progressively smaller, will have more zones containing whole pixels, and as with zone-plates of increasing zone number, resolution will increase [5.4].

The pixelated zone-plate approach to this phenomenon may be extended to non-rectangular regular arrays [5.5]. For example, an hexagonal array of pixels would also act as a pixelated zone-plate, as it falls into the zone-plate structure. Such an array would have a primary focal length given by

$$F = \frac{3l^2}{2\lambda} \qquad -(5.10)$$

As we would expect, sampling of the object by a pixelated zone-plate causes replication of the F.T. in the focal plane. Intensity modulation of the focal plane is determined by pixel size and shape. Both of these subjects have been covered previously for pixelated F.T. filters and have been treated in depth in relation to this particular case elsewhere [5.6].

5.2 Experimental observation

As investigation of self-Fourier transformation was not the purpose of this project, none of the filters was designed with that purpose in mind. For only one filter (G) were the conditions for

FIGURE 5.4

A rectangular array of pixels having $\Delta/l=0.5$, with a superimposed zone structure

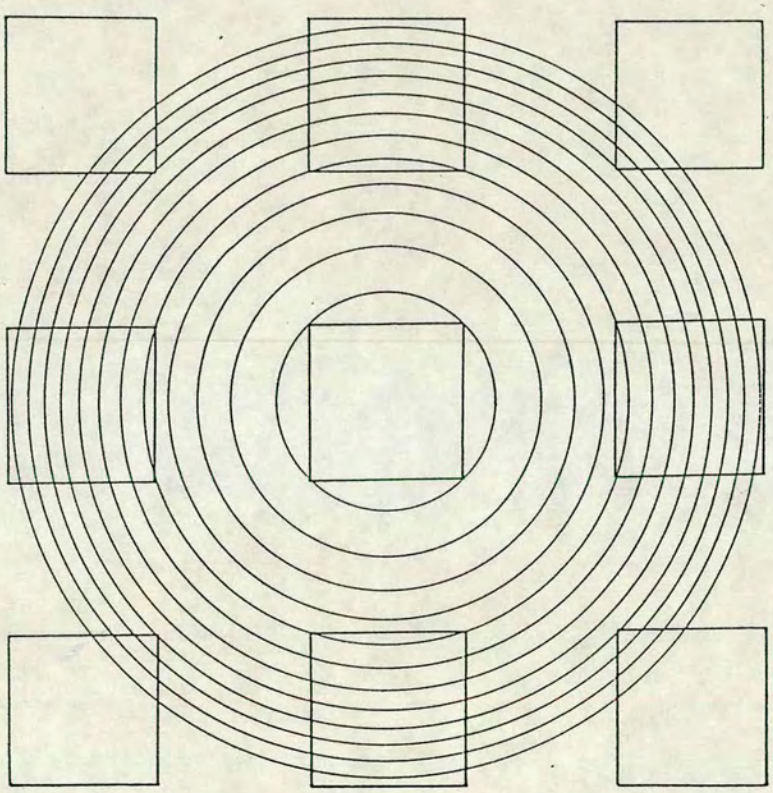

self-transformation satisfied. For all other filters $\Delta/l>=0.5$ and could not display the effect as seen from (5.9). This also shows why self-imaging cannot be performed by any s.l.m.s presently available as such devices are usually designed to have the maximum possible mark to space ratio, which in all cases is greater than 1:1.

The use of array G as a Fourier transform filter has already been illustrated. The variable magnification system was used to form the F.T. of a triangular object in the plane of the filter. The zoom reconstruction system was used to magnify the replicated images resulting from the self-F.T. action of the pixel array on the F.T.

The diameter of the pixels in the filter is 40μm and their separation is 200μm. Thus the smallest zone into which the pixels will wholly fit is the 3rd. The primary focal length of the array is 31mm.

Figure 5.5 is a photograph of the image plane with the pixel array in position. Notice that there is a Fresnel diffraction pattern of the triangular object also visible. This is due to the reflections from the oxide layer between the silicon and the metal discussed in the previous chapter. In previous experimental situations we have seen that this reflection acts to increase the intensity of the central replica in the image plane. In this case, however, there is no lens transforming the F.T. into a bright image. Hence the Fresnel diffraction pattern of the reflection is seen. As the pixels are small most of the light in the F.T. makes up the Fresnel diffraction pattern, which is particularly bright in the

FIGURE 5.5

A photograph of the self-image plane

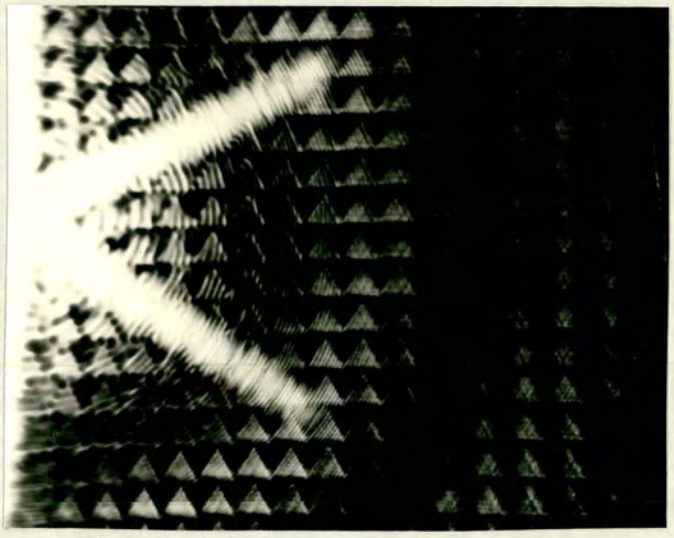

centre and obscures some of the image replicas. The Fresnel diffraction pattern is brightest in an area which is a little larger than that of the filter, whilst the image replicas extend over an infinite area. Thus some replicas are clearly visible. Notice that there is an envelope of intensity which is the F.T. of the pixel shape. Considerable difficulty was encountered in finding the most prominent i.e. the principal focus of the filter. The other maxima, which are very close to the principal in this case could not be distinguished.

5.3 Filtering experiments

Following the manufacture of the filters, the existence of self-filtered images was investigated. That is, using a filter with some pixels removed to see if a filtered image could be formed. It was thought that filtered images should be seen for two reasons, i) by effectively blocking out part of the zone-plate, no destructive interference is introduced to decrease the focussing property, although of course there would be a decrease in intensity. ii) the situation is equivalent to forming the filtered F.T. of a triangle onto a normal pixel array, so the image should be of a filtered triangle.

Unfortunately in practice no self-filtering was observed. Because of the decrease in intensity in the image and the increase in intensity of the central portion of the F.T. reflected from the

surface, the images, if they existed were of an intensity too low to be visible.

5.4 Discussion

We have reported in this chapter for the first time, the demonstration of self-Fourier transforming using a filter produced by V.L.S.I. techniques, and we have presented a previously unreported analysis of the self-transforming phenomenon. As mentioned previously in this chapter, the filter used for the investigation was not designed specifically for the purpose and it is only by happy coincidence that the filter fulfilled the necessary conditions and that the phenomenon was noticed. The conditions for its examination were not perfect, and it is unfortunate that no results could be obtained from the filtering experiments. We shall, however consider the possible implications for s.l.m. design of these observations in the concluding chapter of this thesis.

Chapter 6

Conclusions

In this chapter, the results from work shown in previous chapters will be reviewed, the conclusions derived from them will be discussed and suggestions for future work will be given.

6.1 The variable-scale Fourier transform optical system

It was stated in chapter 1 that our Applied Optics Group is concerned with the design and use of s.l.m.s. The s.l.m.s produced by us are pixelated and electronically addressed liquid-crystal-over-silicon devices which work in reflection. It was in order to have an optical system which could be used for several devices and eliminate the need for a system specifically designed for each one that a variable-scale Fourier transform system was designed.

It was shown in chapter 2 that pixelation in the Fourier transform plane of an optical imaging system puts some constraints on the design of the system. The pixelation causes the image of the object to be replicated, that is an infinite number of images is produced in the image plane. The main constraint on the design of the system is therefore that sampling of the Fourier transform of an object by pixels of the filter is required to be at what we have

termed the Nyquist spacing. If the spacing is larger than this for a given object and Fourier transform, the image replicas will overlap, confusing information in the image plane. If the spacing is smaller, assuming the pixel number to be the same, the high-frequency cutoff of the filter will decrease, causing more severe low-pass filtering and loss of detail. It has been seen that the Fourier transform of an object may be produced by using the transforming property of the converging lens. In the case of the widely used f-f system, where the object is illuminated by a parallel beam of light, the transform is of fixed size for a given transform and lens. However, if the object is illuminated by a converging or diverging beam of radiation, a Fourier transform may still be produced but its scale may be varied simply by changing the relative position of the object and transforming lens. Thus the optimum sampling conditon may be achieved for several different filters, with different specifications in the same optical system. In chapter 2 the conditions under which this variable scale transform is acheivable, and the constraints upon change of scale and the positions of the Fourier transform plane were derived. It was also shown that a varifocal imaging system would be a useful addition to such an optical system, allowing the magnification of the image plane to be varied and/or the position of the image plane to be kept constant as the scale of the Fourier transform was varied. This has enabled us to design a variable scale Fourier transform optical system for the specific purposes of our research.

In chapter 3, the design criteria of the laboratory optical system were described, and its specifications were given. Results

of investigations of the effect of pixel size and overall filter size, using the optical system showed experimentally the effect of varying the scale of the Fourier transform, and the effect of low-pass filtering produced by the small size of the s.l.m. which was initially to be used with the optical system. The effect on the image plane of the shape and size of the pixels was demonstrated.

6.2 Mirror arrays

In chapter 4, the investigation of the shape, size and configuration of pixels within a small pixelated filter was taken further. A set of arrays of mirrors was produced using microfabrication design tools, that is the same techniques used for the production of s.l.m.s. The arrays were fabricated by the e.m.f. and consisted of metal mirrors deposited on an oxide surface with a silicon substrate. These were produced both to simulate designs of the working device and to investigate configurations of pixels which have not been used in s.l.m.s. It was hoped that these simulations would be an inexpensive, simple and useful way of testing new ideas for s.l.m design by simulation. At present most attention in the design of s.l.m.s is paid to the electronics of the device, and rightly so as this is the part of the device where failure is most likely. However, now s.l.m.s are becoming larger, more costly and are required for applications as diverse as holography and optical computing, it may be useful to test the optics of the device separately. Although it has been shown that using methods of integrated circuit design, some of the properties of production

devices may be reproduced exactly, the arrays were of high cost both financially, and technically, pushing the skills of the e.m.f. to the limit in the case of the filtering arrays. However, the problems which have been encountered in the use of the arrays as F.T. filters are surmountable. The most noteable problem, the reflection from the oxide surface could be overcome in future experiments by making the background diffusely reflecting. The optical characteristics of the background material could be varied to produce arrays with different contrast ratios and a photoresist layer over the pixels may be used to simulate phase or grey-scale devices.

Unquestionably, the arrays produced by V.L.S.I. methods are more precise than those produced by other methods such as photographic transparencies, and may be of use in other fields such as computer generated holograms. Some of the designs of simulation produced had faults which would be encountered on s.l.m.s, for example failed pixels. The effect of these failures would be worth investigating for their effect on image quality. A single failed pixel in a device may mean that the device is useless if that pixel is in the centre but not if it is at the edge. The effect of failed pixels in other positions is far less clear. As the size of s.l.m.s increases their production yield decreases; it would therefore be useful to know how many failed pixels and in what positions cause the s.l.m. to be unusable for a particular application.

Although results were achieved with the filters, and optical modification of the image was observed in all cases, the degree of blurring of the image caused by the low-pass filtering effect of 16x16 or 15x17 pixel arrays made it difficult to evaluate their

filtering quality. It was hoped that one configuration would stand out as the obvious choice for a F.T. plane filter, but this was not the case. We have seen that in these arrays and filters, the 'rough' edges of filters consisting of hexagonal arrays seen to have little effect on the filtered image compared to other filters. It appears that in this case, the array of close packed hexagonal pixels may be a good choice for a Fourier transform plane filter, as it creates low intensity first order image replicas, and has a central replica with a higher intensity than filters with rectangular pixels. A detailed comparison with calculations of perfect systems e.g. computer simulations may be useful in future.

6.3 Self-Fourier transformation

Self-Fourier transformation was discussed in chapter 5. This was not a piece of work which was envisaged at the beginning of the project. The phenomenon was observed by accident and is certainly striking and worthy of investigation in the context of pixelated Fourier transform filters. It is hoped that by simplifying the notation, and in this case showing the link between pixelation and the Fresnel zone plate, the phenomenon occuring with pixelated filters will be better understood.

We have seen that using filters which were not specifically designed for the purpose, we may observe image formation using this phenomenon. In our case, the image plane was 31mm away from the Fourier transform plane, which is much closer than would be possible with a lens system. By using the self-Fourier transforming effect

to produce the transform of the object as well, future investigations could produce very small all-diffractive Fourier transform optical systems.

Appendix 1

The Fourier Transform of h(x,y;d)

$$\text{F.T.}[h(x,y;d)] = \text{F.T.}\left[e^{\frac{ik}{2d}(x^2+y^2)}\right]$$

$$= \int_{-\infty}^{\infty}\int_{-\infty}^{\infty} e^{\frac{ik}{2d}(x^2+y^2)} e^{-i2\pi(\xi x+\eta y)}\,dxdy$$

Completing the square in the exponent gives

$$\text{F.T.}[h(x,y;d)] = e^{\frac{-ik\lambda^2 d}{2}(\xi^2+\eta^2)} \int_{-\infty}^{\infty}\int_{-\infty}^{\infty} e^{\frac{ik}{2d}[(x-\lambda\xi d)^2+(y-\lambda\eta d)^2]}\,dxdy$$

$$= i\lambda d\,h(\xi,\eta;-1/(\lambda^2 d))$$

Appendix 2

Fourier Transform Definition and Useful Formulae

The Fourier transform is defined by mathematicians to be a 1-dimensional integral transform of a 1-dimensional function. However, what is usually termed a Fourier transform by optical scientists is 2-dimensional. This useage of the term is well established and when we refer to a Fourier transform throughout the text, we mean the 2- dimensional variety.

We define the Fourier transform of two independent variables as

$$F.T.[f(x,y)] = \int_{-\infty}^{\infty}\int_{-\infty}^{\infty} f(x,y)e^{-i2\pi(\sigma x+\tau y)}dxdy$$

The transform is a complex-valued function of the independent variables σ and τ which we shall refer to as spatial frequencies.

The inverse is defined as

$$F.T.[G(\sigma,\tau)] = \int_{-\infty}^{\infty}\int_{-\infty}^{\infty} G(\sigma,\tau)e^{i2\pi(\sigma x+\tau y)}d\sigma d\tau$$

Some useful mathematical properties of the Fourier transform are given below. Proofs of these can be found in Goodman.

1) Linearity theorem

$$F.T.[\alpha g(x,y) + \beta h(x,y)] = \alpha F.T.[g(x,y)] + \beta F.T.[h(x,y)]$$

2) Similarity theorem

If F.T.[g(x,y)] = $G(\sigma,\tau)$

then F.T.[g(ax,by)] = $\frac{1}{|ab|} G\left[\frac{\sigma}{a}, \frac{\tau}{b}\right]$

3) Shift theorem

If F.T.[g(x,y)] = $G(\sigma,\tau)$

then F.T.[g(x-a,y-b)] = $G(\sigma,\tau)e^{-i2\pi(\sigma a+\tau b)}$

4) Parsevals theorem

If F.T.[g(x,y)] = $G(\sigma,\tau)$

then $\int_{-\infty}^{\infty}\int_{-\infty}^{\infty} |g(x,y)|^2 dxdy = \int_{-\infty}^{\infty}\int_{-\infty}^{\infty} |G(\sigma,\tau)|^2 d\sigma d\tau$

5) Convolution theorem

If F.T.[g(x,y)] = $G(\sigma,\tau)$ and F.T.[h(x,y)] = $H(\sigma,\tau)$

then F.T.$\left[\int_{-\infty}^{\infty}\int_{-\infty}^{\infty} g(\xi,\eta)h(x-\xi,y-\eta)d\xi d\eta\right] = G(\sigma,\tau)H(\sigma,\tau)$

6) Autocorrelation theorem

If $\text{F.T.}[g(x,y)] = G(\sigma,\tau)$

then $\text{F.T.}\left[\int_{-\infty}^{\infty}\int_{-\infty}^{\infty} g(\xi,\eta)g^{*}(\xi-x,\eta-y)d\xi d\eta\right] = |G(\sigma,\tau)|^{2}$

7) Fourier integral theorem

$$\text{F.T.}\{\text{F.T.}^{-1}[g(x,y)]\} = \text{F.T.}^{-1}\{\text{F.T.}[g(x,y)]\} = g(x,y)$$

Appendix 3

Published Papers

1. Underwood I., Willson P.H., Sillitto R.M., Vass D.G.
Real-time image processing :concepts and technologies
Proc. SPIE V860 p2 (1987)

2. Vass D.G., Sillito R.M., Underwood I., McKnight D.J.,
Willson P.H., Ranshaw M.J.
Progress in developing VLSI based spatial light modulators
IEE Colloqium Digest No 1987/105

3. Willson P.H.
Fresnel zone approach to self-Fourier transforming
Applied Optics V30, No8 (1991)

An adaptive Fourier optical processor.

I. Underwood, P.H. Willson, R.M. Sillitto and D.G. Vass.

Department of Physics, University of Edinburgh,
Mayfield Road, Edinburgh, Scotland. EH9 3JZ.

Abstract

A prototype liquid-crystal-over-silicon spatial light modulator (SLM) with 16 x 16 pixels has been fabricated and used as an adaptive filter in the Fourier plane of a coherent optical processor. Preliminary results showing images of simple objects filtered through the SLM are presented. For comparison, images of the same objects obtained using photographic transparencies to simulate the action of the SLM as a filter are also presented.

Introduction

The procedures for Fourier analysis and synthesis of the radiation fields forming optical images in coherent light have been known for about a century. However, applications of spatial frequency filtering techniques in image enhancement and information processing tasks, though very effective, have been limited due to the cumbersome nature of the photographic or lithographic processes required for their implementation.[1,2] The recent progress in the development of two-dimensional spatial light modulators,[3,4] now makes possible the realisation of flexible adaptive processing systems and it is becoming increasingly attractive to investigate such processors and their potential uses in robotics and image-based industrial applications.

A prototype liquid-crystal-over-silicon spatial light modulator (SLM) is being developed in this laboratory for use in the input plane or in the Fourier plane of a coherent optical processor. The SLM operates in the reflection-mode and has a pixellated structure in the form of a square array of mirrors, whose effective reflectivity is controlled by the liquid crystal layer. For efficient information processing, it is necessary to match discrete regions of the radiation field across the light beam incident on the SLM with the fixed areas of its pixels, so that the information content of the light beam is sampled effectively. Also the inherent pixellation of the filter imprints a characteristic modulation on the coherent light beam carrying the information through the processor. We have investigated these aspects using photographic transparencies to simulate the SLM.

Later in this article we present a few simple examples of optical images, which have been filtered in the Fourier plane using transparencies, to illustrate the limitations imposed by the structure of the SLM, namely, filtering with low efficiency over a small aperture. We also present some preliminary results showing the output images obtained by filtering the coherent light from the same objects using the actual SLM. First of all we briefly describe the construction and principle of operation of the SLM in the next section.

The liquid-crystal-over-silicon spatial light modulator

The silicon backplane

The backplane consists of a 16 x 16 array of pixels, each covering an area of 200 x 200 μm^2 and carrying a mirror 110 x 110 μm^2 on the surface of the silicon chip. The mirror is formed during normal wafer fabrication by evaporating a layer of aluminium - copper - silicon (95%: 4%: 1%) alloy on top of a thin silicon oxide layer which has been grown on the wafer surface at an earlier stage in the processing. The oxide layer insulates the aluminium mirror from the substrate, while maintaining the surface flat to within ± 25 nm as judged by white light interferograms. The VLSI circuitry, which does of course spoil the originally flat silicon surface, is confined to the region around the pixel mirror.

The mirror also acts as an electrode for transmitting electrical voltages to the overlying liquid crystal layer. The VLSI circuitry associated with each pixel contains a static memory cell, as indicated in figure 1. The stable (d.c.) output signal from the memory cell is mixed with a universal clock signal in an XNOR gate to generate the a.c. drive signal required for the liquid crystal element immediately above the pixel mirror. To set up an image pattern in the liquid crystal layer, the appropriate array of logic signals is loaded into the memory cells addressed a row at a time (but in a random order if need be) via a special interface connected to the 8-bit port of a microcomputer. Details of the interface and an assessment of the electrical performance of the VLSI backplane have already been published.[5]

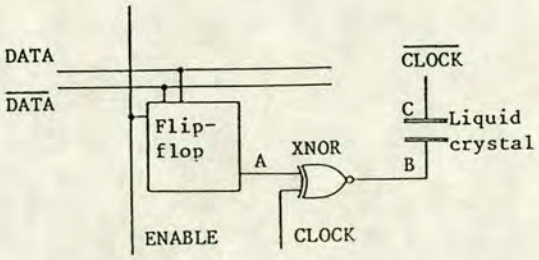

Truth table				Nominal voltage difference between B and C	Liquid crystal state
A	Clock	B	$\overline{\text{Clock}}$		
0	0	1	1	0	OFF
0	1	0	0	0	OFF
1	0	0	1	-5	ON
1	1	1	0	+5	ON

Figure 1. Functional diagram of the pixel circuitry, truth table for logic signals at the nodes indicated, and polarity of voltage signals appearing across the liquid crystal pixel.

The liquid crystal layer

The liquid crystal layer over the VLSI array is formed by mounting a glass cover over the silicon backplane with an intermediate spacer of 12.0 ± 0.1 μm thick polyester to create a cell which is then filled with liquid crystal, see figure 2. The inner surface of the glass cover (a cube of 5 mm side) is coated with a transparent indium tin oxide (ITO) film[6] which is connected to an aluminium contact evaporated onto the side of the cube. Voltage signals are applied across the liquid crystal pixel via the ITO electrode on the glass cover and the mirror electrodes on the VLSI backplane. The front face of the glass cover is coated with an anti-reflection coating matched for He-Ne laser light.

The cell is filled, by capillary action, with a guest-host liquid crystal mixture (Roche type 1263), which consists of a mixture of nematic material (RO-TN-3010) as host doped with a blue dye (2.5% concentration) as guest.[7] [This mixture is used since earlier measurements of the intensity of light transmitted through test cells have shown that contrast ratios above 1000:1 can be achieved between the ON and OFF states for polarised He-Ne laser light.] Both the ITO film and the VLSI backplane have their surfaces treated with rubbed PVA to secure the alignment of the liquid crystal molecules at the cell boundaries. The spatial light modulator is assembled with the rubbing directions on the PVA surfaces at right angles, so that in the quiescent state the liquid crystal molecules form a helical structure with ideally the director always parallel throughout the cell to the electrode surfaces and its orientation twisting through an angle of π/2 between the front and rear electrodes, as in a conventional twisted nematic arrangement.

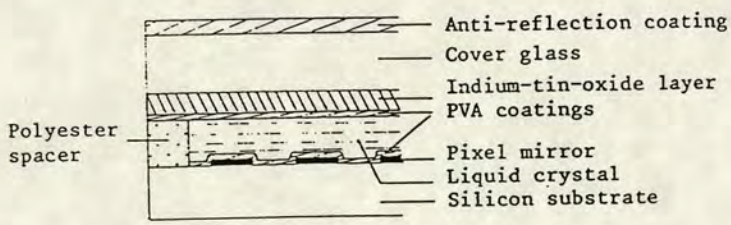

Figure 2. The structure of the spatial light modulator.

SLM operation

The operation of the guest-host liquid crystal layer as a light modulator exploits the polarisation guiding properties of the helical structure of the liquid crystal layer in its quiescent state.[8] When plane polarised light is incident normally with its polarisation vector aligned parallel, as in this case, (or exactly perpendicular) to the director at the front ITO electrode of the SLM, the light propagates with the polarisation vector always parallel (or perpendicular) to the director throughout the liquid crystal layer. The dye molecules exhibit a large anisotropy in their differential absorption coefficient for the He-Ne laser light used in the optical processor. Also the intermolecular forces between the dye and liquid crystal molecules cause the dye molecules to align preferentially parallel to the director of the liquid crystal structure. The resulting strong correlation between the orientations of the dye molecules and the polarisation vector of the light ensures that the light is strongly absorbed as it travels through the guest-host mixture.

The liquid crystal pixels are driven by an a.c. signal applied to the ITO electrode, which is logically the complement of the universal clock signal on board the VLSI chip. The universal clock signal is a square wave train oscillating at a frequency of 1 KHz between voltage levels at 0 V and +5 V.

When a pixel is programmed to store a logic "0", the XNOR arrangement in the VLSI circuitry ensures that the voltage signals on the pixel mirror and the ITO counter electrode are in phase (figure 1), and as a result no electric field is generated in the liquid crystal. The liquid crystal layer remains in, or returns to, the quiescent state; light propagating through the guest-host mixture is strongly absorbed; and therefore little light is reflected from that pixel.

On the other hand, when a logic '1' is stored in a memory cell, the signals on the mirror electrode and the counter electrode are π out of phase (figure 1). In this case an electric field is established in the liquid crystal layer and the field reverses direction on each clock transition. The electric field disrupts the helical structure in the liquid crystal layer, thereby destroying the close alignment between the axes of the dye molecules and the polarisation vector of the light. The light is absorbed only weakly, and there is a strong reflection from the pixel mirror.

The SLM is assembled in a 40 pin dual-in-line IC package and weighs about 8 grams. It is easily mounted, therefore, in an optical processor. The support electronics are modest, since the SLM has its own internal memory. Once a pattern has been loaded into the pixel array, only power and a clock pulse train need be supplied to the SLM in order to maintain that pattern indefinitely. Also the operating conditions of the VLSI chip, which is fabricated using a 6 µm nMOS process, may be changed easily to select clock signals of up to 100 KHz switching between 0 V and up to 10 V. The signal appearing across the liquid crystal layer may have, therefore, peak-to-peak values of up to 20 V. The liquid crystal settling time after a change of pattern is observed to be about 150 ms.

Filtering of 2-D Fourier transforms

Coherent optical processors for Fourier plane filtering

Various optical systems have been designed to perform the Fourier Transform operation on two-dimensional scenes, based on the properties of refracting[9] and reflecting[10,11] optical components. Usually two Fourier Transformers are cascaded so that a filtered image of the input scene is available in the output plane. The essential features of such systems for use with transmissive and reflective spatial light modulators as filters in the Fourier plane are illustrated in figure 3.

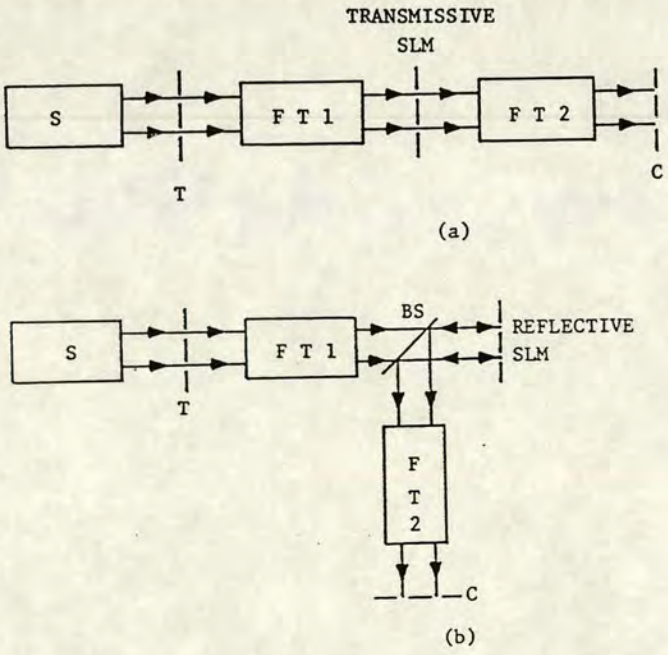

Figure 3. Schematic diagrams of (a) transmissive and (b) reflective coherent optical processors for Fourier plane filtering.

In both cases a source S of monochromatic, coherent light illuminates a transparency T of the input scene and the Fourier Transformer FT1 produces the required transform in the plane of the SLM. In figure 3(a) the light transmitted by the SLM passes through a second Fourier Transformer FT2 to produce the filtered image of the input scene in the output plane C. In figure 3(b), the light reflected from the SLM is steered by the beam splitter BS through a second Fourier Transformer FT2 to form the output image at the plane C. [In passing we point out that the reflective SLM could also be used in a suitable arrangement to create the input scene from electronically stored data.]

Filtering using photographic simulations of SLM

In order to assess the potential for Fourier plane filtering of using a 16 x 16 pixellated filter and to provide "benchmarks" with which to compare the performance of the SLM described above, we have simulated the action of the SLM as a filter using photographic transparencies.

A binary amplitude filter corresponding to the SLM operating with all pixels ON was constructed by photographing a 16 x 16 array pattern drawn using computer graphics. The photographic filter has transparent regions 90 x 90 μm^2 at a repeat distance of 200 μm corresponding to pixel mirrors of 110 x 110 μm^2 spaced 200 μm apart on the actual SLM. It is assumed for simplicity that the areas surrounding the pixel mirrors on the SLM reflect little light, and that a pattern of clear and opaque regions provides, therefore, a good representation of the SLM as a filter. This filter was mounted in the Fourier plane of a conventional 6-f coherent optical processor and used to filter the light from an object $T(x_1,y_1)$ in the form of a clear equilateral triangle of side 3 mm placed in the input plane. The filtered image $I(x_3,y_3)$ recorded photographically in the output plane is shown in figure 4. Of course, the photograph records the intensity distribution and not the complex amplitude distribution of the light in the output plane. The processor - of the type shown in figure 3(a) - performed the first transformation with a scaling factor (k/f) such that the Fourier Transform at the filter is $F(x_2,y_2)$, where

$$F(x_2,y_2) = \iint_A T(x_1,y_1)\exp\{ik(x_1x_2 + y_1y_2)/f\}dx_1dy_1.$$

Here the wave number for He-Ne light is $k = 1.0 \times 10^7\ m^{-1}$; the effective focal length of the Fourier transformer is $f = 1.0$ m; and the area of the aperture in the input plane over which the integration is performed is $A = 5 \times 5\ mm^2$. The second transformation carried out by the processor had similar parameters.

An edge-only triangle of side 3 mm was used as an object and the images recorded in the output plane using photographic filters in the Fourier plane to simulate the SLM with all pixels ON and with all pixels ON EXCEPT FOR THOSE IN THE EIGHTH AND NINTH COLUMNS. The filtered images are illustrated in figures 5(a) and 5(b) respectively.

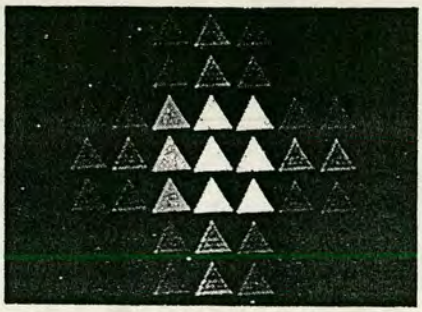

Figure 4. Image, recorded in the output plane, of a clear equilateral triangle of side 3 mm placed in the input plane and filtered in the Fourier plane by a photographic transparency representing the SLM with all pixels ON.

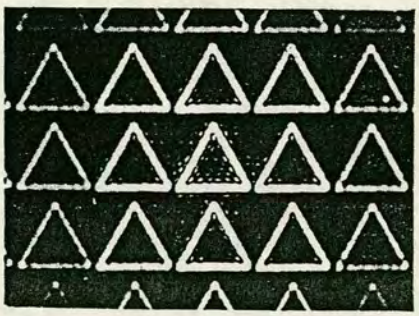

(a)

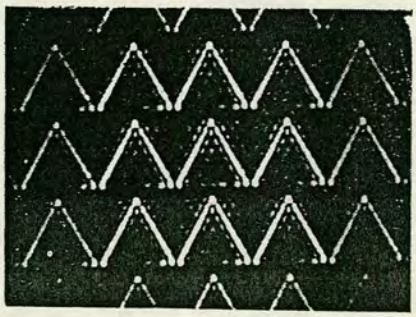

(b)

Figure 5. Image, recorded in the output plane, of an edge-only equilateral triangle of side 3 mm placed in the input plane and filtered in the Fourier plane by a photographic transparency representing the SLM with (a) all pixels ON and (b) all pixels ON EXCEPT THOSE IN THE EIGHTH AND NINTH COLUMNS.

The photographs in figures 4 and 5 exhibit clearly the aliasing (i.e. the replication of the primary image) which is a feature always associated with the use of pixellated array filters in the Fourier plane. Also the 256 pixel array, covering an area of 3.2 x 3.2 mm^2, acts as a low pass filter for the spatial frequency spectrum of the coherent light from the input scene. This is manifest by the lack of sharpness of the edges in figures 4 and 5. The appearance in such images of interference "structures" is a real effect produced by the filtering process, although in this case there may be additional contributions due to phase noise introduced by the use of a photographic transparency as the input. As expected, blocking the central, vertical strip of the filter in the Fourier plane removes the horizontal base of the triangle as seen in figure 5. Also as the strip passes through the central region of the Fourier plane, the low frequency components in the spatial frequency spectrum of the light from all regions of the input scene are suppressed. Thus switching off the pixels in the eighth and ninth columns greatly reduces the intensity of the light transmitted through the processor to form the image in the output plane. The SLM acts as a band-pass filter in this case.

Filtering using the 16 x 16 liquid-crystal-over-silicon SLM

The prototype liquid-crystal-over-silicon SLM was mounted in the Fourier plane of a coherent optical processor of the type shown in figure 3(b). The photographs in figures 6(a) and 6(b) illustrate the images of the clear triangle obtained when filtered by the SLM with all pixels ON and with all pixels OFF. The contrast between ON and OFF states is very good, but unwanted reflections of light from the front and rear surfaces of the cover glass produce the strong spurious image present in both figures.

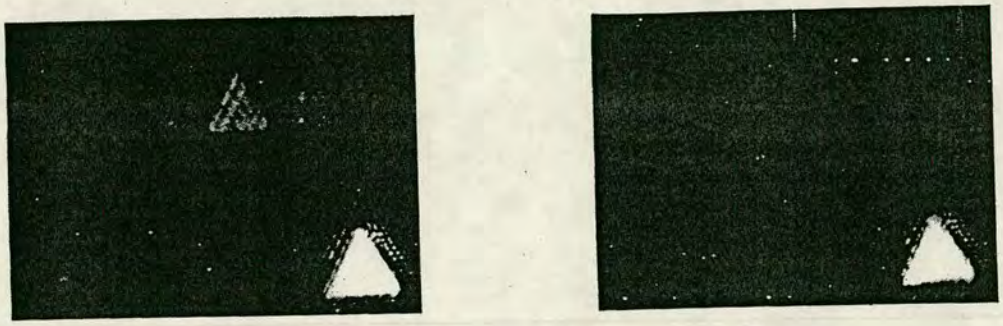

(a) (b)

Figure 6. Image, recorded in the ouput plane, of a clear equilateral triangle of side 3 mm placed in the input plane and filtered in the Fourier plane using the actual SLM with (a) all pixels ON and (b) all pixels OFF. For purposes of comparison, both photographs were obtained under identical conditions and exposure times. (Figures 4 and 6 were recorded under different conditions.)

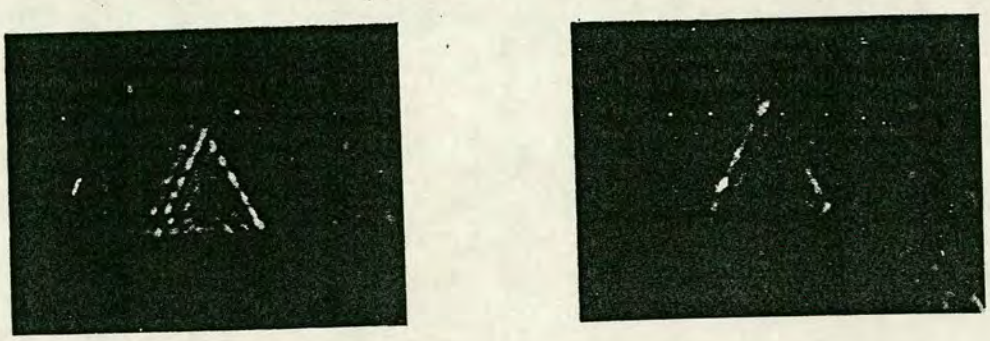

(a) (b)

Figure 7. Image, recorded in the output plane, of an edge-only equilateral triangle of side 3 mm placed in the input plane and filtered in the Fourier plane by the actual SLM with (a) all pixels ON and (b) all pixels ON EXCEPT THOSE IN THE EIGHTH AND NINTH COLUMNS. Different exposure times were used in (a) and (b); see discussion of signal-to-noise ratios in text. (Figures 5 and 7 were recorded under different conditions.)

The edge-only triangle was placed in the input plane and the images recorded with the SLM programmed to have all pixels ON and then to have all pixels ON EXCEPT THOSE IN THE TWO CENTRAL, VERTICAL COLUMNS. The observed images are presented in figures 7(a) and 7(b); the corresponding simulations are those in figures 5(a) and (b). The filtering action of the SLM in the Fourier plane is clearly observed, but the quality of the images is not nearly so good as for the simulations.

When the actual SLM is used as the filter, the coherent light beam carrying the information through the processor is attenuated by the SLM itself and also by the associated polariser. Relative to the simulation studies, longer exposure times are required to record the weaker signals and therefore the photographs in figures 6 and 7 record any noise inherent in the optical system integrated over the longer period. More significant, however, are the contributions to the noise introduced by the spurious reflections occurring at the front and, to a lesser extent, the rear surfaces of the glass cover of the SLM. If these surfaces acted as perfectly flat reflectors, not parallel to each other nor to the surface of the silicon backplane, we would expect simply to observe two additional "ghost" images of the input scene; see figure 6. Unfortunately when dicing the glass sheet to make the front electrodes for this batch of prototype SLMs, the anti-reflection coating on the front surface was severely damaged. In use as a Fourier plane filter, light is scattered from the rough surface at the front face of the SLM resulting in a re-distribution of the light intensity to other regions of the output plane. This scattered light appears as noise in figures 6 and 7.

The noise is most prominent in figure 7(b). This occurs because in this case the SLM suppresses the low frequency components in the spatial frequency spectrum from all regions of the input scene as well as the higher frequency components which are associated predominantly with the horizontal base of the edge-only triangle. The intensity of this band-pass filtered signal is greatly reduced relative to the intensity of the low-pass filtered signal in figure 7(a). The noise contributed by the light scattering at the cover glass is not attenuated by the filtering action of the liquid crystal layer in the SLM, and therefore the signal-to-noise ratio is much reduced.

Discussion and conclusion

The performance of a SLM in the Fourier plane of a coherent optical processor provides a very stringent test of the optical quality of the device, in that both the amplitude and the phase of the coherent light must be controlled precisely and uniformly across the whole active area of the modulator. The present investigation indicates that useful Fourier plane filtering can be achieved with liquid-crystal-over-silicon spatial light modulators, but that high quality optical performance is very important. The results obtained using the photographic transparencies illustrate the image quality which should be attainable from high performance spatial light modulators even with a relatively small number of pixels.

The fabrication of SLMs with undamaged anti-reflection layers to eliminate the spurious scattering, which so severely degrades performance, is underway. Research is being pursued to improve the performance of the liquid crystal layer as a light modulator, and the development of a silicon backplane with a much greater number of smaller pixels is well advanced using the new 1.5 μm nMOS process at the Edinburgh Microfabrication Facility. (The device described here was fabricated using a 6 μm nMOS process.) Work is also in progress on a variable magnification processing bench which enables the scale of the Fourier Transform distribution to be matched to the dimensions of the pixels in order to achieve more efficient and effective filtering.

Acknowledgements

We wish to thank Mr. A. Kurzfeld, Rutherford-Appleton Laboratory, Professor J.M. Robertson, Edinburgh Microfabrication Facility and the staff of both institutions for their generous assistance with VLSI computer design tools, mask-making and wafer fabrication. We gratefully acknowledge the financial support for this project received from the U.K. Science and Engineering Research Council. We are also grateful for the award of studentships for periods of two years each from the U.K., S.E.R.C., and for financial support for a further year each from the Trustees of the Dewar Fund within the University of Edinburgh (I.U., and P.H.W.). We thank Messrs H.J. Stevens, A. Garrie and E. Davidson of our department for their technical assistance with liquid crystal cell fabrication. Finally we record our appreciation of the support and encouragement received from Professors R.A. Cowley and D.J. Wallace and from Drs. G. Bradford, R.C. Dougal, N.E. Fancey and the other members of the Applied Optics Group, who are all contributing to the successful progress of this project.

References

1. Cutrona, L.J., Leith, E.N., Palermo, C.J. and Porcello, L.J., "Optical Data Processing and Filtering Systems", IRE Trans. Inf. Theory, pp.386-400. June 1960.
2. Van der Lugt, A., "Coherent Optical Processing", Proc. IEEE, Vol. 62, pp.1300-1319. 1974.
3. See articles in Opt. Eng. (Spatial Light Modulators: critical issues), Vol. 22. 1983.
4. Fisher, A.D. and Lee, J.N., "The Current Status of Two-Dimensional Spatial Light Modulator Technology", Proc. SPIE, Vol. 634, pp.352-371. 1986.
5. Underwood, I., Vass, D.G. and Sillitto, R.M., "Evaluation of an nMOS VLSI Array for an Adaptive Liquid-Crystal Spatial Light Modulator", IEE Proc.J.: Opto-electronics, Vol. 133, pp.77-82. 1986.
6. Optical and Electronic Coatings (1982) Ltd., Wills Road, Industrial Road, Totnes, Devon, England. TQ9 5XR.

7. Roche: "Liquid Crystal Data Sheet", Ko/sg/0065z/ F. Hoffmann-La Roche and Co., Liquid Crystal Group, R.L.C., CH-4002, Basle, Switzerland, 1984.
8. Vass,D.G., Dougal, R.C., Weir, K. and MacGregor, A.R., "Light Transmission Through Twisted Nematic Liquid Crystal Cells", Proc. SPIE, Vol. 651, pp.112-119. 1986.
9. Goodman, J.W., "Introduction to Fourier Optics", Pub. McGraw-Hill, 1968.
10. Ih, C.S. and Yen, K., "Imaging and Fourier Transform Properties of an All Spherical Mirror System", Appl. Opt., Vol. 19, pp.4146-4149. 1980.
11. Nickolov, I.D., "Fourier Transform Properties of an All Mirror System", Opt. Acta., Vol. 25, pp. 1175-1178. 1982.

PROGRESS IN DEVELOPING VLSI BASED SPATIAL LIGHT MODULATORS

D.G. Vass, R.M. Sillitto, I. Underwood, D.J. McKnight, P.H. Willson and M.J. Ranshaw.

Introduction

The development of high quality spatial light modulators (SLMs) is essential for the realisation of real-time optical information processing systems and optical computers. In particular for those systems where the information is carried by coherent light, the 2-D SLM must impose precisely controlled amplitude and phase modulations on the coherent light beam. In this contribution we discuss the development of VLSI nMOS arrays as the pixel-addressing components in devices, and describe amplitude-only and phase-only SLMs which may be constructed using these nMOS arrays.

Prototype 16x16 pixel liquid-crystal-over-silicon SLM

A 16 x 16 pixel array on a 7 x 7 mm^2 silicon chip has been designed using the VLSI design and mask-making facilities at the Rutherford-Appleton Laboratory (RAL) and fabricated using the 6 μm nMOS process at the Edinburgh Microfabrication Facility (EMF). The pixels are spaced 200 μm apart and each carries a metal pad, insulated from the silicon substrate by an oxide layer, which acts both as an output electrode and as a mirror. The pixel mirrors 110 x 110 μm^2 are flat to within ± 25 nm as judged by white light interferograms obtained using a LINNICK interferometer at Imperial College. A prototype SLM has been fabricated using a guest-host liquid-crystal mixture on the surface of the silicon as the light modulating medium. The VLSI array is addressed as a static random access memory (1 bit deep), and the liquid crystal above each pixel mirror activated to absorb or transmit light according to whether the datum stored in the array element is a logic '0' or a logic '1'. An assessment of the electrical performance of the VLSI array has already been published[1], and the use of the SLM as a binary-amplitude filter in the Fourier plane of a coherent optical processor is being investigated[2].

Development of a 128 x 128 pixel liquid-crystal-over-silicon SLM

Following the successful testing of the 16 x 16 prototype SLM, research has been initiated to fabricate a 128 x 128 nMOS array using a more compact integrated circuit technology. A schematic diagram of the circuitry associated with each pixel in the array is shown in figure 1. A 128 bit data word is applied via shift registers to the 128 inputs of the rows of the pixel array and a sequence of read/hold pulses is applied to each of the 128 column inputs, again by means of shift registers. In this way a logic signal is loaded into each pixel circuit and the datum stored as a voltage level at the node D, figure 1. The voltage signal fed to the mirror electrode to activate the overlying liquid-crystal layer is derived by mixing a universal clock signal with the logic signal at node D. The complement of this clock signal, $\overline{clock}$, is fed to the transparent counter electrode which encapsulates the liquid crystal on top of the IC. With this arrangement, as indicated in the truth table of figure 1, the liquid

The Authors are with the Physics Department, Edinburgh University. Mayfield Road, Edinburgh. EH9 3JZ.

crystal experiences an alternating electric field when the voltage level at node D is nominally +5V, whereas no field is generated when the voltage level is zero.

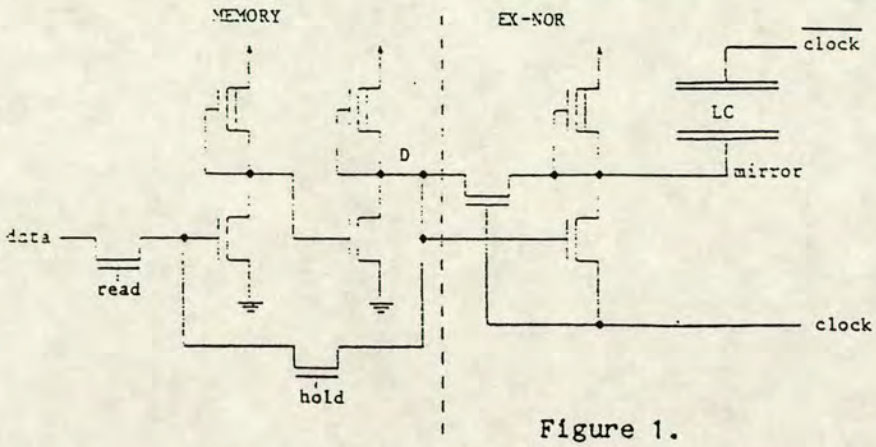

D	ck	mirror	$\overline{ck}$	LC
0	0	1	1	OFF
0	1	0	0	OFF
1	0	0	1	ON
1	1	1	0	ON

Figure 1.

The layouts for a 12 level mask set carrying test structures for this second generation SLM have been produced, and X10 reticles procured through the Silicon Brokerage at RAL. The fabrication of wafers is well advanced using the 1.5 μm nMOS process being developed at the EMF. A block diagram showing the disposition of test structures on the 1 x 1 cm^2 IC surface is given in figure 2; as indicated a 50 x 50 array is included in the top left hand quadrant for test purposes. This array has mirrors of area 45 x 44 μm^2 with the mirror centres 74 μm apart, which means that the mirror surfaces cover just over 33% of the area of the array.

It is intended to construct a SLM for use as a binary-amplitude filter by establishing a 45° twisted nematic arrangement, as described by Grinberg[3], on the surface of the chip. Measurements of the intensity of light reflected from test cells, constructed to simulate the operation of the reflective SLM, show that contrast ratios > 10^3 between the intensities reflected in the ON and OFF states may be obtained. Also the spurious reflections from the glass/ITO/liquid crystal interfaces, which degraded the performance of the guest-host liquid crystal arrangement used with the 16 x 16 pixel SLM[2], may be rejected using the 45° twisted nematic scheme.

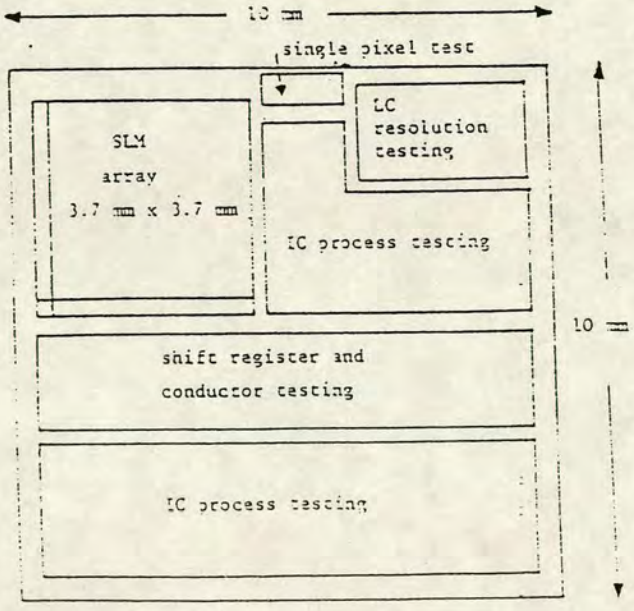

Figure 2.

Development of a deformable-mirror-over-silicon SLM

A phase modulating SLM may be constructed using a deformable mirror to control the lengths of the optical paths travelled by coherent light through the device, as described by Pape and Hornbeck[4]. The imagewise deflection of a deformable mirror may be accomplished using a modified version of either one of the VLSI arrays described above. The structure of a typical deformable-mirror device based on a VLSI array is illustrated in figure 3. An insulating layer of photoresist - 3 μm thick is deposited on the surface of the wafer and "wells" formed in the insulator by etching away the photoresist above the metal electrodes. A thin membrane of nitrocellulose 300-400 nm thick is formed and a layer of aluminium - 30 nm thick evaporated onto one surface. This thin, reflecting, electrically conducting membrane is then stretched across the surface of the integrated circuit and covers each of the "wells" as indicated in figure 3. A static voltage V_m is applied to the aluminium mirror on the membrane and, by applying a steady clock signal to the pixel array, a voltage V_p is applied to the pixel electrode: $V_m \approx 25$ V; $V_p \approx$ 0V or 5V. The local potential difference $(V_m - V_p)$ between each pixel electrode and the aluminium mirror determines the deformation profile of the membrane which is deflected into the well from its equilibrium position. The maximum deflection D of the deformed mirror is given approximately by $D = K(V_m - V_p)^2$, where K is a constant whose value depends on the pixel geometry and the elastic properties of the membrane. The change ΔD in the maximum deflection caused by a change of pixel voltage ΔV_p is given, therefore, by $\Delta D = K\,\Delta V_p(2V_m - \Delta V_p)$. Obviously the dynamic range of the device may be tuned by adjusting the bias voltage V_m.

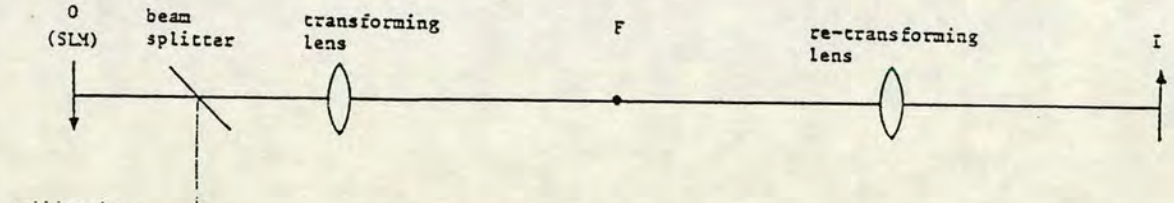

Figure 3.

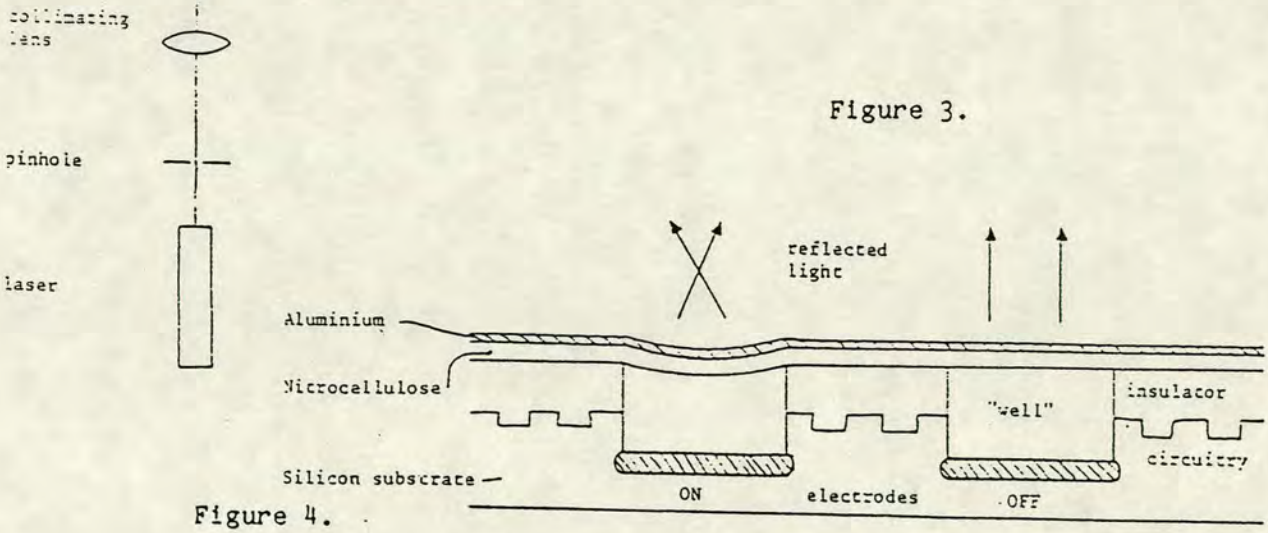

Figure 4.

In order to render visible the phase variations imposed on a coherent light beam by the deformable-mirror SLM under test, the SLM is mounted in the input plane 0 of the Schlieren type optical processing system shown in figure 4. A plane, parallel beam of monochromatic coherent light is

incident on the SLM, and the Fourier transform of the light reflected from its surface formed in the Fourier plane F by the transforming lens. A filtered image of the light is formed in the output plane I by the re-transforming lens. For a perfectly flat mirror most of the light in the Fourier plane is confined to a spot on the axis, where a stop is placed. Any deformation of the mirror causes the light to by-pass the stop and to form in the output plane a visible "image" of the deformed region of the mirror.

The basic principles of operation have been checked using the 16 x 16 pixel array as the backplane. Further work is in progress to improve the metalisation of the membrane, and the tensioning of the membrane over the surface of the integrated circuit.

Conclusion

VLSI circuits, carrying pixellated mirror structures with on-board static memory to support independent addressing of each pixel, are providing versatile backplanes for SLM development. nMOS arrays are capable of operating at frequencies above 1 MHz, and with currently used processing technology statically-addressed pixels with minimum dimensions of ~ 75 x 75 μm^2 are attainable. As the microelectronics industry develops robust sub-micron fabrication processes, smaller pixel structures will become available. We are also considering the fabrication of binary phase only modulators by controlling the refractive index variations in parallel nematic structures above the silicon backplane.

Acknowledgements

The support received from SERC for this project and for research studentships is gratefully acknowledged, as is the supplementary support from the Dewar Fund, Edinburgh University. We wish to thank Mr. A. Kurzfeld, RAL, and Professor J.M. Robertson, EMF, and the staff of both institutions for their generous assistance. We are also grateful to Professor C.J. Dainty for granting us access to the LINNICK interferometer at Imperial College. The work on the 128 x 128 liquid-crystal-over-silicon SLM is being carried out in association with STL Ltd., Harlow. Finally we record our appreciation of the encouragement, helpful advice and technical assistance from our colleagues in the Physics Department.

References

1. UNDERWOOD, I., VASS, D.G. and SILLITTO, R.M.: "Evaluation of an nMOS VLSI array for an adaptive liquid-crystal spatial light modulator", IEE Proc. J.: Opto-electronics, Vol. 133, pp 77-82, 1983.

2. UNDERWOOD, I., WILLSON, P.H., SILLITTO, R.M. and VASS, D.G.: "An adaptive Fourier optical processor", Proc. SPIE, Vol. 860, paper 01, 1987.

3. GRINBERG, J., JACOBSEN, A., BLEHA, W., MILLER, L., FRAAS, L., BOSWELL, D., MYER, G.: "A new real-time Non-coherent-to-coherent light image converter. The hybrid field effect liquid crystal light valve", Hughes Reserach Labs., Opt. Eng., Vol. 14, pp 217-225, 1975.

4. PAPE, D.R. AND HORNBECK, L.J.: "Characteristics of the deformable mirror device for optical information processing", Opt. Eng., Vol. 22, pp 675-681, 1983.

Fresnel zone approach to self-Fourier transforming

Paul H. Willson

University of Strathclyde, Department of Physics & Applied Physics, Glasgow G4 0NG, Scotland, U.K.

Received 25 June 1990.
0003-6935/91/080912-03$05.00/0.

The phenomenon of self-imaging and (in the case of coherent illumination) self-Fourier transforming was first observed over a century and a half ago. [H. Talbot, "Facts Relating to Optical Science NoIV.," Philos. Mag. 9, 403–407 (1836).] There has since been a steady stream of publications in which the phenomenon has been noted and a theoretical analysis presented. Most noteworthy of these papers in recent years have been those by Kolodziejczyk, Kalestynski, and Smolinska. [A. Kolodziejczyk, "Realization of Fourier Images Without Using A Lens By Sampling The Optical Object," Opt. Acta. 32, 741–746 (1985); and A. Kalestynski and B. Smolinska, "Multiple Image Formation By Sampling Fraunhoffer Diffraction Patterns," Opt. Acta. 24, 1115–1124 (1977).]

Kolodziejczyk has described the case in which a self-Fourier transform of an object is obtained by illuminating with coherent monochromatic light the object sampled by a pinhole array.[1] It is the purpose of this Technical Note to draw attention to the fact that such a sampling array of pinholes may be considered as a pixelated Fresnel zone plate.

Let us first consider the theory as presented by Kolodziejczyk. Figure 1 is a schematic diagram showing the object, pinhole array, and Fourier transform plane. A rectangular array of infinitesimally small pixels may be represented by the transmission function

$$t_o(x_o,y_o) = \sum_{m=-\infty}^{\infty}\sum_{n=-\infty}^{\infty} \delta(x_o - ml, y_o - nl) = \frac{1}{l^2}\,\mathrm{comb}\left(\frac{x_o}{l}, \frac{y_o}{l}\right), \quad (1)$$

where l is the pixel separation and m and n are integers. An object in the same plane as the pixels may be denoted by $U_o(x_o,y_o)$. The complex amplitude in the $z = d$ plane may be represented by the Fresnel diffraction integral and written

$$U_1(x,y) = \frac{\exp(ikd)}{i\lambda d}\exp\left[\frac{ik}{2d}(x^2+y^2)(+\infty)\right]\iint_{-\infty}^{+\infty} U_o(x_o,y_o) \times \sum_{m=-\infty}^{\infty}\sum_{n=-\infty}^{\infty}\delta(x_o - ml, y_o - nl)\exp\left[\frac{ik}{2d}(x_o^2+y_o^2)\right] \times \exp\left[-\frac{ik}{d}(xx_o + yy_o)\right]dx_o dy_o. \quad (2)$$

This is the Fourier transform of the product

$$U_o(x_o,y_o)\sum_{n=-\infty}^{\infty}\sum_{m=-\infty}^{\infty}\delta(x_o - ml, y_o - nl) \quad (3)$$

if the condition

$$\exp\left[\frac{ik}{2d}(x_o^2 + y_o^2)\right] = 1 \quad (4)$$

is fulfilled.

We see that for this particular array or sampling filter,

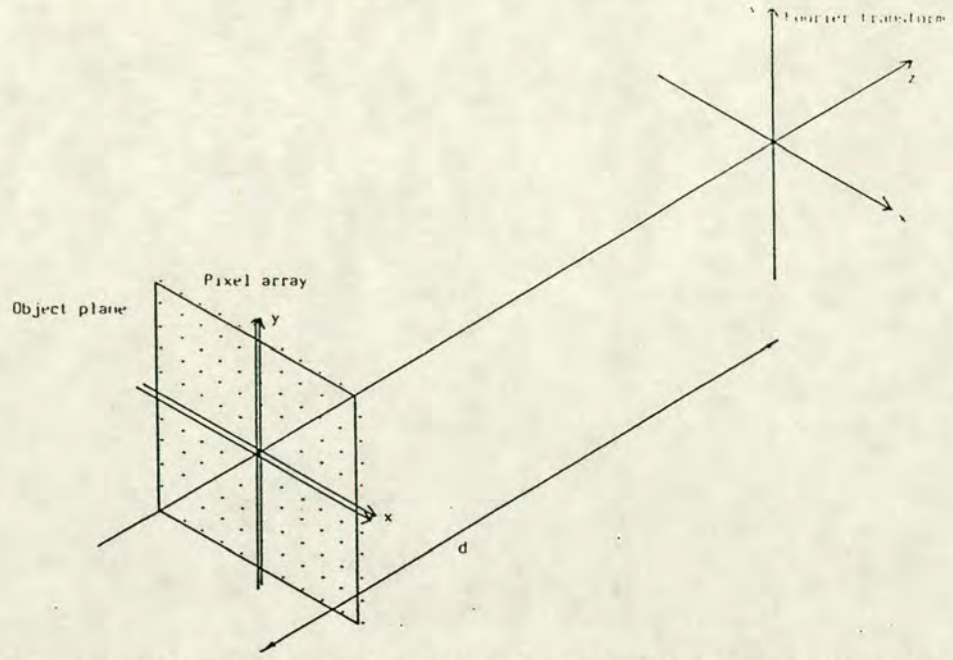

Fig. 1. Schematic diagram showing a 2-D object and pixel array in the same plane and the Fourier transform plane separated from them by a distance d.

$$x_o = ml, \qquad y_o = nl, \tag{5}$$

and thus the conditions for self-Fourier transformation from Eq. (4) become

$$d = \frac{l^2}{2\lambda N}, \tag{6}$$

where N is a positive odd integer.

Consider now the array of pinholes as a pixelated zone plate of the Soret type, that is, with zones either completely opaque or perfectly transparent. Figure 2 shows an array of pixels with Fresnel zone boundaries indicated. The radius of the central zone is the distance from the center of a group of four pixels to any one of those pixels. Let us call these four pixels the first shell. The distance is $\sqrt{(2l)}/2$. A zone plate with a central zone of this radius would have a primary focal length:

$$F = \frac{r^2}{\lambda} = \frac{l^2}{2\lambda}, \tag{7}$$

which is the focal length arrived at in Eq. (6) by a different method.

If we continue in this manner and consider other zone radii, we see that pixel shells do not fall on each zone boundary but on every fourth. Changing the zone radii by an infinitely small amount so that the first shell of pixels is included in either the center zone or the second zone and adjusting the other zone radii accordingly, we see that pixels only fall into zones which we would expect to be transparent in a zone plate of the same primary focal length. If we had chosen a pixel as the center of our zone plate structure, as shown in Fig. 3, we see that the same zone plate radii would include pixels in each alternate zone.

This type of analysis, although alluded to in the published literature, has not been given explicity.

When considering sampling arrays with pixels of finite size, the condition for the formation of the Fourier transform according to Kolodziejczyk becomes

$$\exp(2\pi i)\left\{\frac{(ml+\Delta)^2 + (nl+\Delta)^2}{2\lambda d}\right\} = 1, \tag{8}$$

where Δ is the radius of a pixel (assuming them to be circular).

For practical filters, this reduces to the inequality

$$\frac{2(m+n)N\Delta}{l} \ll 1, \tag{9}$$

which is satisfied if d is large or Δ/l is small.

Consider now a sampling array with square pixels with sides of length Δ as a pixelated zone plate. As shown in Fig. 4, where $\Delta/l = 0.5$, only one pixel falls completely into a zone. Pixels which fall across two or more adjacent zones have a diminished focusing effect as light from these zones destructively interferes. A set of sampling arrays for which Δ/l is progressively smaller will have more zones containing whole pixels, and, as with zone plates of increasing zone number, resolution will increase.[4]

The pixelated zone plate approach to this phenomenon may be extended to nonrectangular regular arrays. For example, an hexagonal array of pixels would also act as a pixelated zone plate, as it falls into the zone plate structure. Such an array would have a primary focal length given by

$$F = \frac{3l^2}{2\lambda}. \tag{10}$$

This result was shown by Bryngdahl[5] but determined by a different method.

As we would expect, sampling of the object by a pixelated zone plate causes replication of the Fourier transform in the focal plane. The intensity modulation of the focal plane is determined by the pixel size and shape. Both of these subjects have been described in great depth elsewhere.[6]

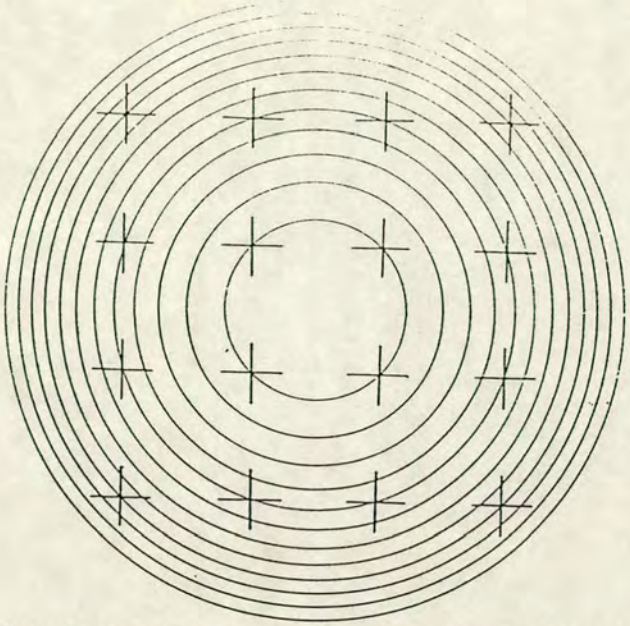

Fig. 2. Rectangular array of pixels (considered to be small and lying at the center of the crosses) with superimposed Fresnel zones.

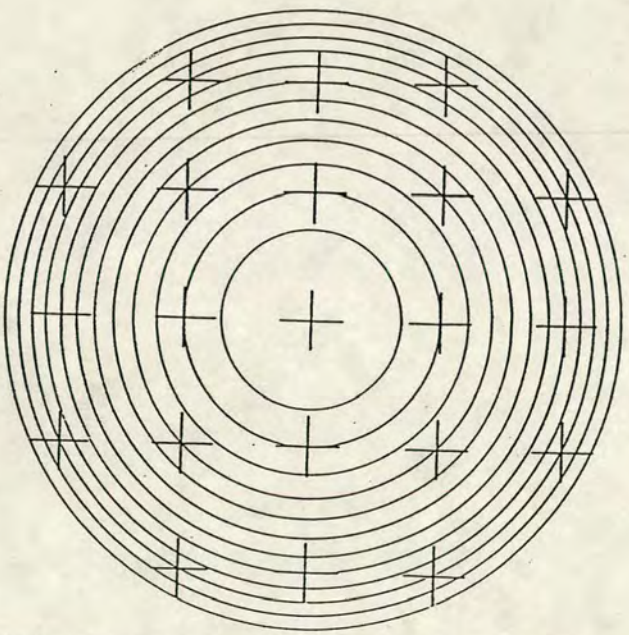

Fig. 3. Fresnel zones centered on a pixel. The pixel and zone spacing is the same as that in Fig. 2.

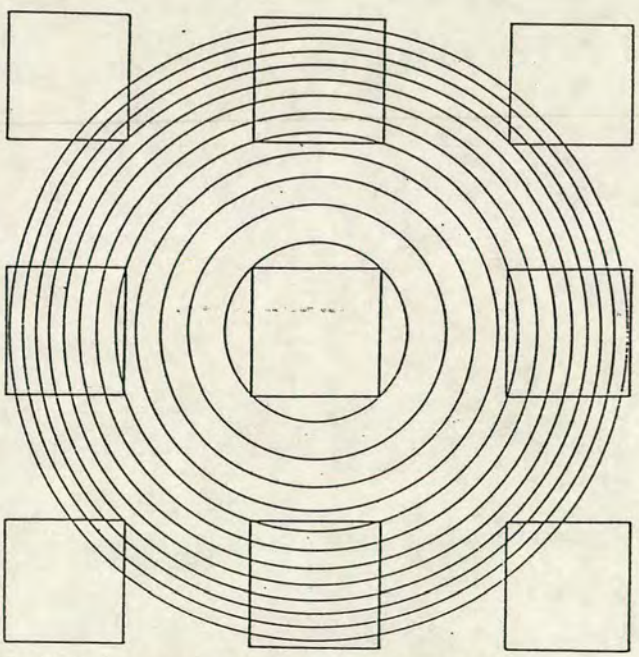

Fig. 4. Rectangular array of pixels with $\Delta/l = 0.5$ with a superimposed zone structure.

In conclusion, it should be noted that while the phenomenon of self-imaging and self-Fourier transforming by a rectangular or hexagonal array of pixels may be investigated using rigorous diffraction theory, in some cases the same results can be obtained by considering the array as a pixelated zone plate. Thus we may apply zone plate rules (which are analogous to lens formulas) to find focal planes and magnification.

I would like to thank R. M. Sillitto of the Applied Optics Group at the University of Edinburgh for his comments.

References

1. P. H. Willson, "Theory of the Fresnel Zone Plate," M.Sc. Dissertation, Reading (1985).

2. O. Bryngdahl, "Self-Imaging Techniques in Image Formation," J. Opt. Soc. Am. 63, 418 (1972).

3. J. W. Goodman, *Introduction to Fourier Optics* (McGraw-Hill, New York, 1968).

Appendix 4

Mask plots and specifications

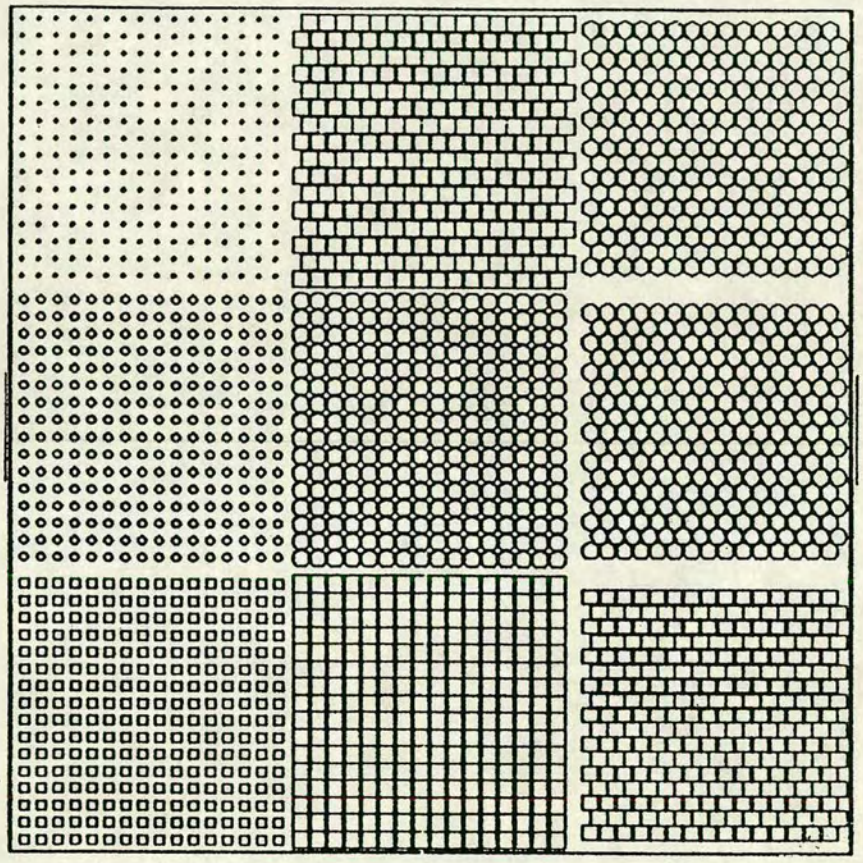

A plot of a mask to be used for the production of 9 pixelated mirror designs

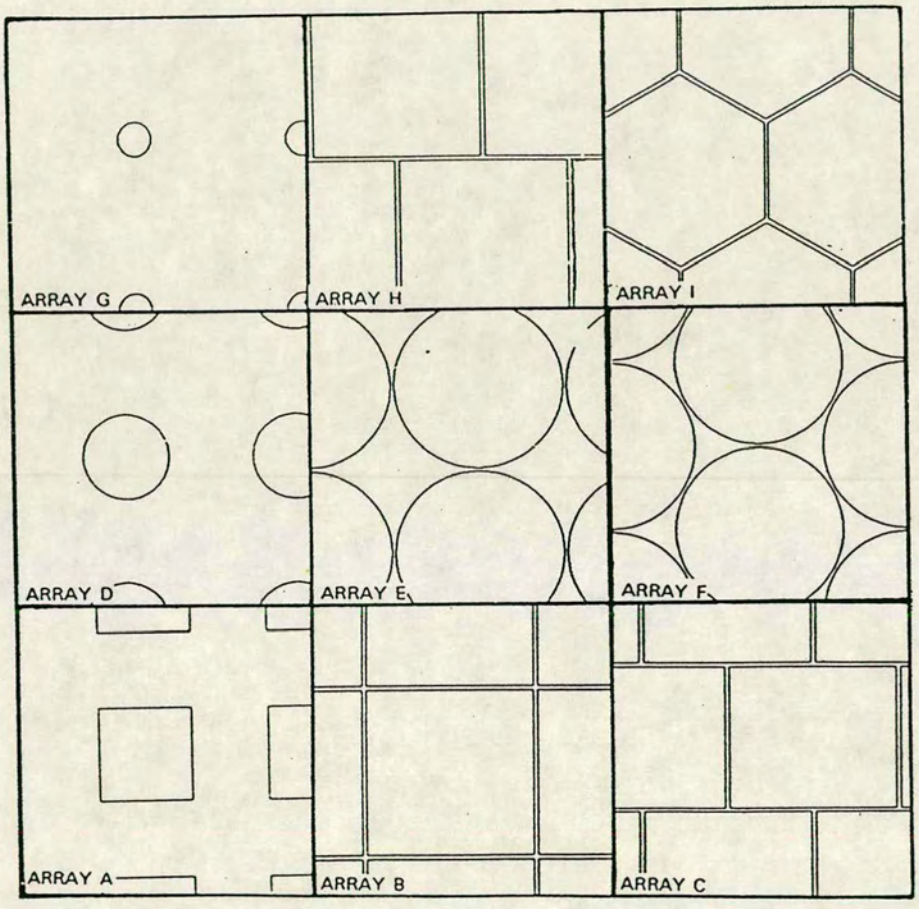

Magnified plots of the 9 designs.

A)16x16 square array of square mirrors 200 µm centre to centre horizontally and 200 µm centre to centre vertically (200-200 µm). 100x100 µm mirrors.

This mimics the 16x16 device already described with perfect shielding, to determine by comparison the actual degree of shielding achieved by the liquid crystal.

B)16x16 square array of square mirrors 200-200 µm centre to centre 196x196 µm mirrors.

A similar array to the previous one but with mirrors as large as possible. If the mirrors were made any larger there would be the possibility of their joining during fabrication.

C)15x16 hexagonal array of Rectangular mirrors 200-173 µm centre to centre 196x169 µm mirrors.

These are rectangular mirrors on a regular hexagonal lattice, again as closely packed as possible.

D)16x16 array of circular mirrors 200-200 µm centre to centre 100 µm diameter.

Circular mirrors replacing square ones in a cell of the same dimensions as previously.

E)16x16 square array of Circular mirrors 200-200 µms centre to centre, 196 µm diameter mirrors.

Circular mirrors of same diameter as the sides of the large square mirrors.

F)15x17 hexagonal array of circular mirrors 200-173 µms centre to centre 196 µm diameter mirrors.

Closest possible packing of circular mirrors with almost the same number of mirrors as the square array for comparison.

G)16x16 square array of circular mirrors 200-200 µm centre to centre 20 µm diameter mirrors.

Mirrors are as small as possible whilst still giving a reasonable reflection intensity.

H)15x17 hexagonal array of square mirrors 200-200 µms centre to centre 196x196 µm mirrors.

Array of large square mirrors with alternate rows shifted to investigate any increase in efficiency.

I)15x17 hexagonal array of hexagonal mirrors 200-173 µms centre to centre 196 µm mirrors A/F.

Hexagonal array of hexagonal mirrors which makes better use of space than the circular mirrors, but with higher symmetry than the square.

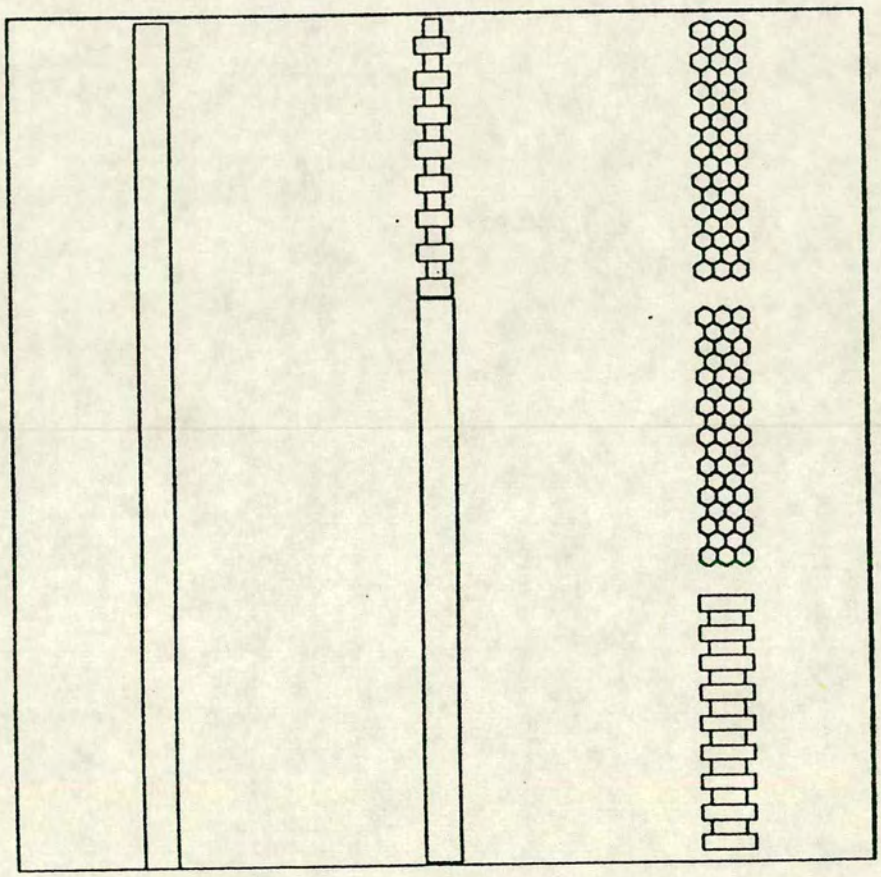

Leg filter (mask 1)

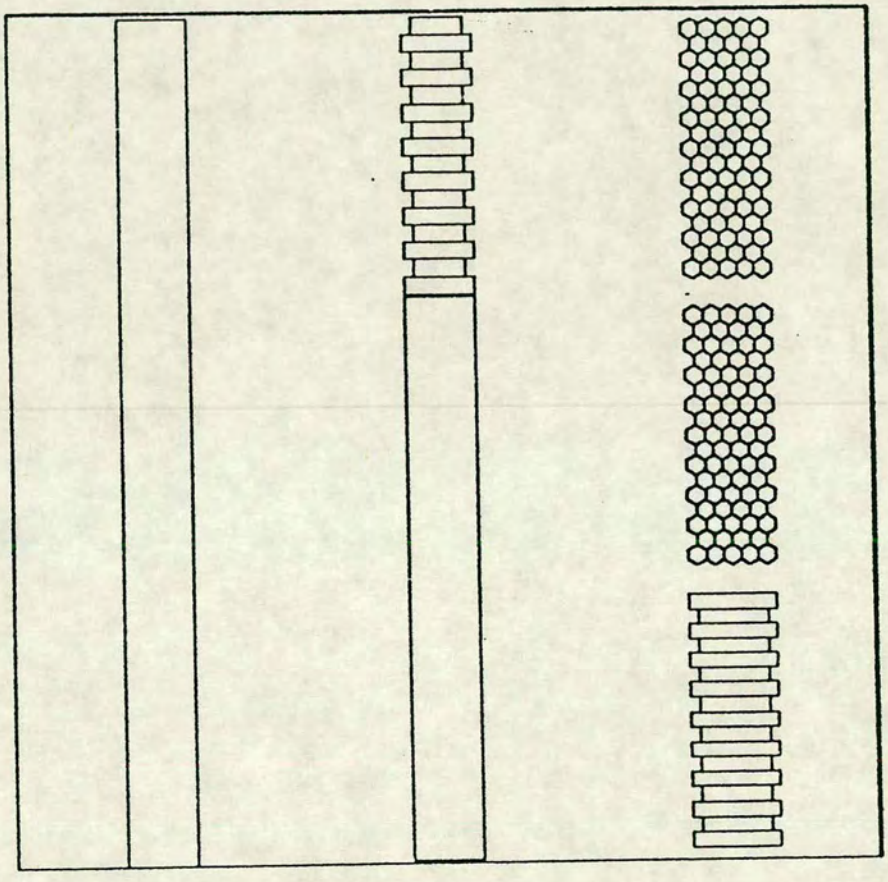

Leg filter (mask 2)

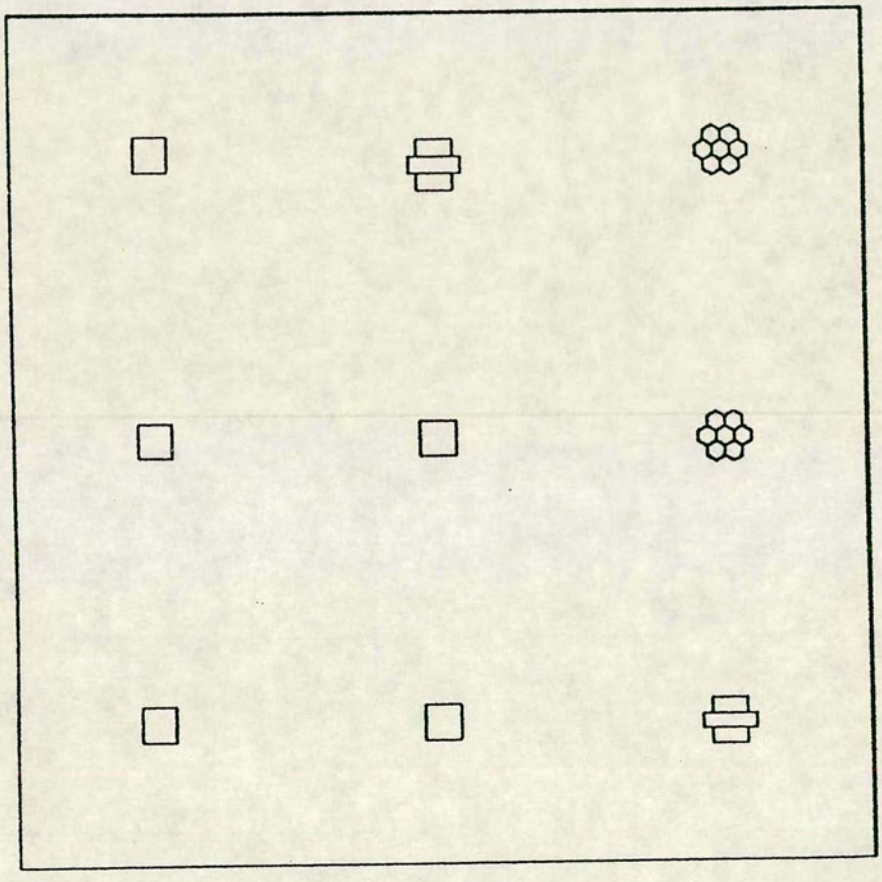

High-pass filter (mask 3)

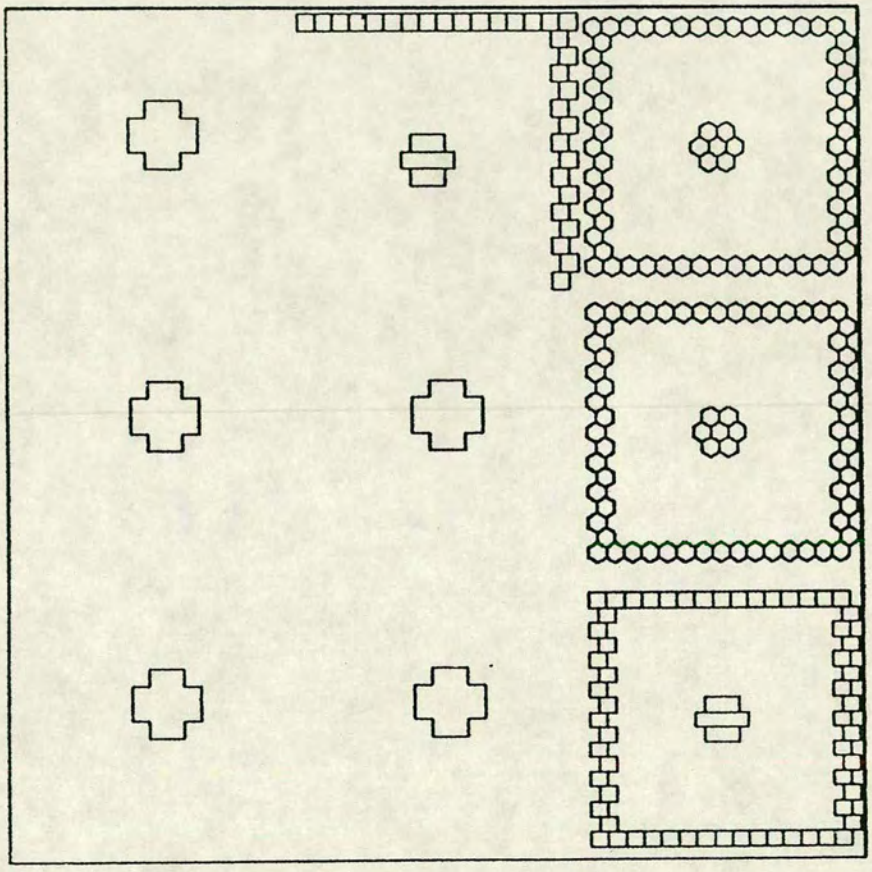

High-pass filter (mask 4)

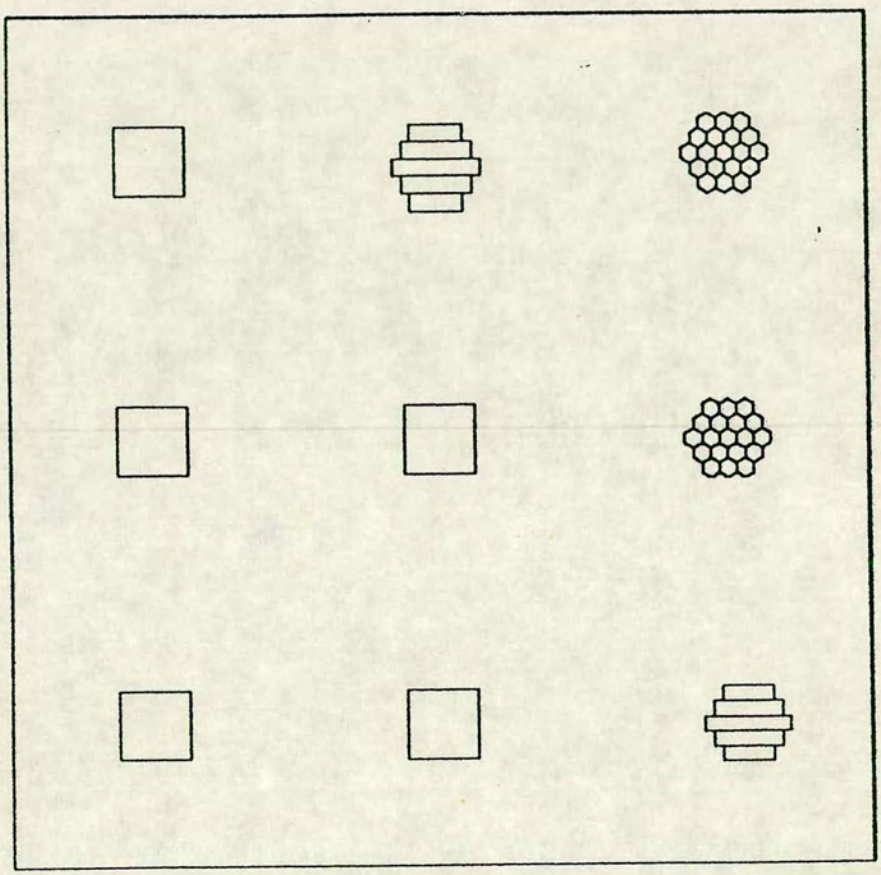

High-pass filter (mask 5)

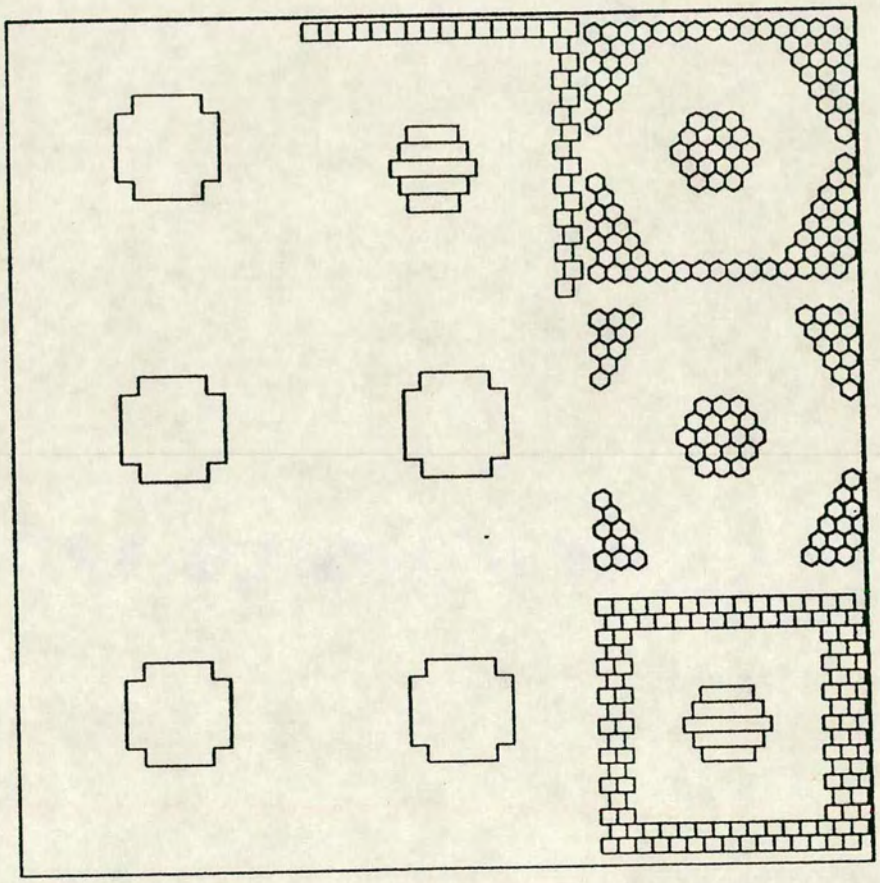

High-pass filter (mask 6)

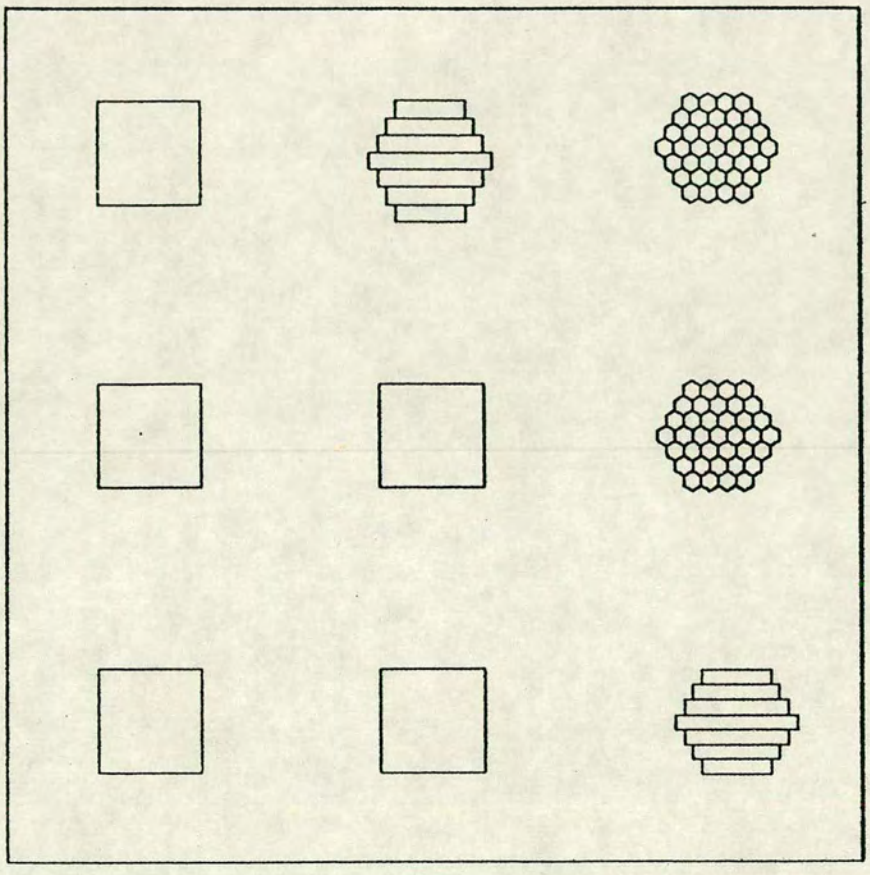

High-pass filter (mask 7)

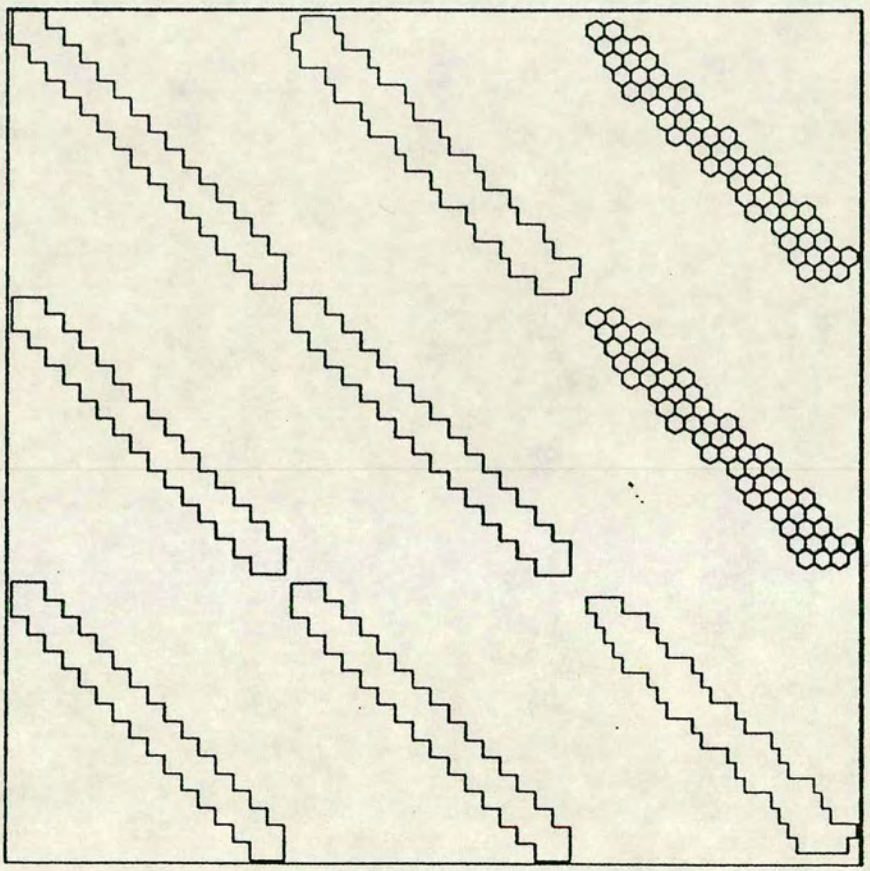

Diagonal leg filter (mask 8)

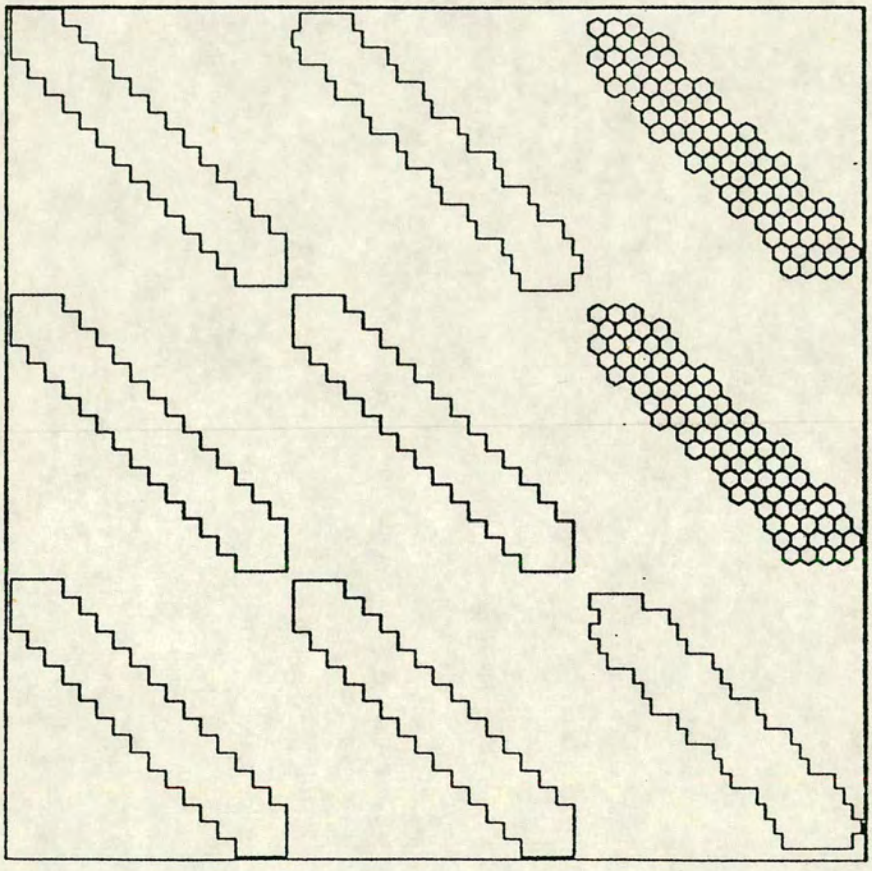

Diagonal leg filter (mask 9)

1) A mask to remove two columns of pixels, or the equivalent in the hexagonal grid structures.

When used to form a filter, this would be used to remove a leg of the Fourier transform, which would cause high-pass filtering and the removal of an edge in the image.

2) A wider version of the last mask, this time to remove four columns of pixels or the equivalent.

A filter formed using this mask would have a similar effect to the last but with a higher low-frequency cutoff

3) A group of four pixels in the rectangular structures or five in the hexagonal, would be removed.

This is a mask to form a high-pass filter.

4) A similar mask to the last, with more pixels removed. Some pixels are also removed from the outer edges of some arrays, to increase the low-pass filtering effect.

5) A high-pass filter with more pixels removed.

6) Again, a mask to remove more pixels to form a high-pass filter. Also, with pixels removed from the edges of the arrays to investigate the increased low-pass filtering effect

7) The high-pass filter mask with the highest low-frequency cutoff.

8) A mask to remove pixels on a diagonal across the filter. This would have the same use as the first two filter masks, but used to investigate the effect of the jagged edges which must be used with diagonal filters.

9) A similar mask to the previous one but with more pixels removed.

References

1.1 Abbe E.

Archiv. fur Microscopicische Anatomie ix, p413 (1873)

1.2 Porter A.B.

On the diffractive theory of microscopic vision

Phil. Mag. V11, No6, p154 (1906)

1.3 Vander Lugt, A.

A review of optical data-processing techniques

Optica acta V15, #1, p1-33 (1968)

1.4 Zernike F.

Das phasenkontrastverfahren bei der mikroscopischer beobachtung

Z. Tech. Phys. V16 p454 (1935)

1.5 Goodman J.W.

Introduction to Fourier optics

McGraw-Hill (1968)

1.6 Schelling A.D.

Liquid crystal displays

Elec. comp. and appl. V5, No4, p233 (1983)

1.7 Sehi H., Uchida T., Shibata Y.

Evaluation of brightness and contrast in twisted nematic guest-host cells

Proc. SID V24/5, p273 (1984)

1.8 Young M.

Low-cost LCD video display for optical processing

Applied Optics V25, No7 (1984)

1.9 Underwood I., Vass D.G., Sillitto R.M.

Evaluation of an nMOS VLSI array for an adaptive liquid crystal SLM

IEE Proc. V133/J, No1, p77 (1986)

1.10 McKnight D.J., Vass D.G., Sillitto R.M.

Development of a spatial light modulator - a randomly addressed liquid crystal over silicon array

1988 Technical Digest Series V8, p151 (1988)

1.11 Latham S.G., Owen M.P.

A silicon-liquid crystal SLM

GEC Journal of Research V4, No3, p220 (1986)

2.1 Born, M. and Wolf, E.

Principles of optics

Pergamon press, 6th edition, 1980, p382

2.2 Cathey, W.T.

Optical Information Processing and Holography

Wiley, 1974, p102

2.3 Goodman, J.W.

Introduction to Fourier Optics

McGraw-Hill, 1968, p86

2.4 Pernick,B.J.

Variable-Scale Single-Lens Optical Transform Systems

Applied Optics, V19, #5, 1980, p651-2

2.5 Gaskill, J.D.

Linear Systems, Fourier Transforms and Optics

Wiley, 1978, p451

3.1 Joyeux D., Lowenthal S.

Optical Fourier transforms:what is the optimum setup?

Applied Optics V21, No23, p4368 (1982)

4.1 Petersen D.P., Middleton D.

Sampling and reconstruction of wave-number-limited functions in N-dimensional Euclidian spaces

5.1 Talbot, H.

Lond., Edin., Dubl., Phil. Mag. V9, 1836, p407

5.2 Kolodziejczyk, A.

Optica Acta V32, 1985, p741

5.3 Smolinska, B., Kalestynski, A.

Optica Acta V25, 1978, p256

5.4 Willson, P.H.

M.Sc. Dissertation, Reading, 1985

5.5 Bryngdahl, O.

J. Opt. Soc. America, V63, 1972, p416

5.6 Goodman, J.W.

Introduction to Fourier Optics

McGraw-Hill, 1968